Creation of a structural plasticity model consistent with memory consolidation

Auteur : Magis, Justine
Promoteur(s) : Drion, Guillaume
Faculté : Faculté des Sciences appliquées
Diplôme : Master en ingénieur civil biomédical, à finalité spécialisée
Année académique : 2022-2023
URI/URL : http://hdl.handle.net/2268.2/17703

Creation of a structural plasticity model consistent with memory consolidation

Master thesis realised with the aim of obtaining the degree of Master in Biomedical Engineering

Justine Magis

Promotor:
Guillaume Drion

Jury members:
Guillaume Drion
Pierre Sacré
Kathleen Jacquerie
Vincent Seutin

University of Liège
Faculty of Applied Sciences
Academic year 2022 - 2023

Creation of a structural plasticity model consistent with memory consolidation

Justine Magis

Supervisor: G. Drion
Master in Biomedical Engineering, University of Liège
Academic year 2022-2023

Abstract

In our daily lives, every individual is inevitably faced with the need to memorize new things. Whether it is at school or university, where entire courses need to be memorized, or even when we have to remember a shopping list to do our groceries. It is easy to think that to maximize our performance when memorizing, it is necessary to work as hard as possible. However, experimental studies have contradicted this thinking and shown that punctuating learning phases with phases of rest helps to strengthen memory. This transition between learning and resting phases is directed by our brain, which moves from a state of active waking to one of quiet waking. This is reflected in changes in neuronal firing patterns. During learning (active waking state), neurons display tonic activity, whereas in the quiet waking state, they display burst activity. The role of these state switches on learning and memory consolidation is now considered to be well established, but the mechanisms underlying this phenomenon are still not well understood. Various approaches can be adopted to better understand them, including a computational approach.

It has been demonstrated that the brain stores memories in the neuronal connections, which are constantly modified through synaptic plasticity. Several models exist in the literature to model synaptic plasticity, and have proved effective when used in the active waking state. However, these models are not adapted to the changes in neuronal firing patterns that take place during state changes, and applied as they are, they do not prove the link between memory consolidation and quiet waking states. Indeed, they lead to a "homeostatic reset", which refers to the fact that no matter whether neurons have learned more or less information during active waking states, they follow the same evolution during quiet waking states. This means that all the information learned is forgotten when the quiet waking state is reached.

The aim of this thesis is to propose a structural plasticity model which, combined with traditional synaptic plasticity models, will be able to solve this homeostatic reset problem which is not consistent with memory consolidation. The structural plasticity model will then be used to transfer learning through lasting morphological changes in synapses. To achieve this goal, structural plasticity is first investigated from a biological point of view to understand the main mechanisms underlying it. Next, the various models of structural plasticity that exist in the literature are reviewed. A new structural plasticity rule is then proposed and tested in different experiments. In addition, an analysis of the model parameters is provided. The results were convincing, and the rule was able to take advantage of homeostatic reset to consolidate memory. The effectiveness of the model is then tested in a simple task. The results showed that combining the structural plasticity rule with a traditional plasticity rule in the presence of switches from tonic to burst activity improved the signal-to-noise ratio (SNR) across several tonic/burst cycles. Finally, the effectiveness of our model is illustrated in a simple pattern recognition learning task and the results showed that neurons learned better in the presence of structural plasticity. To conclude, future prospects aiming to further explore the rule of structural plasticity developed in this thesis are proposed.

Acknowledgements

First and foremost, I would like to express my gratitude to Professor Drion for his trust, and for his availability throughout this thesis. I am thankful for the time he allocated to our regular meetings, our discussions, and his valuable research suggestions.

The successful completion of this work would not have been possible without the close guidance and supervision of Kathleen Jacquerie, and I am forever grateful for her availability throughout the entire thesis. Her meticulous proofreading and insightful suggestions have been invaluable.

I had the privilege of closely collaborating with Emmy Kellens during this work. I am thankful to her for contributing to an enjoyable working experience, engaging in stimulating discussions, and generously devoting her time to proofread sections of this work.

I am sincerely thankful to Sven Goffin for taking the time to help me, on numerous occasions, in formalizing and mathematically demonstrating experimental observations.

Beyond this thesis, I would like to thank my family and my friends for accompanying me on my studies, and making it an awesome journey.

Liège, June 9^{th}, 2023

Justine Magis

Contents

Chapter 1

Introduction

1.1 Motivation

It has been shown that the brain is able to store memories thanks to the ability of neurons to constantly modify their neuronal connections. This is achieved through *synaptic plasticity*, which is driven by the spike activity of neurons. What's more, throughout the day, the brain passes through different cerebral states and, more specifically, can move from a state of *active waking* to one of *quiet waking*. These transitions from one state to another are reflected in changes in the firing patterns of neurons. Scientific research has shown that these quiet waking states play a predominant role in memory consolidation. However, the underlying mechanisms that explain the role of these quiet waking states in memory are still under investigation. Computational studies can help to understand these mechanisms and overcome the limitations of experimental studies on living subjects.

Several computational models exist in the literature to model synaptic plasticity and have been shown to be effective when used in waking states. These models describe the evolution of neuronal connections through what is known as *synaptic weight* (which characterizes the strength or efficiency of neuronal connections). However, it has recently been shown by [Jacquerie et al., 2022a] that these models are not suitable when used for the transition from an active waking state to a quiet waking state. Indeed, these models lead to *homeostatic reset*, in which synaptic weights converge to the same basal value, regardless of their initial value. This means that all the information learned during the active waking state would be forgotten when switching to the quiet waking state.

Furthermore, it has been shown in the literature that *structural plasticity* (which refers to long-lasting morphological changes in synapses) is essential for long-term memory storage. The aim of this thesis is to propose a model of structural plasticity that will take advantage of homeostatic reset and provide a model compatible with memory consolidation. To this end, the following questions will be answered:

- *What is synaptic plasticity, how is it modeled, and what are the limitations of these models for changes in neuronal firing pattern?* (Chapter 2)
- *What is structural plasticity from a biological point of view* (Chapter 3) *and how is it modeled in the literature?* (Chapter 4)
- *Can we create a structural plasticity rule that takes advantage of homeostatic reset to transfer learning and be consistent with memory consolidation?* (Chapter 5)
- *Is the proposed model effective for memory consolidation?* (Chapter 6)

1.2 Structure

To answer these questions, this thesis is divided into 4 main parts:

Part I introduces the various basic neuroscience concepts useful for understanding this thesis. The different *brain states* with their associated neuronal activities will be discussed. The way neurons communicate with each other and certain morphological aspects of neurons (in particular *dendritic spines*) will be presented. *Synaptic plasticity* will then be investigated, where we will distinguish between *E-LTP* (or *plasticity induction*) and *L-LTP* (or *plasticity maintenance*). The mechanisms involved in plasticity induction will be described. Then, the way to model a neural network capable of switching neural activity will be briefly described. To conclude this section, the two traditional synaptic plasticity rules used to model E-LTP (*biophysical models* and *phenomenological models*) will be presented. The *homeostatic reset* phenomenon, which results from the application of these traditional rules during neuronal activity switches, will be introduced (Chapter 2).

Part II focuses on *structural plasticity*. First, it will be approached from a biological point of view. The molecular mechanisms responsible for morphological changes in dendritic spines will be investigated. In particular, the role of small GTPases will be examined. In addition, the Synaptic Tagging and Capture hypothesis, which links E-LTP to L-LTP, will be presented (Chapter 3). Chapter 4 reviews the various structural plasticity models available in the literature. The models will be presented according to 3 categories: *mathematical models*, *biophysical models* and *phenomenological models*.

Part III is the computational study. First, the structural plasticity model proposed by [Jacquerie, 2023] will be investigated in different experiments and the limitations of this model will be given. Then, to overcome these limitations, a new structural plasticity model is introduced. It is tested in various experiments and its parameters are analyzed (Chapter 5). The effectiveness of the model will then be tested in a simple memory task. This will be done through an in-depth analysis of the signal-to-noise ratio (SNR) in different experiments. We will see that the model we've developed improves SNR compared to the case where traditional plasticity rules are applied alone. Finally, the effectiveness of our model will be illustrated in a simple pattern recognition learning task (Chapter 6).

Part IV draws the conclusion. To summarize the thesis, answers are provided to the 4 key thesis questions presented on the previous page. In addition, future perspectives to be explored are proposed and some limitations are outlined.

Part I

Background

Chapter 2

Elements of neurophysiology

This chapter briefly introduces the different notions in neuroscience necessary for a clear understanding of this master thesis.

2.1 Brain and neuron electrical activity

Our *brain*, composed of *neurons* that are connected to each other to form *neural circuits*, is constantly active. Throughout the day, it is able to go from a state of sleep to a state of wakefulness, from a state of inattention to a state of attention [Zagha and McCormick, 2014, Lee and Dan, 2012]. A *brain state* refers to the functional state in which the brain is at a given moment. They can be studied at several spatial scales, but also at several temporal scales.

At the cellular level, neurons can switch from *tonic firing* to *bursting* in less than a second [Jacquerie, 2023].

Tonic firing: characterized by trains of action potential, in response to a stimulus.

Bursting: characterized by a series of grouped high-frequency action potentials interrupted by periods of silence [Jacquerie, 2023].

At the neuronal circuit scale, the state can switch from active to quiet waking in a few minutes. In this case, the circuit rhythm will change from a small amplitude, high frequency oscillation to a large amplitude, low frequency oscillation. Finally, on a brain scale, the state can change from arousal to sleep on an hourly scale [Jacquerie, 2023].

The mechanisms involved in the transition from one brain state to another are not yet fully understood. However, it has been shown that neuromodulators are partly responsible for these changes. The different states just described are illustrated in Figure 2.1.

2.2 Communication between neurons

The connections formed between neurons are of great interest since, in addition to allowing neurons to communicate with each other, they are considered the seat of learning and long-term memory [Fauth and van Rossum, 2019].

The area of contact between two neurons is called the *synapse* and allows the transmission of information. Information is transmitted from a *presynaptic neuron* to a *postsynaptic neuron*, called *synaptic transmission* [Bear et al., 2007]. There are two types of synapse: *electrical synapses* and *chemical synapses*. However, the most abundant type is the chemical synapse, in which information is transmitted through chemical compounds, called *neurotransmitters*.

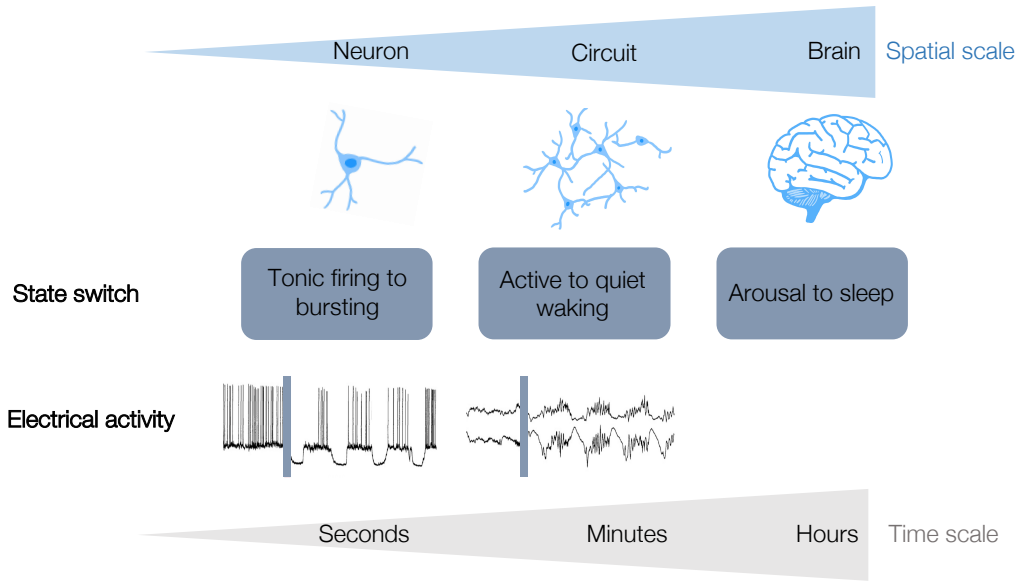

Figure 2.1 – **Brain states at different scales.** A neuron can change its electrical activity in less than a second and switch from tonic firing to bursting. The neurons form neural circuits. The circuits can go from an active to a quiet state of waking on a minute scale. The brain can go from an awake state to a sleep state on a time scale of an hour. *Adapted from [Jacquerie, 2023].*

In practice, how is information transmitted across a chemical synapse?

The process is illustrated in Figure 2.2.

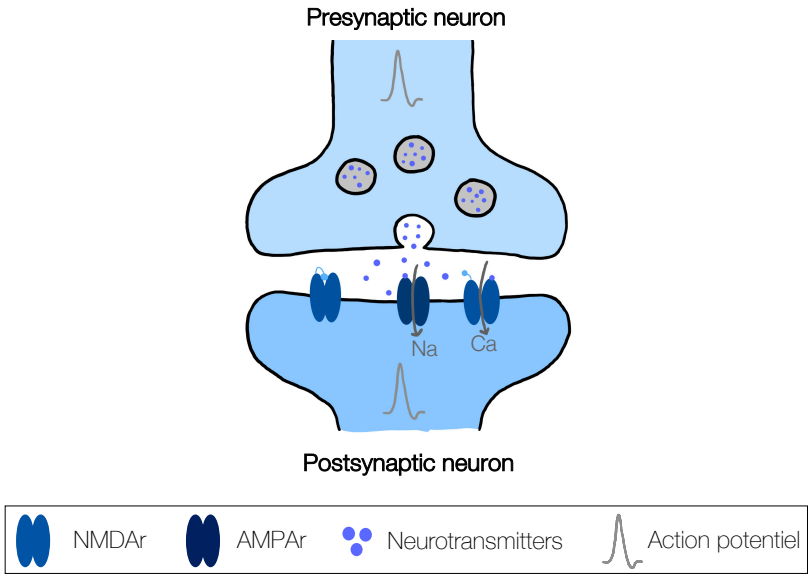

Figure 2.2 – **Chemical synapse.** An action potential in the presynaptic neuron triggers the release of neurotransmitters. These interact with receptors on the postsynaptic neuron, in particular the glutamate receptors AMPA (α-amino- 3-hydroxy-5-methyl-4-isoxazole propionic acid) and NMDA (N-methyl-D-aspartate). The activation of these receptors induces an influx of sodium (Na) and calcium (Ca) respectively into the postsynaptic neuron. *Inspired from* [Jacquerie et al., 2022b, Lamprecht and LeDoux, 2004].

The neuron presynaptic, also called *presynaptic button*, will generate an action potential. This will result in an influx of calcium into this neuron, which causes the neuron to release neurotransmitters. These neurotransmitters then interact with the receptors of the postsynaptic neuron and eventually trigger a response in it [Bear et al., 2007]. Receptors playing a key role in synaptic transmission are the AMPA (α-amino- 3-hydroxy-5-methyl-4-isoxazole propionic acid) and NMDA (N-methyl-D-aspartate) glutamate receptors [Bear et al., 2007].

2.3 Dendritic spines

The connection between two neurons takes place between the synaptic terminal of the presynaptic neuron and the dendrites of the postsynaptic neuron. On the dendrites, small protuberances called *dendritic spines* can be found [Bear et al., 2007]. Figure 2.3 shows where these dendritic spines are located in relation to the neuron. They are the points of contact with the neighboring neurons and thus represent the postynaptic site of the synapses. On this figure, the main structures of the neuron are also represented.

Dendritic spines are dynamic structures and their size, shape and number constantly change in response to neuronal activity. Changes can occur on vastly different time scales, ranging from seconds to minutes or even hours to days. Moreover, they are constantly renewing themselves, i.e. there is a constant formation of new spines and elimination of others [Runge et al., 2020, Hering and Sheng, 2001]. Changes in the size, shape and density of synaptic spines is associated with learning and memory [Pchitskaya and Bezprozvanny, 2020].

It should be noted that not all types of neurons have dendritic spines [Hering and Sheng, 2001]. Indeed, there are for example motor neurons, sensory neurons, some are excitatory, others inhibitory [Furness, 2000]. Dendritic spines are more common in advanced nervous systems (such as the mammalian brain) and are rarely present in less complex organisms [Hering and Sheng, 2001].

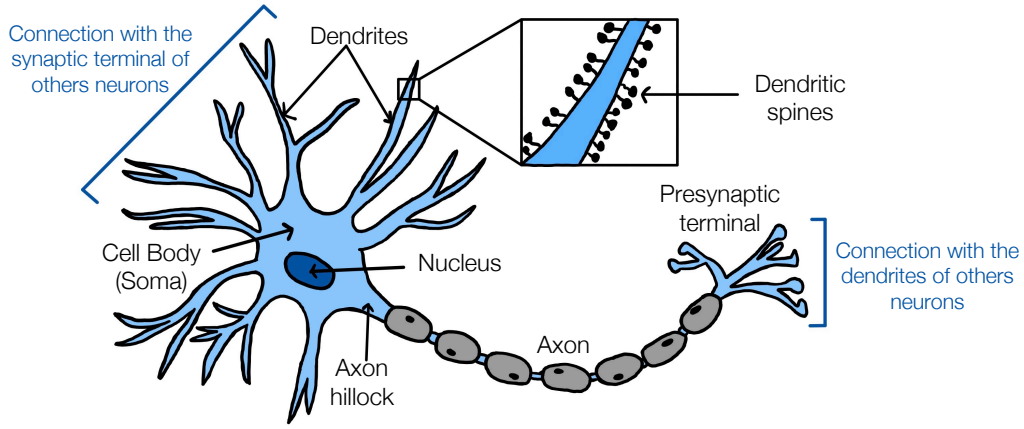

Figure 2.3 – **Structure of the neuron.** A neuron contains an axon, a nucleus, a cell body, an axon hillock, a presynaptic terminal and dendrites. The connection between two neurons is made between the presynaptic terminal of one neuron and the dendrites of a neighboring neuron. Dendritic spines are located on the dendrites. *Inspired from [Adem et al., 2016].*

2.3.1 Structure of dendritic spines

The dendritic spines have a typical length of 0.5 to 2 μm. The spines contain globular tips called *spine heads*, from which synapses are formed. The tight links that connect the spine heads to the dendrites are called *spine necks* [Bear et al., 2007]. Figure 2.4 illustrates the dendritic spine structure.

Spines are characterized by *postsynaptic density* (PSD) which is a thickening of the membrane typically located at the head of the spine. The PSD is composed of hundreds of densely organized signaling molecules and proteins,

including ion channels and receptors [Pchitskaya and Bezprozvanny, 2020, Hering and Sheng, 2001]. One of the most abundant proteins in PSD is the CaMKII (calcium/calmodulin-dependent protein kinase II). This protein plays a major role in changes in synaptic transmission efficacy, which will be described in more details later in this master thesis [Muller et al., 2002].

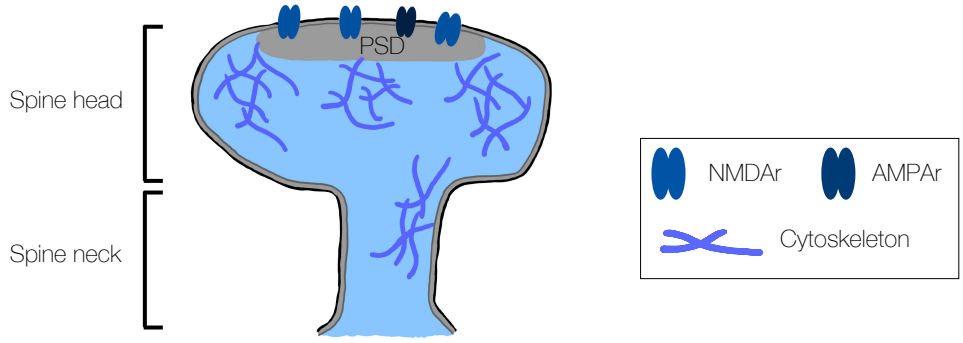

Figure 2.4 – **Simplified structure of a dendritic spine.**The spine is composed of two parts: the spine head and the spine neck. Inside the spine, there is a cytoskeleton that maintains its structure and a postsynaptic density (PSD). The PSD is dense in signalling molecules, ion channels and receptors. In particular, there are glutamate receptors such as AMPAr and NMDAr. *Inspired from* [Domart, 2019]

The structure of the spine is maintained by a network of *actin cytoskeleton*, which also serves as a scaffold for the various proteins that constitute it and for the PSD [Nakahata and Yasuda, 2018, Pchitskaya and Bezprozvanny, 2020]. Regulation of this actin cytoskeleton can induce morphological changes in spines [Patterson and Yasuda, 2011]. This aspect will be discussed in more detail later in the Chapter 3 of this thesis. It is noteworthy that, like the synapse as a whole, PSDs have also been shown to be morphologically dynamic [Muller et al., 2002].

Dendritic spines exist in a wide variety of shapes and sizes depending on their location in the brain. According to their morphological characteristics, they are classified into several classes. In this thesis, we focus only on the so-called *mushroom* and *thin* spines. Indeed, mushroom-shaped spines, which have a large head and a small neck (like the one in Figure 2.4), are considered as long-term memory storage sites. This is because they form strong synaptic connections and are long-lived. In addition, thin spines, which have a structure similar to mushroom spines but with smaller heads, are considered learning sites. Indeed, they are more dynamic and their head will expand in response to a learning event [Pchitskaya and Bezprozvanny, 2020].

2.3.2 Fonction of dendritic spines

The primary function of dendritic spines is that they allow the separation of postsynaptic chemical responses, such as calcium responses. Indeed, spines can be considered as small closed chemical compartments that are semi-autonomous. They are separated from the dendritic tree by their rather thin neck which would prevent the diffusion of biochemical signals from the head of the spine to the rest of the dendritic [Bear et al., 2007, Hering and Sheng, 2001]. Moreover, the geometry of the neck would control the kinetics and magnitude of postsynaptic calcium responses. For example, calcium responses in dendritic spines with a long neck are faster than in spines with a short neck [Hering and Sheng, 2001].
In addition, the spine heads have a small volume which allows for rapid and efficient responses to input signals [Bear et al., 2007].

Dendritic spines, by their dynamic morphology, also play an important role in learning and long-term memory [Lamprecht and LeDoux, 2004]. It is this role that is of great interest in this thesis and will be discussed in depth in the following.

2.4 Synaptic plasticity

The brain of mammals has the fascinating property of being able to change and adapt according to the experience they live. This property of plasticity occurs in particular during the learning and memorization process. *Synaptic plasticity* refers to the ability to change the strength or efficiency of synaptic transmission of existing synapses according to activity [Citri and Malenka, 2008]. The literature distinguishes several types of plasticity. Firstly, there is *short-term plasticity* and *long-term plasticity*. Short-term plasticity temporarily modifies synaptic transmission and lasts only a few milliseconds. This type of plasticity is not the focus of this thesis and will therefore not be discussed at length here, but its mechanisms are discussed in Appendix A.1. With regard to long-term plasticity, several forms are also discussed in the literature, the most frequently addressed of which are described below.

2.4.1 Long-term plasticity

In the 1940s, Hebb proposed that when presynaptic activity is correlated with postsynaptic activity, there is a change in the strength of synaptic connections between the two neurons involved. This phenomenon, named after its discoverer, is called Hebbian plasticity. *Long-Term Potentiation* (LTP) and *Long-Term Depression* (LTD) are examples of this type of plasticity. LTP therefore occurs when synapses are repeatedly stimulated, leading to potentiation of synaptic strength between the two neurons and allowing rapid storage of information. Like memory, LTP can be rapidly generated and is strengthened and prolonged by repetition. These mechanisms have been extensively studied because they are believed to play a crucial role in the formation of memories and learning [Citri and Malenka, 2008].

In the literature, there are often two types of LTP: *early LTP* (E-LTP), also referred to as synaptic plasticity *induction* and *late LTP* (L-LTP), also referred to as plasticity *maintenance*. E-LTP lasts 1-2 hours and is characterized by a change in receptor efficacy and rapid insertion of new receptors. However, this type of plasticity is independent of protein synthesis [Patterson and Yasuda, 2011].

L-LTP, on the other hand, lasts longer and requires the synthesis of new proteins and is associated with the induction of many genes [Smolen et al., 2006]. In addition, it involves structural changes in synapses. Therefore, in this thesis, L-LTP will refer to structural plasticity and will be investigated at length in Chapter 3 [Patterson and Yasuda, 2011] .

Mechanisms involved in the induction of synaptic plasticity (E-LTP)

Synaptic plasticity is induced in 3 stages, as described in Figure 2.5.

- Firstly, by its activity, the presynaptic neuron releases glutamate which binds to and activates AMPAr and NMDAr. However, only AMPA receptors allow the passage of ions to which they are permeable since NMDAr are blocked by magnesium. Sodium therefore enters the postsynaptic neuron through the AMPAr and depolarizes it. (Figure 2.5 **i.**)

- Secondly, depolarization of the postsynaptic neuron causes the magnesium blocking NMDAr to be removed. Calcium can then enter the postsynaptic neuron through NMDAr. In other words, NMDAr only allow calcium to pass when both pre- and postsynaptic neurons are active at the same time. (Figure 2.5 **ii.**)

- Thirdly, this massive influx of calcium results in the activation of a cascade of events that lead to a change in synaptic strength (LTP or LTD). Thus, calcium plays a key role in the induction of synaptic plasticity. Depending on the amount of calcium entering the postsynaptic neuron, an LTP or LTD will be induced. It should be noted that another source of calcium entry into the postsynaptic neuron is possible through voltage-gated calcium channels (VGCC) [Lamprecht and LeDoux, 2004, Citri and Malenka, 2008]. (Figure 2.5 **iii.**)

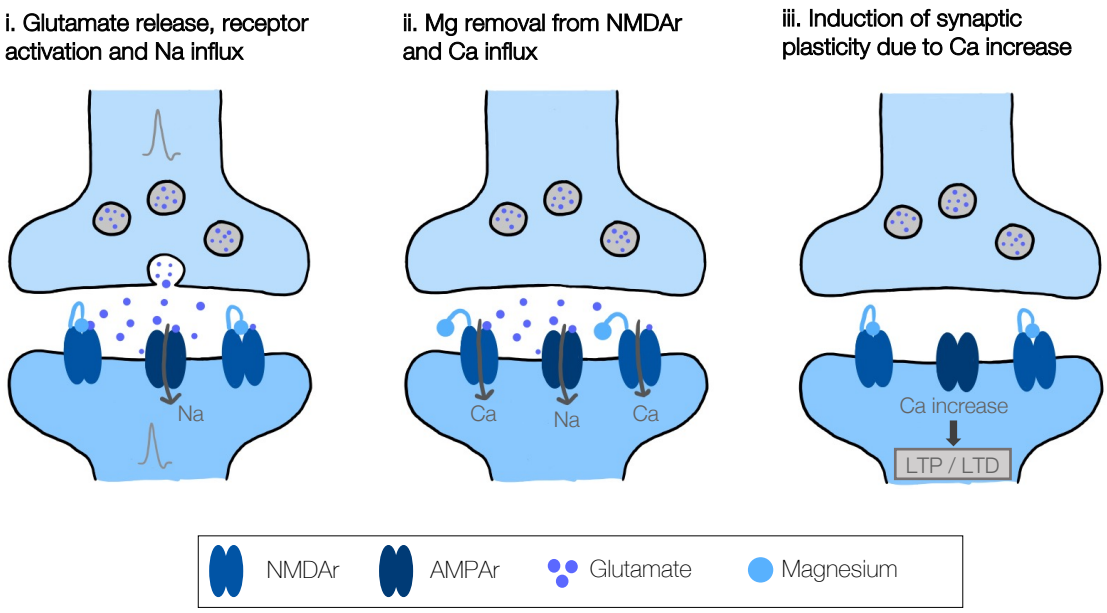

Figure 2.5 – **Mechanisms invloved in the induction of synaptic plasticity. i.** Activity-dependent release of glutamate from presynaptic neurons leads to the activation of AMPAr and to the depolarization of the postsynaptic neuron. **ii.** Magnesium (Mg) is then moved from NMDAr and calcium can flow through into the post-synaptic neuron. **iii.** The increase in calcium in the postsynaptic neuron leads to the induction of LTP or LTD. *Inspired from* [Lamprecht and LeDoux, 2004].

LTP induction vs LTD induction

Before looking at how this calcium influx leads to LTP or LTD, it's important to understand that in dendritic spines, there's a continuous recycling of AMPAr. This is because AMPAr move from the postsynaptic membrane to areas of endocytosis closer to the intracellular side. There, the receptors are endocytosed and recycled in endosmoses, called *recycling endosomes*. They are then exocytosed to the plasma membrane and return to the postsynaptic membrane. The endocytosis and exocytosis phenomena balance each other so that the number of AMP receptors remains unchanged [Citri and Malenka, 2008, Patterson and Yasuda, 2011]. This phenomenon is illustrated in Figure 2.6 (left-hand diagram).

Endocytosis: process by which a cell captures external substances by enclosing them in an internal vesicle formed by its membrane, in order to transport them inside the cell [Larousse, 2023a].

Exocytosis: process by which a cell releases substances to the outside by fusing a vesicle filled with these substances with the cell membrane [Larousse, 2023b].

Endosome: small membrane vesicles found inside eukaryotic cells (e.g. neurons), which play a crucial role in sorting and transporting molecules captured by endocytosis [Wikipédia, 2023].

LTP induction It occurs when the calcium influx into the postsynaptic neuron exceeds a certain critical value. This increase in calcium leads to the activation of protein kinases such as CaMKII. This kinase then reinforces the phenomenon of exocytosis, which disrupts the pre-existing balance. An increase in the number of receptors is then observed [Citri and Malenka, 2008, Patterson and Yasuda, 2011]. LTP induction is illustrated in the top right-hand diagram of Figure 2.6.

LTD induction It occurs when the increase in calcium in the postsynaptic neuron is modest. This results in the activation of phosphatases such as calcineurin and protein phosphatase 1 (PP1). These activations will, in turn, reinforce the phenomenon of endocytosis. A decrease in the number of receptors will then be observed [Citri and Malenka, 2008, Patterson and Yasuda, 2011]. Illustrated in the bottom right-hand diagram of Figure 2.6.

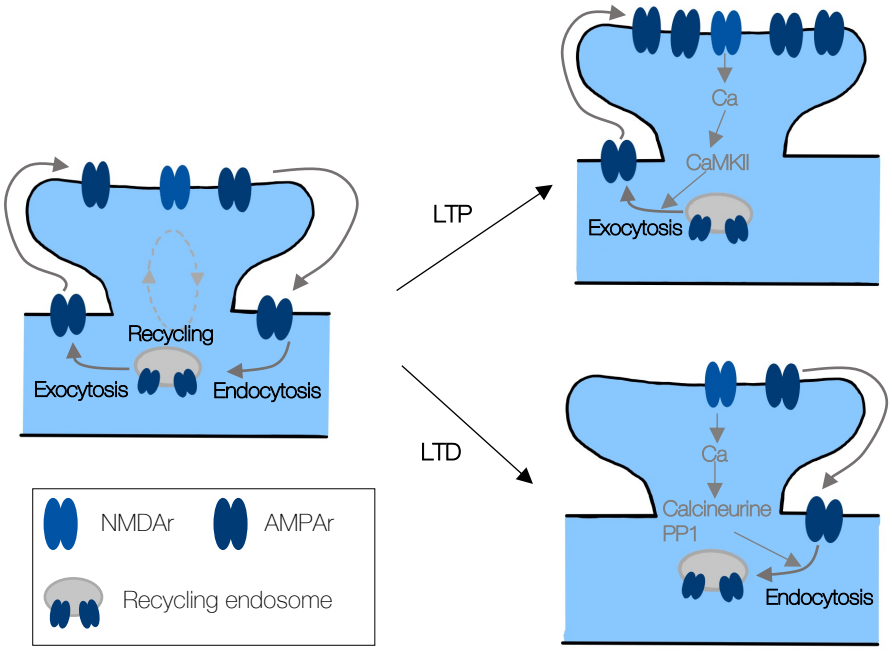

Figure 2.6 – **Rapid trafficking of AMPA receptors.** Receptor recycling occurs continuously with the help of recycling endosomes. There is a balance between endocytosis and exocytosis. When an LTP or LTD is induced, this balance is disturbed. An LTP will reinforce the phenomenon of exocytosis and will increase the number of receptors. A LTD will reinforce the phenomenon of exocytosis and will decrease the number of receptors. *Inspired from* [Citri and Malenka, 2008, Sheng and Lee, 2001].

Here we are dealing with a fast traffic of AMPAr in which protein synthesis is not required [Citri and Malenka, 2008]. The molecular mechanisms by which LTD and LTP occur are more complex than those described here, but there is little point in describing them in detail in this thesis.

2.4.2 Synaptic plasticity from a modeling point of view

Now that synaptic plasticity has been briefly described from a biological point of view, we can see how it is modelled from an information point of view. As a reminder, synaptic plasticity is defined as the ability of neurons to change the synaptic strength between them. Modeling synaptic plasticity consists in creating a model (a kind of black box) that takes as input the activities of pre- and postsynaptic neurons and provides as output the synaptic strength [Jacquerie, 2023].

Neuron model

Before synaptic plasticity can be modeled, it is necessary to model the activity of neurons. To do this, there are several types of models, the most common of which are the *conductances-based models* and the *integrate-and-fire models* [Minne, 2021].

- The conductance-based models are more biological models that represent in a complete way the behavior of neurons [Minne, 2021]. In this type of model, the neuron membrane voltage is described by a Hodgkin and Huxley type equation [Jacquerie, 2023].
- The integrate-and-fire models, on the other hand, are more mathematical models that describe the qualitative aspects of neurons such as spike times [Minne, 2021]. These models are based on the following process: neurons accumulate electrical signals from other neurons and add them up over time. When the sum of these signals reaches a threshold, the neuron generates an action potential. Then the neuron resets and the process begins again.

The model that will be used in the computational part of this thesis (Chapter 5 and Chapter 6) is a conductance-based model able to switch between activities and is based on the one proposed by [Jacquerie et al., 2022a]. A simplified illustration is shown in Figure 2.7. It is composed of an inhibitory neuron and excitatory pre- and postsynaptic neurons. Here, in the diagram, the network is made up of a presynaptic neuron and a postsynaptic neuron. However, depending on the experiment required, the size of the network can be modulated and we can form much larger networks. The inhibitory neuron (I) is connected to all the excitatory neurons and the presynaptic neurons are connected to the postsynaptic neurons, in a feedforward manner. Moreover, in order for the circuit to change its type of activity, a current I_{app} is applied to the inhibitory neuron. By adjusting the value of this current, we can modulate the activity of the neurons, i.e. make them change from tonic activity to burst activity.

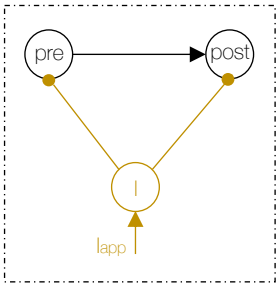

Figure 2.7 – **Neural circuit used in the computational part.** Presynaptic neurons are connected to postsynaptic neurons in a feedforward manner. An inhibitory neuron is connected to all neurons and an I_{app} current is applied to it. *Adapted from* [Jacquerie, 2023].

Thanks to this model, in which neurons are able to switch electrical activity, we can study the role of these activity switches on memory. Figure 2.8 shows examples of the activities we can give to the neurons in the network, and these are the ones we'll be using in the experiments in Chapter 5 and Chapter 6. Neurons will either have *inactivity*, in which they spike very little, or *tonic activity*, in which they spike at a chosen frequency, or *burst activity*.

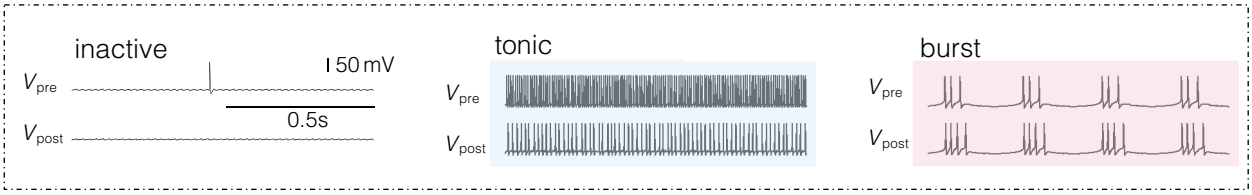

Figure 2.8 – **Example of possible neuronal activity.** The following types of activity will be considered in the experiments: inactive activity, tonic activity or burst activity. *From* [Jacquerie, 2023]

.

Synaptic plasticty model

As far as modeling synaptic plasticity is concerned, E-LTP models have been widely studied and are now well established in the literature, which is not the case for L-LTP models. In this section, the traditional rules for modeling E-LTP are described. The models will characterize changes in synaptic strength by changes in the variable w, representing the synaptic weight between two neurons. For an LTP, there will be an increase in w while for an LTD there will be a decrease in w.

There are two main traditional rules of synaptic plasticity: *biophysical models* and *phenomenological models*.

- Biophysical models are based on the molecular processes responsible for synaptic plasticity. They will therefore take as input biological variables such as calcium influx resulting from neuronal activity in order to govern

changes in synaptic weight.

- Phenomenological models are mathematical models that are not concerned with the molecular processes underlying synaptic plasticity. They are constructed using an input-output relationship between neuronal activity and synaptic plasticity [Benghalem, 2022]. The input of this type of model will be for example the spike times of pre- and postsynaptic neurons [Jacquerie, 2023].

These two models are illustrated schematically in Figure 2.9 and will both be used in this thesis.

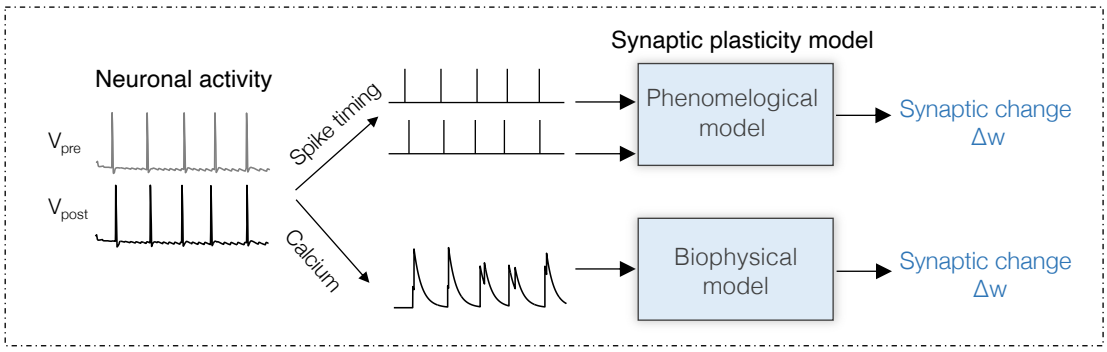

Figure 2.9 – **The two main traditional models of synaptic plasticity.** Synaptic plasticity can be translated into changes in synaptic weight from neuronal activity via phenomenological models or biophysical models. Phenomenological models take as input the spike times of the two neurons and convert them into synaptic changes. Biophysical models take calcium as input and convert it into synaptic changes. *Adapted from* [Jacquerie, 2023].

2.4.3 Switch to burst activity leads to homeostatic reset

We have seen in Section 2.1 that, throughout the day, neural networks switch from one state to another. In particular, they go from an active waking state (reflecting learning) to a quiet waking state. This transition is reflected in a change in the electrical activity of the neurons. Indeed, in this case, they will switch from a tonic activity to a burst activity.

Using the traditional rules of synaptic plasticity just described above (calcium rule and phenomenological model), [Jacquerie et al., 2022a] studied the evolution of the synaptic weight w during these switches from tonic to burst activity. The results (Figure 2.10) showed that, regardless of the learning of neurons during tonic activity, all synaptic weights (high weights, shown in blue, and low weights, shown in grey on figure) converge to the same value in burst activity. The transition to burst activity therefore results in a reset of the synaptic weights. [Jacquerie et al., 2022a] called this phenomenon the *homeostatic reset*.

It's important to note that this homeostatic reset stems from the use of soft-bounds in synaptic plasticity rules. The soft-bound method consists in adding a weight dependency. In other words, synaptic plasticity itself depends on synaptic weight. In this way, a synaptic connection with a low weight is more likely to undergo potentiation than depression. Conversely, a synaptic connection with a high weight will be more easily depressed than potentiated. In this thesis, we will consistently utilize this soft-bound method.

This reset phenomenon is robust to the variability of neuronal circuit properties. In fact, it is consistently observed when variability is introduced in the conductance of neuronal channels or in the size of the network. It has a good side and a bad side. On the one hand, this regularization of synaptic weights makes it possible to learn new things. However, on the other hand, all the information learned during the tonic activity is forgotten [Jacquerie et al., 2022a]. This is the problematic of this thesis. We will try to take advantage of this homeostatic reset to provide a model that is consistent with memory consolidation and therefore for which the information learned during tonic is not completely forgotten at the transition to burst activity. To this end, we're going to try to use structural plasticity to transfer learning and thus avoid losing all the information. Structural plasticity is therefore discussed at length in the following chapters. From a biological point of view, in Chapter 3 and from a computational point of view in Chapter 5.

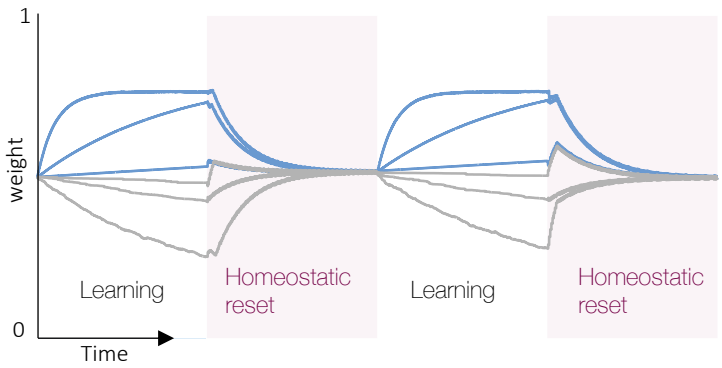

Figure 2.10 – **Homeostatic reset.** Evolution of synaptic weight during 2 tonic/burst cycles for 3 correlated connections (blue) and 3 uncorrelated connections (gray). The tonic phases correspond to learning. Regardless of learning, all synaptic weights converge to the same point when the activity switches to burst activity. *Adapted from* [Jacquerie et al., 2022a]

.

Chap 2 : synaptic plasticity

Definition

Ability of neurons to modify their neuronal connections

E-LTP

Modification of receptor efficiency and rapid insertion of new receptors.

L-LTP

Structural changes in dendritic spines. Involves protein synthesis.

E-LTP computational models

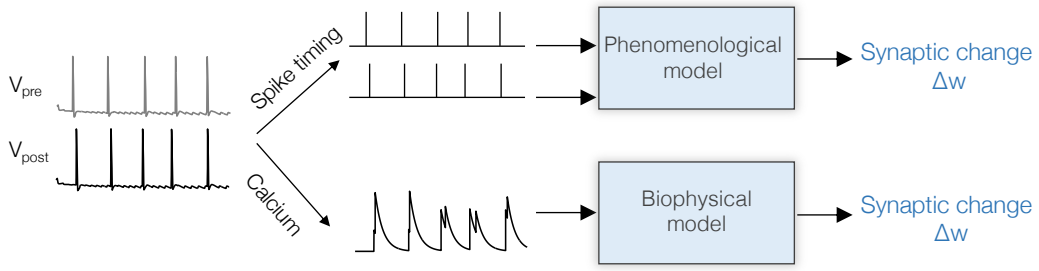

Limitations

The use of these traditional rules of synaptic plasticity leads to homeostatic reset when they are used in changes in firing pattern.

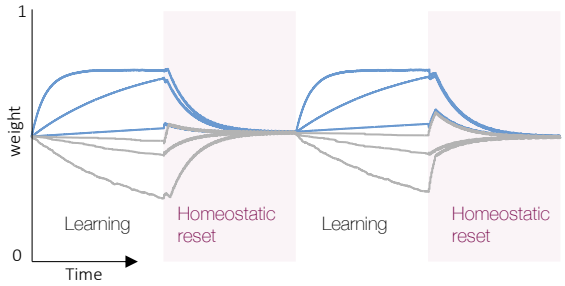

Good feature

Reset of synaptic weights makes it possible to learn new things

Bad feature

Information is forgotten

Research question

Is it possible to take advantage of this homeostatic reset and transfer learning through structural plasticity?

Part II

Structural plasticity

Chapter 3

Structural plasticity from a biological point of view

First of all, before getting to the heart of the matter, it is important to clearly define what is considered structural plasticity in this thesis. Indeed, in the literature, it is presented under a good number of terms, which sometimes makes its definition complicated. Here, we consider everything defined in the literature as *L-LTP*, *LTP maintenance* to be part of structural plasticity. On the contrary, everything defined as *E-LTP*, *LTP induction* is considered as simple synaptic plasticity in this thesis and not as structural plasticity. As a reminder, this type of plasticity induces changes in receptor efficiency as well as the rapid insertion of new receptors directly from the recycling endosome of dendritic spines. We define structural plasticity as follows:

Structural plasticity: A process that occurs in the hour following the LTP induction, usually based on protein synthesis, and causes structural changes in spines.

Structural plasticity occurs in different ways, as illustrated in Figure 3.1:

- Firstly, it can manifest through changes in the morphology of the pre-existing spines. Indeed, an increase in spine head volume with their PSDs and a widening and shortening of the spine neck have been observed upon induction of LTP. These changes are accompanied by changes in the number and distribution of receptors, resulting in higher neurotransmitter sensitivity in spines with larger heads. The influx of calcium into the dendrite will therefore also be affected [Lamprecht and LeDoux, 2004]. (Figure 3.1 **i.**)

- Next, LTP induced the formation of *multiple synapse boutons* (MSBs), i.e. several dendritic spines are in contact with the same presynaptic terminal [Muller et al., 2002, Lamprecht and LeDoux, 2004]. It is interesting to note that in basal activity (i.e. without LTP induction), most of the MSBs found are formed by spines from different dendrites. Whereas after LTP induction, MSBs are observed formed by spines belonging to the same dendrite. This shows that LTP leads to synapse duplication and thus probably to the creation of new spines [Muller et al., 2002]. (Figure 3.1 **ii.**)

- Moreover, *synaptic rearrangement* is one of the most important forms of structural plasticity. It involves the elimination of synapses in certain locations to allow for the formation of new synapses in other locations. In other words, there is a constant elimination of some dendritic spines and the formation of others [Butz et al., 2009]. (Figure 3.1 **iii.**)

Structural plasticity is crucial for the retention of learning in long-term memory. It enables the stabilization or consolidation of changes induced in the short term by synaptic plasticity. Indeed, changes in spine morphology and number could be responsible for converting these short-term changes into lasting changes in synapse structure,

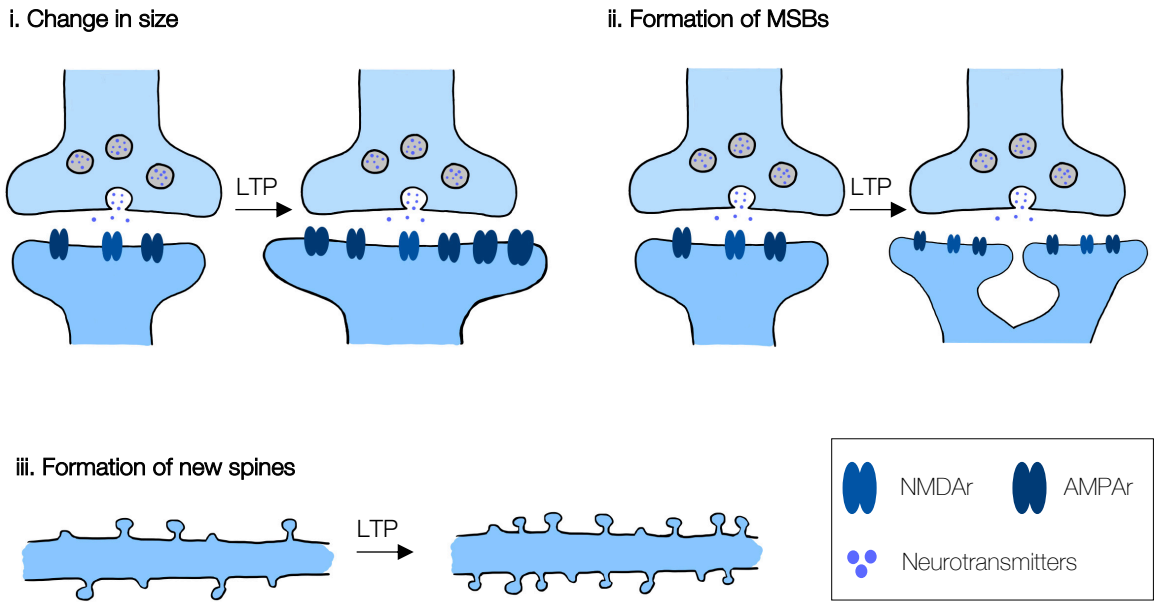

Figure 3.1 – **Morphological changes in dendritic spines induced by LTP.** LTP induces an increase in spine head volume and a widening and shortening of the spine neck (**i.**), in the number of MSBs (**ii.**) and induces the formation of new dendritic spines (**iii.**). *Inspired from* [Lamprecht and LeDoux, 2004, Muller et al., 2002].

connectivity, and function [Lamprecht and LeDoux, 2004, Hering and Sheng, 2001].

3.1 Molecular mechanisms involved in the morphological changes of dendritic spines

We have seen in Chapter 2 that the structure of dendritic spines is maintained by the actin cytoskeleton. It has been shown that after LTP induction, the cytoskeleton undergoes a rearrangement that is responsible for morphological changes in dendritic spines during strucutrelle plasticity [Lamprecht and LeDoux, 2004].

Changes in the actin cytoskeleton are regulated by numerous *actin-binding proteins* (ABPs). These proteins play different roles in actin dynamics such as depolymerization and polymerization.

Depolymerisation: process of breaking down the actin cytoskeleton into its individual subunits, called *actin monomers*.

Polymerisation: process by which actin monomers assemble to form the actin cytoskeleton.

The main ABPs involved in actin cystoskeleton rearrangement during structural plasticity and their role are illustrated in Figure 3.2:

- *Cofilin* will promote actin depolymerization and thus dismantle actin cystoskeleton [Lamprecht and LeDoux, 2004].
- *Actin-Related Protein 2/3* (Arp2/3) complex plays an important role in actin rearrangement during structural plasticity. Indeed, this complex will promote the formation of new actin cystoskeleton [Nakahata and Yasuda, 2018].

- *Epidermal growth factor receptor Pathway Substrate 8* (Eps8) binds to actin cystoskeleton and stabilizes them [Nakahata and Yasuda, 2018].

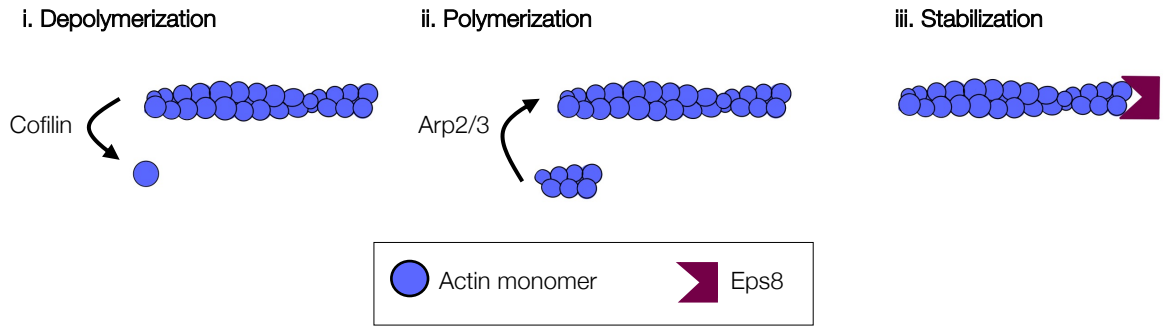

Figure 3.2 – **Actin cystoskeleton dynamics are regulated by ABPs. i.** Actin depolymerization is promoted by cofilin. **ii.** Actin polymerization is promoted by Arp2/3. **iii.** Actin filaments are stabilized by Eps8. *Inspired from* [Nakahata and Yasuda, 2018, Lamprecht and LeDoux, 2004].

How will these ABPs be activated?
Similar to LTP induction, CaMKII plays an important role in the activation of these proteins and thus in structural plasticity [Patterson and Yasuda, 2011]. Indeed, once activated, CaMKII undergoes autophosphorylation which will activate a whole series of downstream signaling molecules and eventually activate Arp2/3, cofilin and Eps8. First, CaMKII will activate a series of *small Guanosine Triphosphatase* (small GTPases) including Rac1, Cdc42, RhoA and Ras. In turn, these GTPases will activate a series of downstream molecules that will eventually lead to the rearrangement of the cytoskeleton [Runge et al., 2020, Nakahata and Yasuda, 2018, Costa et al., 2020, Nishiyama and Yasuda, 2015]. The activation process of these GTPases as well as the activation of their downstream molecules is described below.

Small GTPases: family of proteins that act as molecular switches to regulate various essential cellular processes [Pereira-Leal and Seabra, 2000].

3.1.1 Small GTPases

The activation process of small GTPases is illustrated in Figure 3.3.

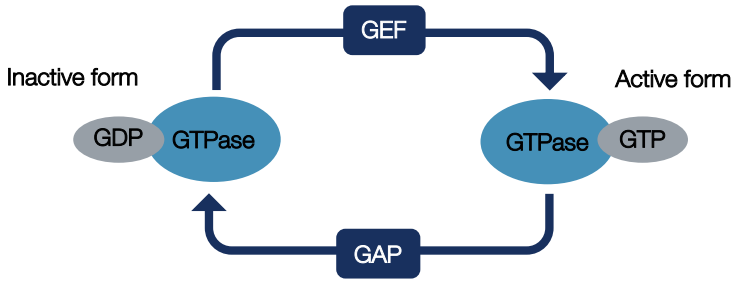

Figure 3.3 – **Regulation of small GTPase activity.** GTPases switch from an inactive form bound to GDP to an active form bound to GTP thanks to GEF. The reverse proccesus is realized thanks to GAP. *Inspired from* [Song et al., 2019, Lamprecht and LeDoux, 2004]

When small GTPases are inactive, they are bound to *Guanosine diphosphate* (GDP), whereas when they are active, they are bound to *Guanosine triphosphate* (GTP) [Song et al., 2019, Lamprecht and LeDoux, 2004]. *Guanine Nucleotide Exchange Factor* (GEF) promote the exchange of GDP for GTP, activating small GTPases, while *GTPase*

Activating Protein (GAP) promote the hydrolysis of GTP to GDP, inactivating small GTPases [Song et al., 2019]. GEF and GAP activity is regulated by CaMKII [Shibata et al., 2021, Hering and Sheng, 2001].

The signaling cascade that follows activation of these small GTPases to modify the actin cytoskeleton is described below and illustrated in Figure 3.4.

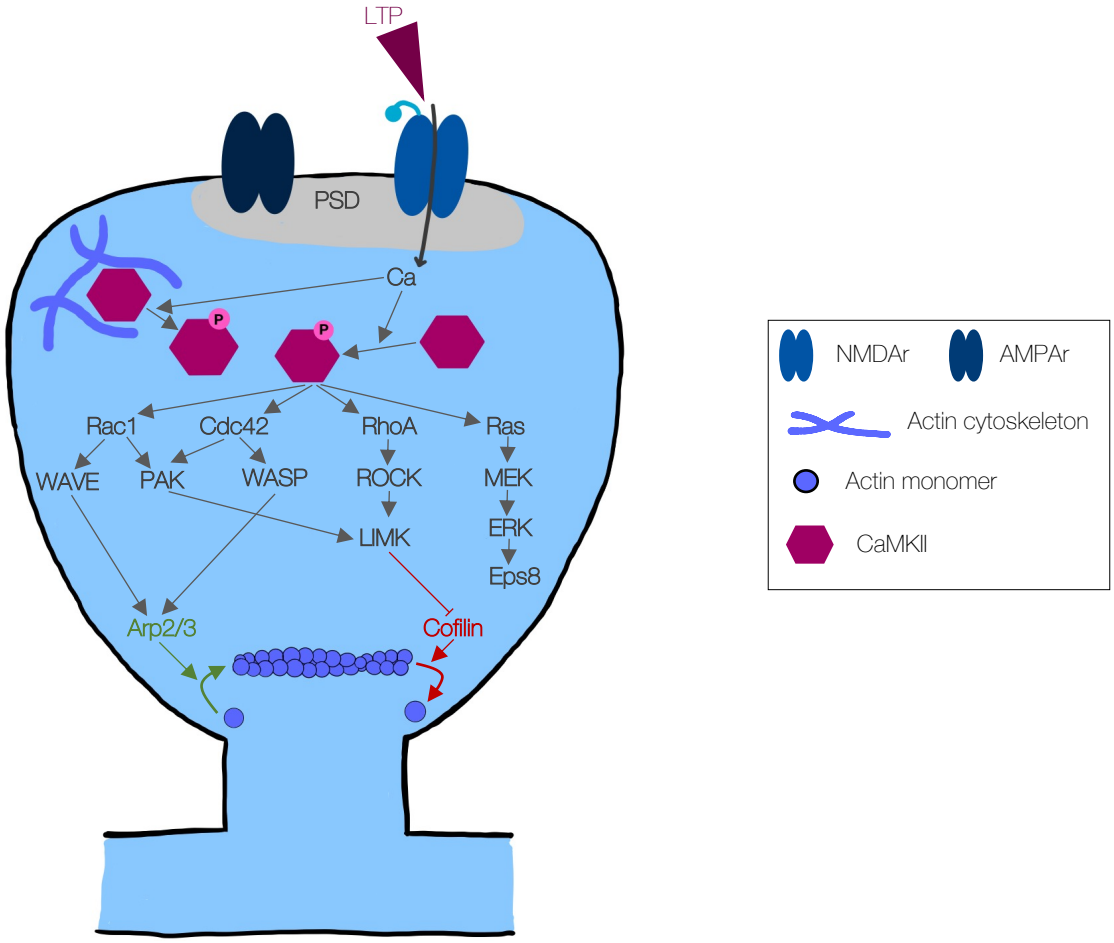

Figure 3.4 – **Molecular mechanisms involved in the cytoskeletal rearrangments.** Increased calcium in the spine following LTP induction activates CaMKII. Once activated, CaMKIIs play two major roles in cytoskeletal rearrangement. First, they detach from actin filaments, which allows them to undergo modifications. Second, CaMKIIs activate small GTPases (Rac1, Cdc42, RhoA and Ras) and their downstream molecules that activate modifications in actin filaments. *Inspired from* [Runge et al., 2020, Nishiyama and Yasuda, 2015, Costa et al., 2020].

Rac1 On the one hand, this protein will activate WAVE which will, in turn, bind to Arp2/3 and regulate it. This will promote the formation of new actin filaments. On the other hand, Rac1 will also activate PAK which, in turn, will activate and regulate the activity of LIMK [Runge et al., 2020, Nakahata and Yasuda, 2018]. In this way, LIMK can inhibit cofilin and thus block its actin depolymerization effect [Lamprecht and LeDoux, 2004].

Cdc42 Like Rac1, this protein has a double effect on actin dynamics. Indeed, through WASP, Cdc42 regulates Arp2/3 and thus promotes actin polymerization. Moreover, it also activates PAK and then LIMK which inhibits cofilin [Runge et al., 2020, Nakahata and Yasuda, 2018].

RhoA Like Rac1, RhoA will have an impact on LIMK and thus on cofilin activity. Indeed, RhoA will activate downstream effectors such as Rho-associated protein kinase (ROCK). And once activated, the latter will phosphorylate LIMK [Nakahata and Yasuda, 2018].

Ras This protein will activate the MEK/ERK pathway which will then regulate the activity of Eps8. Indeed, MEK and ERK will be able to phosphorylate Eps8 and thus modify its activity [Nakahata and Yasuda, 2018].

Furthermore, it is important to note that in addition to activating these GTPases, CaMKII plays a second important role in actin dynamics. Indeed, as also shown in Figure 3.4, CaMKII is initially attached to actin. And once it has autophosphorylated, CaMKII can detach from actin and the actin filaments can then undergo changes [Runge et al., 2020].

In summary, CaMKII plays two important roles in the rearrangement of actin filaments that underlies structural plasticity: it allows actin filaments to undergo modifications by detaching from them and it activates small GTPases that will modify these filaments.

3.1.2 Remodeling of dendritic spines by extracellular factors

In addition to intracellular regulation of spine structure directed by CaMKII activity, there are also external factors that control spine remodeling. Among these factors is autocrine *Brain-Derived Neurotrophic Factor* (BDNF) signaling [Nakahata and Yasuda, 2018], the effect of which is illustrated in Figure 3.5:

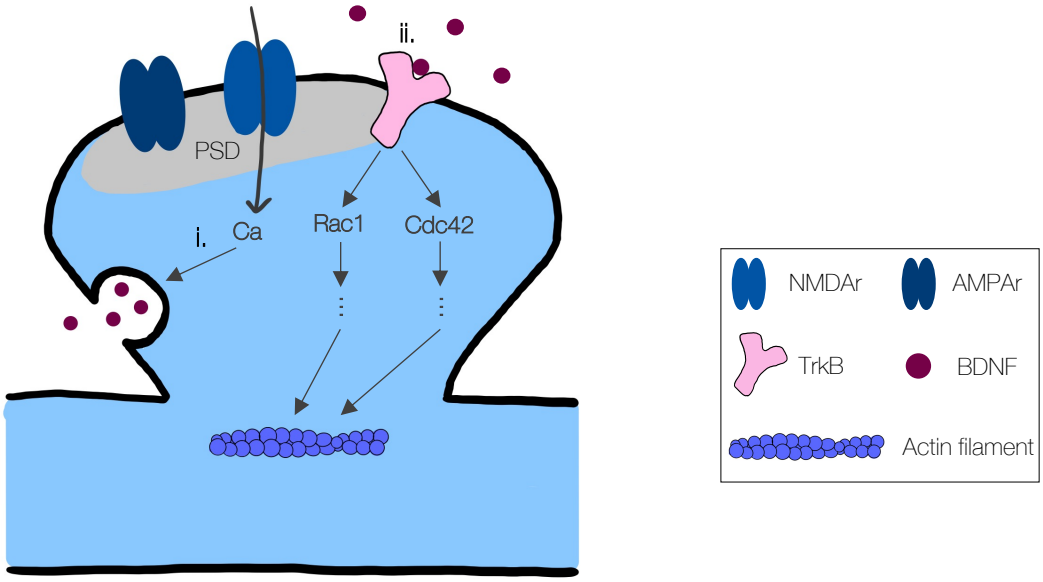

Figure 3.5 – **Role of BDNF in cytoskeletal rearrangement. i.** BDNF can be released into the extracellular environment by the activity of the synapse itself (due to calcium influx). **ii.** BDNF bind to and activate TrkB receptors. This leads to activation of GTPases Rac1 and Cdc42, resulting in rearrangement of the cytoskeleton. *Inspired from* [Fu and Ip, 2017, Hedrick and Yasuda, 2017].

- In addition to being present in the extracellular environment of the synapse, according to [Fu and Ip, 2017], BDNF may originate directly from the dendritic spines. Indeed, its synthesis and secretion are thought to be regulated by the activity of the synapse itself, and can therefore be released from dendritic spines during LTP (following calcium influx). (Figure 3.5 **i.**)

- BDNF will then bind to and activate *Tyrosine kinase B* (TrkB) receptors. These receptors will, in turn, regulate the activity of the small GTPases Rac1 and Cdc42 and thus regulate the structural reorganization of spines [Lai and Ip, 2013, Nakahata and Yasuda, 2018]. However, RhoA does not appear to be dependent on BDNF secretion, so not all GTPases are activated by this signal [Hedrick and Yasuda, 2017]. (Figure 3.5 **ii.**)

To summarize, the activation of small GTPases that leads to actin filament rearrangement is mediated both intracellularly through CaMKII activity and also extracellularly through BDNF.

3.2 Protein synthesis and Synaptic-tagging and capture hypothesis

We have seen in Chapter 2 that E-LTP induces the rapid insertion of new receptors, directly from recycling endosomes. In structural plasticity, new receptors are also introduced but these come from protein synthesis and their insertion is slower. This process of synthesis and insertion of new receptors is illustrated in Figure 3.6.

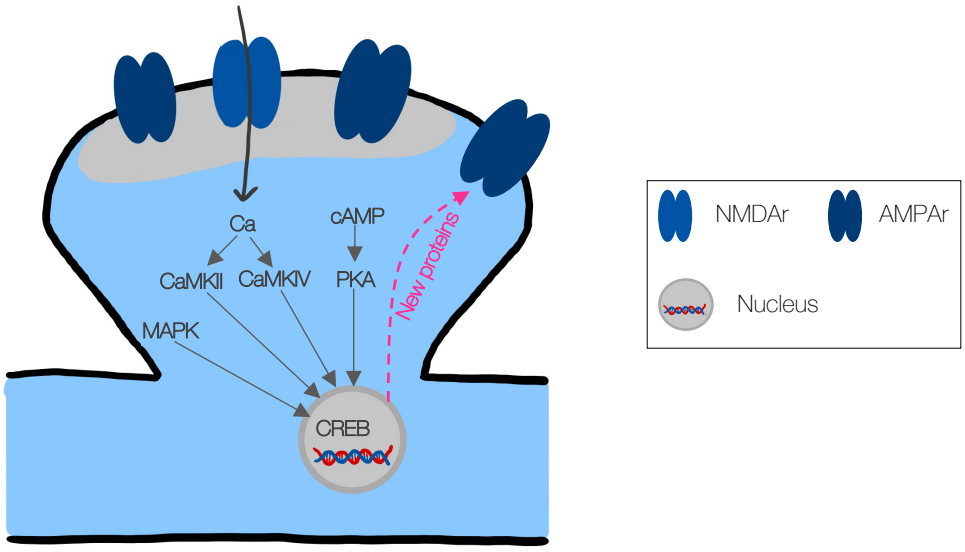

Figure 3.6 – **Synthesis and insertion of new receptors.** The synthesis of new receptors is triggered by the activation of the transcription factor cAMP-response binding protein (CREB). This is activated by the CaMKII and CaMKIV signaling pathways activated by calcium influx. In addition, the cAMP/PKA and MAPK signaling pathways also regulate CREB activity. *Inspired from* [Carlezonjr et al., 2005, Saura and Valero, 2011].

Gene transcription in the nucleus is required to induce protein synthesis. The transcription factor *cAMP-response binding protein* (CREB) has been shown to be essential for sustained changes in synaptic plasticity [Saura and Valero, 2011]. It can induce the expression of genes that code for AMPr in particular. Once synthesized, these receptors will be introduced into the synapse [Jacquerie, 2023]. CREB will be activated by a cascade of signaling pathways from the dendritic spine to the nucleus induced by calcium influx [Runge et al., 2020]. Indeed, the increase in calcium will activate CaMKII or CaMKIV which, in turn, will activate CREB. Moreover, CREB will also be activated by the *Protein Kinase A* (PKA), which is itself activated by cAMP. In addition, the *Mitogen-Activated Protein Kinase* (MAPK) signaling pathway also plays a role in the activation of CREB [Carlezonjr et al., 2005, Saura and Valero, 2011].

Synaptic-tagging and capture hypothesis (STC)

In the previous sections, we defined E-LTP and L-LTP and their underlying mechanisms. The next question then arises: *what is the process for switching from one to the other?*

One hypothesis recognized in the literature is the *Synaptic Tagging and Capture hypothesis* (STC). Several models of structural plasticity rely on STC, as we will see in part II of this thesis. The principles of this hypothesis are described in Figure 3.7.

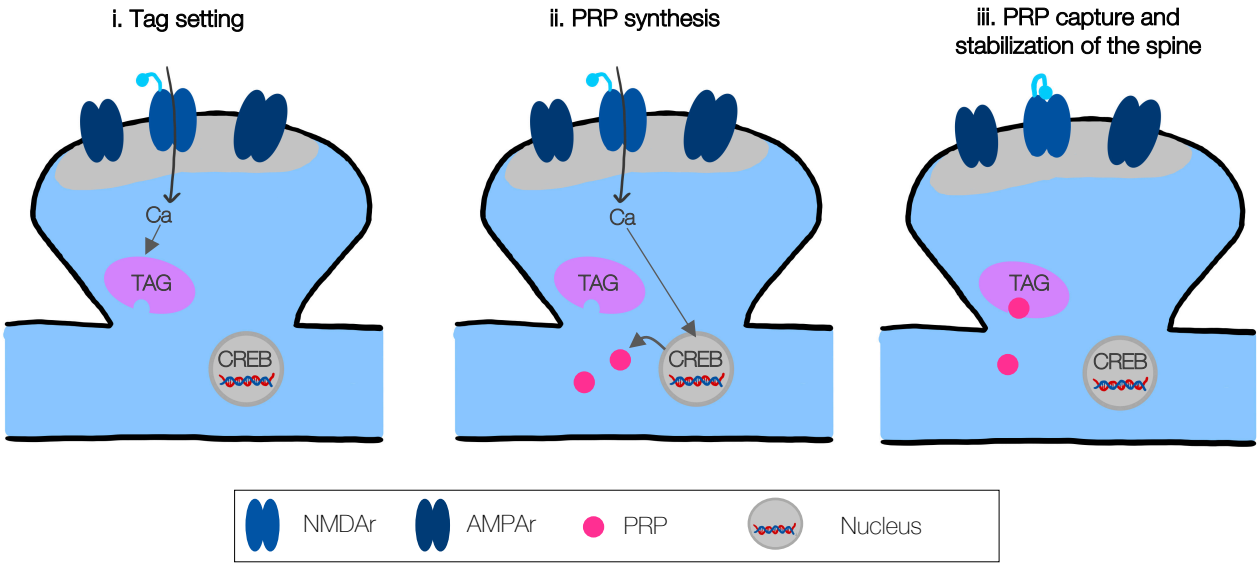

Figure 3.7 – **Synaptic and capture (STC) hypothesis. 1.** LTP induction leads to a tag setting. **2.** Calcium influx induces CREB activation and thus the synthesis of plasticity related products (PRP). **3.** PRP captured by synaptic tags. *Adapted from* [Jacquerie, 2023].

Briefly, the hypothesis assumes that LTP induction results in instantaneous local *tagging* of the dendrite (Figure 3.7 **i.**). Then, the synthesis of *Plasticity-Related Products* (PRP) is triggered by the activation of transcription factors such as CREB (Figure 3.7 **ii.**). They are finally "captured" by synaptic tags, which leads to the long-term stabilization of dendritic spines (Figure 3.7 **iii.**) [Shivarama Shetty and Sajikumar, 2017, Jacquerie, 2023]

Chap 3 : structural plasticity

Definition

Process that occurs in the hour following the LTP induction, usually based on protein synthesis, and causes structural changes in spines.

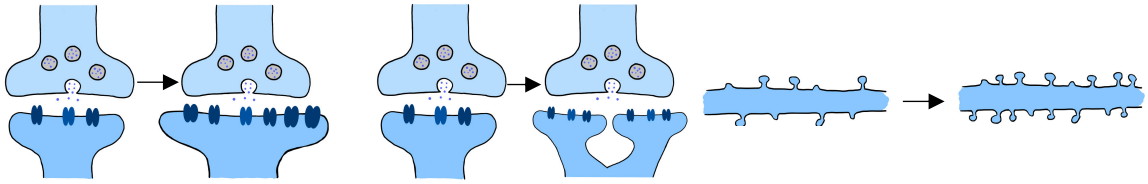

Molecular mechanisms involved in the morphological changes

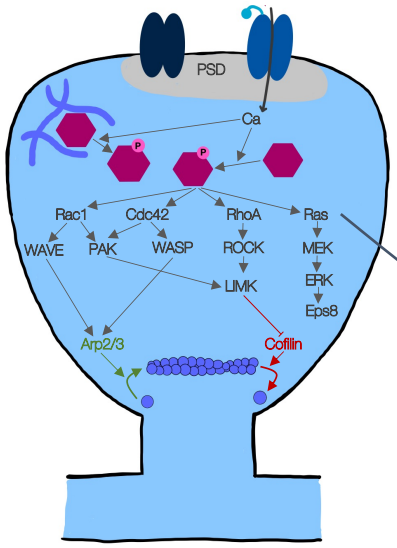

LTP triggers a whole cascade of biochemical reactions leading to the rearrangement of the actin cytoskeleton

Small GTPases play a key role

Synthesis of new receptors

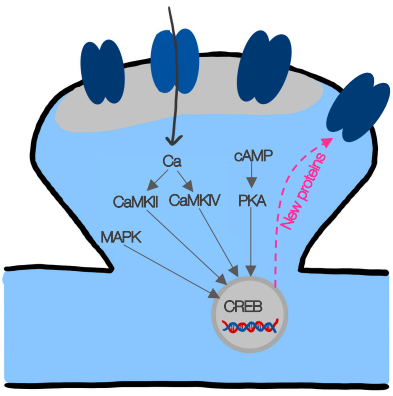

Activation of CREB induces expression of genes encoding AMPr.

Chapter 4

Structural plasticity from a modeling point of view

4.1 Introduction

Modeling structural plasticity is important to help understand the complex mechanisms underlying L-LTP and the resulting structural changes [Smolen et al., 2006]. Furthermore, it has been shown that the traditional rules of synaptic plasticity used to model E-LTP are not sufficient to explain long-term memory and information storage [Poirazi and Mel, 2001]. This is not surprising, since L-LTP has been shown to be essential for learning and memory [Smolen et al., 2006]. To obtain a synaptic plasticity model consistent with memory consolidation, it appears necessary to incorporate a model of structural plasticity.

There are many different strategies for modeling structural plasticity. [Jacquerie, 2023] proposed a classification of these into three categories: *mathematical models*, *biophysical models* and *phenomenological models*.

Below, I review these three categories identified by [Jacquerie, 2023], giving examples for each. For each category, I decided to describe in detail one or two models that I considered to be the most representative of their category. This will give a concrete idea of how the different models are implemented. Of course, the examples given here are not exhaustive, and many more can be found in the literature.

4.2 Mathematical models

These models use mathematical and statistical variables to model structural plasticity and are often based on the activities of pre- and postsynaptic neurons. Their goal is to minimize the involvement of biophysical processes. The model proposed by [Deger et al., 2012] falls into this category [Jacquerie, 2023]. It is described in more detail below.

4.2.1 Model proposed by [Deger et al., 2012]

[Deger et al., 2012] describes structural plasticity using purely mathematical equations. Moreover, they have explicitly given their intention to make minimal assumptions about biophysical processes. If we take a look at their paper, we can see that it is composed of a multitude of equations with a lot of statistics and stochastic. All these equations will not be described in details but only the foundamental ones in order to understand in a global way the model they implement.

Model basics

First, as illustrated in Figure 4.1, the model proposed by [Deger et al., 2012] considers pairs of neurons (a presynaptic neuron and a postsynaptic neuron) that are each composed of multiple synapses.

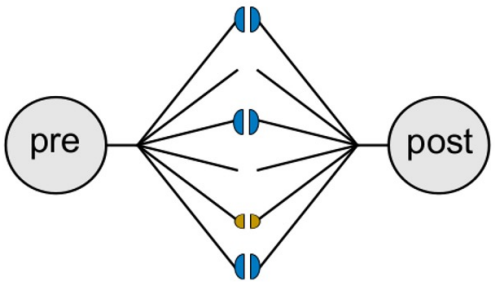

Figure 4.1 – **Schematic of the synaptic connections between a pair of neurons (pre- and postsynaptic) in the model proposed by [Deger et al., 2012].** The connection between a pre- and postsynaptic neuron is made through several synapses. Synapses can be active (in blue, larger), inactive (in orange, smaller), or unrealized. *From* [Deger et al., 2012].

Synapses can be in one of three states: *active*, *inactive*, or *not realized*. Active synapses, shown in blue in Figure 4.1, are considered as large dendritic spines. [Deger et al., 2012] considers these to be dendritic spines that contain AMPA receptors and NMDA receptors. Inactive synapses, on the other hand, are shown in orange and correspond to small newly formed or recently shrunken synapses. These synapses contain far fewer AMPA receptors. Finally, unrealized synapses can be considered as *non-functional* synapses. Here, a non-functional synapse is considered to be a location where the pre- and postsynaptic neurons are in close proximity but no synaptic contact is formed. At this location, there is therefore no connection and so no communication between the two neurons. However, in the future a synaptic contact may form at this location and the non-functional synapse may turn into a *functional* synapse. In a way, they are potential locations for functional synapses. A synapse is then considered functional when it forms a connection between the two neurons, which allows for communization between the neurons.

Basics of structural plasticity

The structural plasticity model proposed by the authors is illustrated in Figure 4.2.

[Deger et al., 2012] considers that a synapse can undergo three forms of structural plasticity: *maturation*, *shrinkage* and *pruning*. Maturation corresponds to the transition of the synapse from an inactive to an active state and thus to an enlargement of the dendritic spine. Shrinkage, on the other hand, corresponds to the opposite process and thus to the transition from an active to an inactive state. The pruning corresponds to the passage from the inactive state to the unrealized state and thus in a way to the elimination of a synapse. Each of these structural changes occurs at its own rate: λ_m is the rate of maturation, λ_s is the rate of shrinkage and λ_p is the rate of pruning. It is important to note that these structural changes depend on the activity of the neurons. Indeed, the dynamics of these changes rely on the spike times of pre- and postsynaptic neurons.

In addition to this structural plasticity, [Deger et al., 2012] includes in their model intrinsic fluctuations in synapse configuration that also each occur with their own rate. Indeed, they consider that new synapses can be created with a rate λ_c or eliminated with a rate λ_i. Synapses can grow or shrink with a rate λ_i.

Moreover, [Deger et al., 2012] consider that there is number N of synapses between a presynaptic neuron and a postsynaptic neuron (whether inactive, active or not realized). The variables x, y, and z represent the number of synapses in the active, inactive, and unrealized states, respectively.

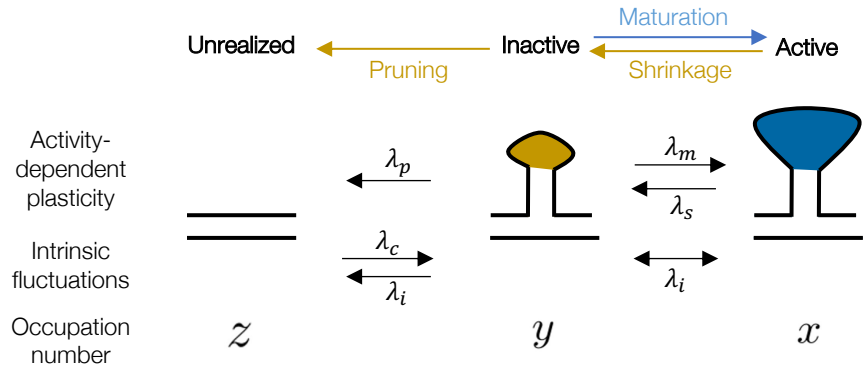

Figure 4.2 – **State diagram of the structural plasticity model prosposed by [Deger et al., 2012].** A synapse can undergo 3 forms of structural plasticity: maturation, which takes it from an inactive to an active state with a rate λ_m; shrinkage, which takes it from an active to an inactive state with a rate λ_s; and pruning, which takes it from an inactive to an unrealized state with a rate λ_p. These structural changes are dependent on the activity of pre- and postsynaptic neurons. The transition from one state to the other is also done by intrinsic fluctuations: from inactive to non-realized state with a rate λ_i and from inactive to active state and vice versa with the same rate λ_i. In addition, synapse creation (transition from non-realized to inactive state) with a rate λ_c. The number of occupancy of the three states, active, inactive, unrealized, is represented by x, y and z, respectively. *Adapted from* [Deger et al., 2012].

How are these processes transformed into mathematics?

Model equations

[Deger et al., 2012] decides to base structural plasticity on the *synaptic correlation trace* formed at each synapse. As the name suggests, the correlation trace represents the correlation between pre- and postsynaptic spike times and is based on a phenomenological model. In other words, if the presynaptic neuron spikes a little bit before the postsynaptic neuron, the correlation trace is increased. In this case, the event is called *causal*. In the opposite case, if the presynaptic neuron spikes a little after the postsynaptic neuron, the trace is decreased. This event is called *anti-causal*. In their model, [Deger et al., 2012] assumes that the values of the correlation trace of each synapse follow a normal distribution. Moreover, this distribution depends on the number of active synapses (x). Indeed, these active synapses contribute to the activity of the postsynaptic neuron, so the authors added this dependence.

Assuming that structural plasticity is a slow phenomenon relative to neuronal activity and is triggered when the correlation trace reaches a θ threshold, [Deger et al., 2012] proposes that rates of structural change follow the following law:

$$\lambda_k(x) = \begin{cases} |\alpha| e^{-(\theta-\mu(x))^2/\sigma^2} & if \quad \alpha(\theta-\mu(x)) > 0 \\ |\alpha| & else \end{cases} \tag{4.1}$$

where $k = \{m, s, p\}$ depending on the type of structural change considered (maturation, shrinkage or pruning). Parameters θ, α and σ are also specific to the type of structural change and thus differ in value from one type to another. $\mu(x)$ and σ are parameters of the synaptic correlation trace: the mean and the variance respectively. Here we see that the mean of the correlation trace depends on x since, as said before, it depends on the number of active synapses. α scales the rates of change, that is, it determines the value to which these rates will converge. Indeed, the cellular machinery of biological systems has limits and will not be able to respond to rates that exceed its limits. This is why it is important to introduce a maximum rate of convergence and [Deger et al., 2012] does so by means of the α variable.

The rates of structural change, defined by equation 4.1, evolve as a function of the correlation trace and therefore as a function of the activity of the neurons following the curve illustrated in Figure 4.3.
When the sign of alpha is positive (solid curve on the figure), the rate of structural changes (λ) approaches the saturation plateau (the maximum rate) when $\mu(x)$ increases. On the contrary, when the sign of alpha is negative (dashed curve), λ moves away from the plateau with the increase of $\mu(x)$.

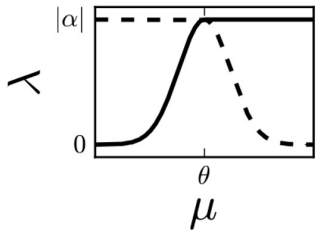

Figure 4.3 – **Shape of the evolution of structural change rates as a function of the synaptic correlation trace.** μ is the average value of the correlation trace. The solid curve represents the case where α is positive while the dashed curve represents the case where α is negative. The absolute value of α defines the λ scale. θ is the threshold of the saturation plateau. Curves drawn from equation 4.1. *From* [Deger et al., 2012].

In the model just described, we see that individual synapses can change continuously. However, the overall state of the connection between the pre- and postsynaptic neuron (i.e. the number of active synapses (x), the number of inactive synapses (y) and the number of unrealized synapses (z) that exist between the two neurons) evolves towards a stable state.

Given that there is a number N of synapses between two neurons of which x are active, y inactive and z not realized, at any time $x + y + z = N$. [Deger et al., 2012] were therefore able to state that the state of a connection between two neurons can be defined by the combination of the number of active and inactive synapses (x, y). They then defined that the probability $p_{x,y}$ of a connection to be in state (x, y) evolves as follows:

$$\begin{aligned}\frac{d}{dt}p_{(x,y)} = &-p_{(x,y)}\left[(x+2y)\lambda_i + (N-x-y)\lambda_c + x\lambda_s(x) + y\lambda_p(x) + y\lambda_m(x)\right] \\ &+ (x+1)p_{(x+1,y-1)}\left[\lambda_s(x+1) + \lambda_i\right] \\ &+ (y+1)p_{(x,y+1)}\left[\lambda_p(x) + \lambda_i\right] \\ &+ (y+1)p_{(x-1,y+1)}\left[\lambda_m(x-1) + \lambda_i\right] \\ &+ (N-x-y+1)p_{(x,y-1)}\lambda_c\end{aligned} \tag{4.2}$$

The first term of the equation represents the rate at which the (x, y) state evolves to other states through different transitions. In other words it describes the rate at which the system leaves this state to reach a new one. The second, third, and fourth terms of the equation, meanwhile, represent all possible ways to reach the (x, y) state from other states by shrinking, pruning, or maturation, respectively. Finally, the last term takes into account transitions resulting from the creation of inactive synapses and thus due to intrinsic fluctuations.

The model proposed by [Deger et al., 2012] is therefore based on equation 4.2. From this equation, they will derive a whole series of equations that give for example the configuration of the stable state of the connection or the lifetime of a connection. However, we are not going to go into details in these equations because the goal here was to understand the foundations of the model.

Model summary

The model introduced by [Deger et al., 2012] is based on the fact that at each synapse a correlation trace is formed based on the spikes of pre- and postsynaptic neurons. The structural plasticity model is then defined based on this correlation trace. Indeed, the rates of structural change are based on the average value of this correlation trace. Moreover, each synapse can be in one of three states: active, inactive, and unrealized. Finally, the model also includes the intrinsic fluctuations of the synapse configuration. This model is illustrated in Figure 4.4.

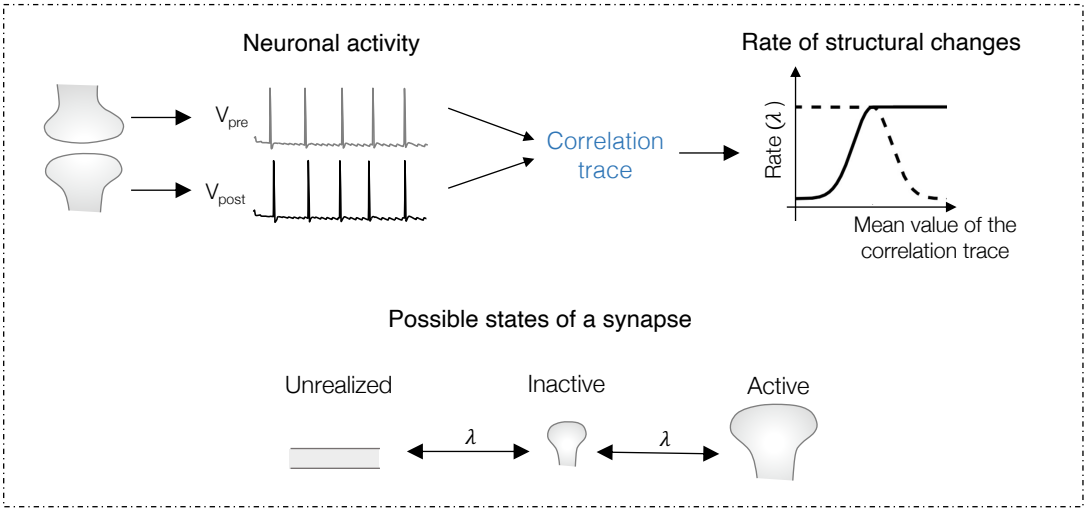

Figure 4.4 – **Diagram of the model proposed by [Deger et al., 2012].** From the pre- and postsynaptic neuronal activity, a correlation trace is formed. The rates of structural change and thus the structural plasticity is then directed by this correlation trace. *Inspired from* [Deger et al., 2012].

The model proposed by [Deger et al., 2012] has been verified with experimental data and is capable of representing the state of the synapses in a correct way. However, the model has several limitations. In particular, it assumes that synapses between different pairs of neurons are independent of each other, which is not quite the case in reality. A major advantage of this model is that it does not require detailed knowledge of the bio-molecular mechanisms underlying structural plasticity. However, it does require a lot of mathematical equations, which can make it difficult to understand.

4.2.2 Others mathematical models

Among the mathematical models, we can also find those of [Helias, 2008] and [Zheng et al., 2013] [Jacquerie, 2023].

The model proposed by [Helias, 2008] is based on many probabilities and like the model proposed by [Deger et al., 2012], relies on detecting the correlation between pre- and postsynaptic activity. For the detection of the correlation, it is based on the calcium influx mediated by NMDA receptors and resulting from the activation of neurons. The model describes the mechanisms by which synapses are formed and eliminated. To do so, it is based on the dynamics of each individual synapse.

As for the model proposed by [Zheng et al., 2013], it combines several different forms of plasticity including structural plasticity. In their paper, this plasticity models the creation of new synapses that occurs continuously. This creation is done with a probability p=0.1 and the new synapse is created randomly between two neurons not yet connected to each other.

4.3 Biophysical models

Unlike the first approach, this approach focuses on the biochemical processes that lead to structural plasticity. Indeed, the modeling, in this case, is based on the signaling cascade between the calcium influx and the morphological changes of the synapses. A typical article that utilizes this approach is the one by [Smolen et al., 2006], which is described in more details below [Jacquerie, 2023].

4.3.1 Model proposed by [Smolen et al., 2006]

The model proposed by [Smolen et al., 2006] is based on the molecular processes involved in structural plasticity, which the authors consider as the key processes of structural plasticity. Specifically, the model consists of several differential equations representing the dynamics of various protein kinases. It incorporates the PKA, MAPK and CaMII and CaMKIV.

It is important to note that the model here does not take into account all the signaling pathways involved in structural plasticity and only focuses on a portion. They explicitly state in their article that they do not consider, for example, the pathways involved in E-LTP.

Biophysical model

The cascade of biochemical reactions that [Smolen et al., 2006] propose in their model are those shown in Figure 4.5 and are described in detail in their paper.

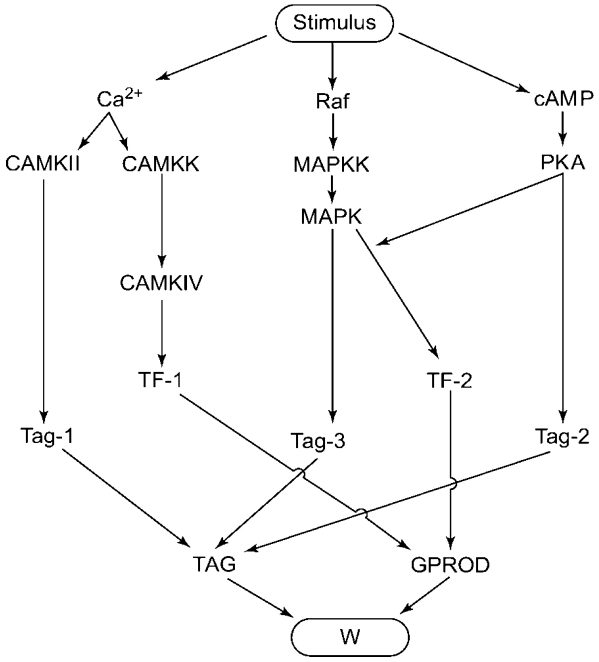

Figure 4.5 – **Scheme of the model proposed by [Smolen et al., 2006].** The model is based on cascades of biochemical processes essential in L-LTP. It translates an electrical stimulus into a change in synaptic weight (w) through the activation of a series of kinases. *From* [Smolen et al., 2006].

In all, they use 23 ordinary differential equations to implement this model. The goal of the model is to transform electrical stimuli into changes in synaptic weight w. In summary, the biochemical cascades occurring between stimulus induction and change of w can be described as follows:

- First, induction of the electrical stimulus results in an increase in Ca and cAMP and activation of Raf.

- A series of protein kinases are then activated: CaMKII and CaMKK (which activates CaMKIV) are activated by Ca; the MAPK cascade is activated by Raf; PKA is activated by cAMP.

- Tag-1, Tag-2, Tag-3 as well as TF-1 and TF-2 are then phosphorylated by protein kinases.

- A synaptic TAG is formed by Tag-1, Tag-2 and Tag-3. Furthermore, the induction of a gene product (GPROD), i.e. resulting from the expression of a gene [Mark Lefers, 2004], is induced by the phosphorylation of TF-1 and TF-2.

- Finally, the combination of the synaptic tag (TAG) with the gene product (GPROD) results in a change in synaptic weight (w).

Model equations

The equations governing the activation of the different protein kinases are of the following form:

$$\frac{d[x]}{dt} = k_1 f([y]) - k_2 g([x]) \tag{4.3}$$

where x is the protein under consideration, y encompasses the molecules that influence the activation of the protein under consideration and k_1 and k_2 are kinetic constants.
As an example, the equation describing the dynamics of CaMKII is the following:

$$\frac{d[CaMKII]}{dt} = k_{act1}\frac{[Ca]^4}{[Ca]^4 + K^4} - k_{deact1}[CaMKII]$$

in which, k_{act1}, k_{deact1} and K are rate constants. In this equation, as in the model diagram shown in Figure 4.5, CaMKII is activated by calcium. The principle is therefore the same for the equations governing the dynamics of other proteins.

The dynamics of the three substrates Tag-1, Tag-2 and Tag-3 as well as the transcription factors TF-1 and TF-2 are described by an equation of the type:

$$\frac{d(x)}{dt} = [y]k_1(1 - x) - k_2 x \tag{4.4}$$

where x corresponds to Tag-1, Tag-2, Tag-3, TF-1 or TF-2 and y the kinase that regulates the activity of the substrate or factor considered. k1 and k2 are rate constants.

The amount of synaptic TAG is simply the product of the Tag-1, Tag-2 and Tag-3 kinase substrates. GPROD activity, on the other hand, is a function of TF-1 and TF-2 and GPROD itself.

This brings us to what we are most interested in: the change in synaptic weight w. This is proportional to the product of the synaptic TAG with the gene product level (GPROD). However, a saturation mechanism is added to limit the increase of w. This mechanism is added using a precursor molecume P defined so that P decreases as w increases. The equation governing the change of w is then the following:

$$\frac{dw}{dt} = k_w(TAG)[GPROD]\frac{[P]}{[P] + K_P} - \frac{w}{\tau_w} \tag{4.5}$$

where K_p and τ_w are the rate and time constants for synaptic weight changes, respectively.

Model simulations

Concretely, what does this model proposed by [Smolen et al., 2006] give when it is simulated?

First, to induce an L-LTP, [Smolen et al., 2006] induces 3 tetanic stimuli (continuous high frequency stimulation: 1 second at 100 Hz) spaced 5 minutes apart. Each tetanus causes an increase in Ca for 3 seconds, Raf rate constant for 1 minute, and cAMP for 1 minute. Thanks to these increases, the cascade of molecular processes in Figure 4.5 may have been triggered.

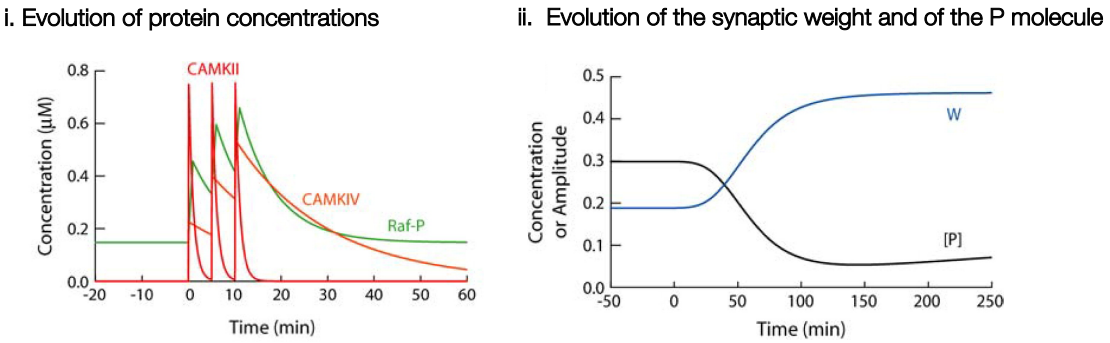

Figure 4.6 – **Results of the model proposed by [Smolen et al., 2006] i.** Changes in levels of active CaMKII, active CaMKIV, and active Raf during and after three simulated tetanic stimuli that allow induction of L-LTP. **ii.** Changes in the synaptic weight (w) and changes in the level of P protein. *Adapted from* [Smolen et al., 2006].

In Figure 4.6 **i.**, we see the evolution of the concentration of CaMKII, CaMKIV and Raf. The three peaks of increase in protein concentration due to the three induced tetanus are clearly visible. Furthermore, after tetany, the times during which the proteins remain active correspond to the data. Indeed, for example, we see in the Figure that CaMKIV remains active for about 45 min, which is similar to the data.

Concerning the evolution of the synaptic weight, it is visible in Figure 4.6 **i.** and we can see that it increases during the induction of L-LTP. Moreover, around 2 hours, w stops increasing and therefore it is the end of the L-LTP induction. This result is consistent with the data since the induction of L-LTP by the BDNF signaling pathway (a signaling pathway external to those of E-LTP induction) also requires 2 hours. Moreover, the amplitude of the increase is also similar to what was observed experimentally. Concerning the evolution of P molecule, as expected, its concentration decreases as w increases. This allows w to be limited when prolonged stimuli are induced. Indeed, according to Smolen, the simulation of 4 tetanics generates an increase of 174% of w while a simulation of 10 tetanics causes an increase of w only slightly higher, of 186%.

Model summary

To summarize, the model proposed by [Smolen et al., 2006] is schematically illustrated in Figure 4.7.

The results of the model proposed by [Smolen et al., 2006] were consistent with the experimental data and observations. This is a good indicator of the accuracy of the model. Although the model represents well the important kinase dynamics essential for L-LTP, not all important biochemical pathways involved are present. Indeed, E-LTP-dependent signaling pathways are for example not taken into account in the model. However, the model remains flexible to the integration of new pathways. The strength of this type of model is that it allows us to clarify the roles of biochemical pathways . Moreover, it allows to understand and interpret some effects of manipulations that affect L-LTP. Indeed, through this model, we can for example understand the effect of inhibiting a certain kinase. On the contrary, a big disadvantage of this type of model is that it consists of a large cascade of events,

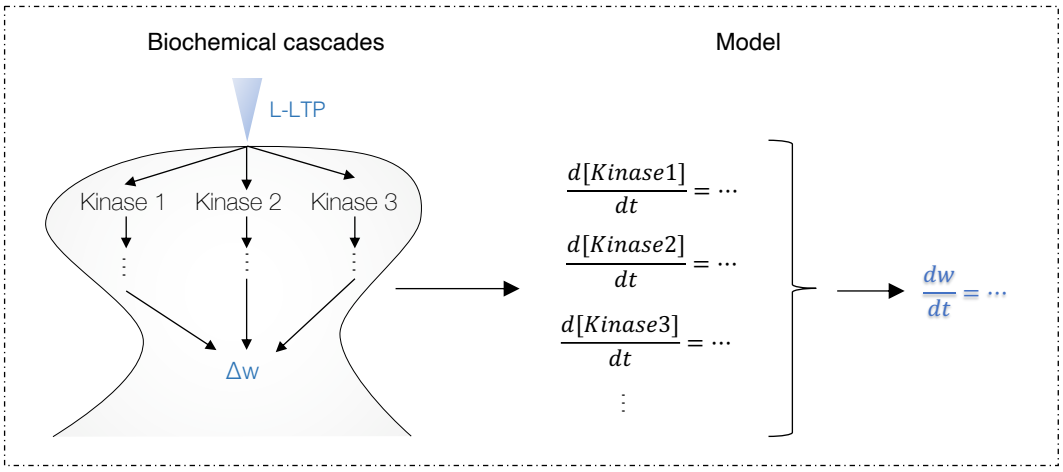

Figure 4.7 – **Diagram of the model proposed by [Smolen et al., 2006]** The model is based on the cascade of reactions that are triggered by an L-LTP. The dynamics of the molecules involved in this cascade is then described by equations. The change of the synaptic weight depends on all the dynamics of the molecules. *Inspired from* [Smolen et al., 2006].

which can make the implementation difficult. Indeed, the evolution of the synaptic weight (defined by equation 4.5) depends on about twenty other equations, which is a lot.

4.3.2 Others biophysical models

[Smolen et al., 2020] and [Amano et al., 2022] have also proposed models that can be categorized as biophysical models [Jacquerie, 2023].

The model proposed by [Smolen et al., 2020] is based on the same principle as the one of [Smolen et al., 2006]. Indeed, the model also describes the dynamics of kinases involved in L-LTP. However, it is simplified compared to the [Smolen et al., 2006] model and the cascade of reactions leading to a change in synaptic weight differs. For example, PKMζ is modeled in this model whereas it was not in the previous one. Here, the model proposed by [Smolen et al., 2020] includes and focuses on positive feedback loops.

The model proposed by [Amano et al., 2022] is slightly different from the previous two. Indeed, it models the structural plasticity by the dynamics of the spine head volume. The volume of the spine head, which depends on the actin remodeling due to the activation of the Ca^{2+} cascade, drives the synaptic force. The model is schematized in Figure 4.8 and is described by 8 differential equations, each of them modeling the dynamics of a model variable.

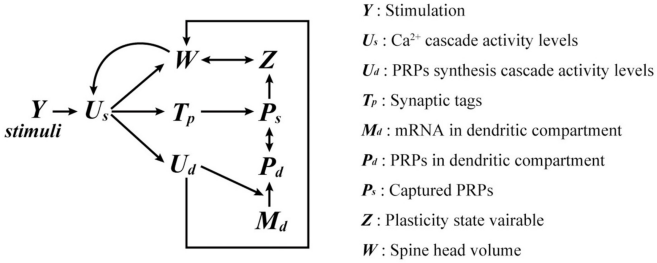

Figure 4.8 – **Diagram of the model proposed by [Amano et al., 2022]** The synaptic force W is directed by the volume of spines and depends in particular on the Ca^{2+} cascade and protein synthesis. The arrows represent the dependencies between the different variables in the model *From* [Amano et al., 2022].

4.4 Phenomenological models

This approach is situated between the two previous approaches, i.e. between the mathematical and biophysical approaches. In other words, structural plasticity is modeled by equations describing biochemical signaling cascades but in a simplified way. The models proposed by [Fauth and van Rossum, 2019] and [Zenke et al., 2015] belong to this category [Jacquerie, 2023].

4.4.1 Model proposed by [Fauth and van Rossum, 2019]

To study information storage in neurons, [Fauth and van Rossum, 2019] uses a neural network model that includes both synaptic and structural plasticity. Synaptic plasticity occurs through changes in synaptic weight between neurons and structural plasticity occurs through the creation and deletion of synapses.

Model basics

The Figure 4.9 **i.** illustrates the considered neuronal model. It assumes an all-to-all potential connectivity, meaning that each neuron can potentially communicate with all other neurons in the network. Moreover, [Fauth and van Rossum, 2019] considers that a presynaptic neuron j connects to a postsynaptic neuron i through multiple synapses. It considers a maximum number S_{max} of synapses for a neuron pair. Notably, some synapses may be non-functional (dashed synapses in the Figure), while others are functional (solid synapses). For instance, in Figure 4.9 **i.**, four synapses are formed, but there could be a maximum of $S_{max} = 7$ synapses if they were all functional. Each synapse formed is characterized by a synaptic weight w_{ij} that evolves according to traditional Hebbian plasticity rules.

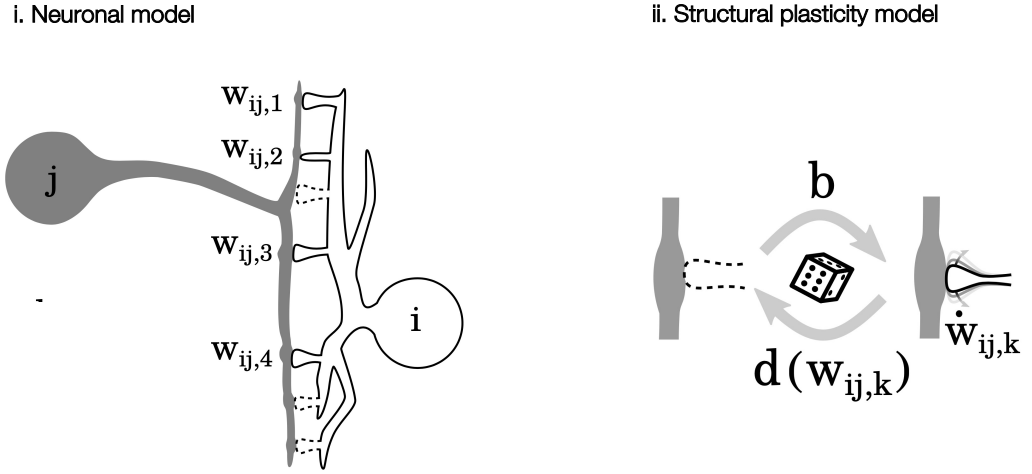

Figure 4.9 – **Scheme of the model proposed by [Fauth and van Rossum, 2019]**. **i.** A neuron j connects to a neuron i through S_{max} synaptic connections (here $S_{max} = 7$). Dashed synapses represent non-functional synapses while solid synapses are functional synapses. Each formed synaptic connection k is characterized by a synaptic weight $w_{ij,k}$. **ii.** Non-functional synapses (dashed) transforming into functional synapses with a rate b. Functional synapses are eliminated with a probability b dependent on the synaptic weight $w_{ij,k}$ of the synapse. *From* [Fauth and van Rossum, 2019].

Structural plasticity

Concerning structural plasticity, [Fauth and van Rossum, 2019] proposes the model shown in Figure 4.9 **ii.**. Non-functional synapses are continuously converted to functional synapses with a constant rate $b = 1/day$. When these new synapses are formed, they are initialized with a low synaptic weight, i.e. $w_0 = 0.001$. This synaptic weight

then evolves according to the traditional rules of synaptic plasticity. Moreover, at the same time as this process of creation of new synapses, functional synapses will be eliminated with a certain probability.

The probability of elimination of a synapse is dependent on its synaptic weight and is given by equation :

$$d(w_{ij,k}) = d_1 + \frac{d_0 - d_1}{1 + e^{(-\beta(w_{off} - w_{ij,k}))}} \tag{4.6}$$

where $d_1 = 0.03/day$, $d_0 = 24/day$, $w_{off} = 0.35 w_{max}$ and $\beta = 20$. d_1 represents the probability of elimination when the synaptic weight is maximal, i.e. when $w_{ij,k} = 0.7$, whereas d_0 represents this probability when the synaptic weight is minimal, i.e. $w_{ij,k} = 0$.

In order to have a simpler understanding of the evolution of this synapse elimination probability, equation 4.6 is plotted in Figure 4.10.

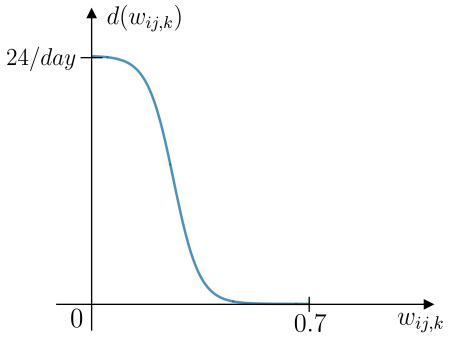

Figure 4.10 – **Evolution of the elimination rate of functional synapses as a function of their synaptic weight.** When the synaptic weight is zero, the rate of synapse removal is 24 per day. When the synaptic weight is maximal ([Fauth and van Rossum, 2019] defined the maximum synaptic weight as 0.7), the rate of synapse elimination is very low. Plot drawn from equation 4.6 with the parameters of the article.

When the synaptic weight is large, the probability of synapse elimination is low, whereas when the synaptic weight is low, this probability is higher. This ensures that larger synapses are more stable than smaller ones and therefore are less easily eliminated.

Synaptic weight evolution

In [Fauth and van Rossum, 2019], the evolution of synaptic weight follows a Hebbian plasticity rule and is described as follows:

$$\frac{dw_{ij,k}}{dt} = \begin{cases} -\Delta_{decay} w_{ij,k} & if \quad \nu_i < 0.5 \quad and \quad \nu_j < 0.5 \\ +\Delta_{LTP}(w_{max} - w_{ij,k}) & if \quad \nu_i < 0.5 \quad and \quad \nu_j < 0.5 \\ -\Delta_{LTD} w_{ij,k} & otherwise \end{cases}$$

where $\Delta_{decay} = (2days)^{-1}$, $\Delta_{LTP} = 0.1s^{-1}$ and $\Delta_{LTD} = 0.01s^{-1}$, ν_j and ν_i are the firing rate of the pre- and postsynaptic neuron, respectively. When both pre- and postsynaptic neurons are highly active, there is LTP and thus synaptic weight increases. When only one of the two neurons is active, there is LTD and thus the synaptic weight decreases. In addition, there is also a decrease in synaptic weight when both neurons have low activity.

Model results

Within assemblies, there is continuous creation and withdrawal of synapses so that in one day about 10% of the synapse population is changed. However, [Fauth and van Rossum, 2019] showed that, immediately after learning, the creation of new synapses increases sharply while the removal of synapses remains low. Then, the creation of new

synapses gradually decreases over the days after learning and falls back to the same level as synapse elimination. However, the net result of simultaneous creation and elimination results in more synapses being stabilized than deleted. Learning therefore results in a net increase in the number of synapses. These results are shown in Figure 4.11.

Assemblies Groups of neurons that are connected to each other through synaptic connections, usually as a result of a learning process. They activate in a synchronized and coordinated way in the brain. The assemblies of neurons could represent the physical basis of memories [Holtmaat and Caroni, 2016].

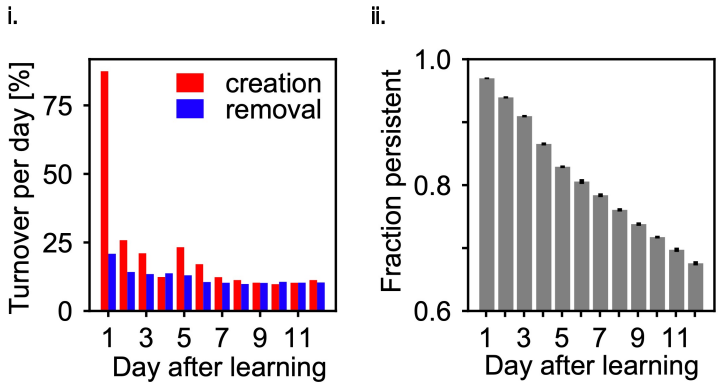

Figure 4.11 – **Structural plasticity after learning. i.** Creation (in red) and elimination (in blue) of synapses compared to the synapses present on the previous day. There is a strong creation of new synapses just after learning while the elimination remains quite low. **ii.** Sketch of the structural changes after learning. Some synapses are eliminated (-) while new ones are created (+) but the net result is an increase in the number of synapses after learning. *From* [Fauth and van Rossum, 2019].

In addition, [Fauth and van Rossum, 2019] showed in their paper some interesting results that deserve to be briefly discussed as they will be useful for part III of this master thesis. Indeed, they showed in particular that rest phases were crucial for the maintenance of memory. Moreover, they have shown that in the absence of structural plasticity, the maintenance of memories is more difficult or impossible. Indeed, as shown in the results of Figure 4.12 **i.**, when the phase is only sensory, within an assembly, without rest phases, the synaptic weight drops as well as the number of synapses. It is logical that the number of synapses falls since the rate of synapse elimination is faster for small synaptic weights (see Figure 4.10). On the contrary, when sensory phases are alternated with resting phases (Figure 4.12 **ii.**), we see that the synaptic weight is preserved and that the number of synapses increases within the assembly. Under the same conditions (alternating sensory and resting phases) but in the absence of structural plasticity (Figure 4.12 **iii.**), memory maintenance is more difficult. Indeed, we see that the synaptic weight drops after a certain time. In fact, it drops off the moment there is a longer period without a rest phase. In this figure, the number of synapses remains constant since there is no structural plasticity. It will therefore be important to consider resting phases and structural plasticity in the computational study.

Sensory phase In [Fauth and van Rossum, 2019], during this phase, the neurons receive permanent information and therefore rapidly changing stimuli.

Rest phase The neurons do not receive any external stimulation but reactivate spontaneously [Fauth and van Rossum, 2019].

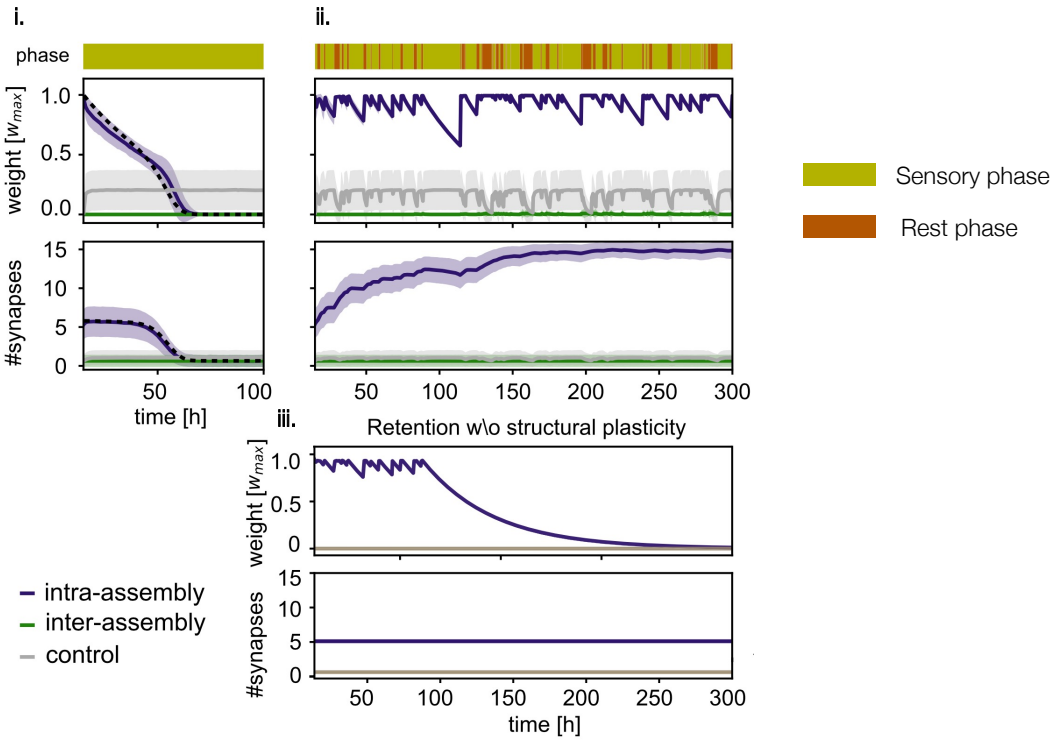

Figure 4.12 – **Evolution of synaptic weight and number of synapses in different cases. i.** Without rest phases, the synaptic weight and the number of synapses decrease (within an assembly). **ii.** When sensory and rest phases alternate, the synaptic weight is maintained and the number of synapses increases (within an assembly). **iii.** Without structural plasticity, the synaptic weight drops after a certain point. *Adapted from* [Fauth and van Rossum, 2019].

To conclude, the model proposed by [Fauth and van Rossum, 2019], which incorporates synaptic and structural plasticity, has been demonstrated to be effective in managing long-term memory. Indeed, on the one hand, it allows to consolidate and reinforce memories by regulating upwards the connectivity within the memory representations. And on the other hand, it allows neurons to remain sensitive to future learning by decreasing synaptic weights and the number of synapses in the rest of the network.

4.4.2 Model proposed by [Zenke et al., 2015]

[Zenke et al., 2015] suggest that the induction of synaptic plasticity must be distinguished from synaptic consolidation and maintenance. This is consistent with the synaptic and structural plasticity proposed by [Lamprecht and LeDoux, 2004] as discussed in the first part of this master thesis.

To this end, [Zenke et al., 2015] proposes a model of plasticity considering several forms of plasticity on different time scales.

Synaptic plasticity

First, on a small time scale (seconds time scale), they model the induction of plasticity by a combination of traditional Hebbian plasticity rules with heterosynaptic plasticity. [Zenke et al., 2015] then schematically describe

the change in synaptic weight between a presynaptic neuron j and postsynaptic i by the following equation:

$$\Delta w_{ij}(t) = \underbrace{A \times (\text{pre})_j \times (\text{post})_i^2 - B \times (\text{pre})_j \times (\text{post})_i}_{\text{Hebbian plasticity}} - \underbrace{\beta(w_{ij} - \tilde{w}_{ij}(t)) \times (\text{post})_i^4}_{\text{Heterosynaptic}} + \underbrace{\delta(\text{pre})_j}_{\text{Transmitter-induced}} \quad . \tag{4.7}$$

In this equation, A and B represent the rates of LTP and LTD, respectively; β and δ are the strength of heterosynaptic and transmitter-induced plasticity. $(\text{pre})_j$ and $(\text{post})_i$ refer to presynaptic and postsynaptic activity (spikes of neurons), respectively. Finally, w_{ij} is the current synaptic weight and $\tilde{w}_{ij}$ is what they call the reference weight, which corresponds to the state of the synapse. The state of the synapse can be seen as the size of the synapse so for example if the synapse has a low reference weight, it could mean that it is a small synapse. On the contrary, if its reference weight is high, we can see the synapse as a large synapse.

Structural plasticity

[Zenke et al., 2015] introduces slow plasticity into this fast plasticity described by equation 4.7. Indeed, they consider that the consolidation of plasticity is reflected by a change in the reference synaptic weight $\tilde{w}_{ij}$. This change occurs on a longer time scale (hour time scale) than the change in synaptic weight and is directed by the following equation:

$$\tau^{cons} \frac{d}{dt} \tilde{w}_{ij}(t) = w_{ij} - \tilde{w}_{ij} - P\tilde{w}_{ij}(t) \left(\frac{w^P}{2} - \tilde{w}_{ij}(t) \right) \left(w^P - \tilde{w}_{ij}(t) \right) \tag{4.8}$$

where τ^{cons} is the consolidation time constant (set to 20 minutes in the paper), which characterizes the rate of convergence of $\tilde{w}_{ij}$ to a stable equilibrium point. P and w^P are fixed parameters.
[Zenke et al., 2015] say that the evolution of $\tilde{w}_{ij}(t)$ is therefore directed by the difference between the current synaptic weight w_{ij} and the current reference weight $\tilde{w}_{ij}$. This difference can therefore be seen as a fixed parameter in this equation and if it is zero, it gives

$$\tau^{cons} \frac{d}{dt} \tilde{w}_{ij}(t) = -P\tilde{w}_{ij}(t) \left(\frac{w^P}{2} - \tilde{w}_{ij}(t) \right) \left(w^P - \tilde{w}_{ij}(t) \right), \tag{4.9}$$

which corresponds to the curve in Figure 4.13.

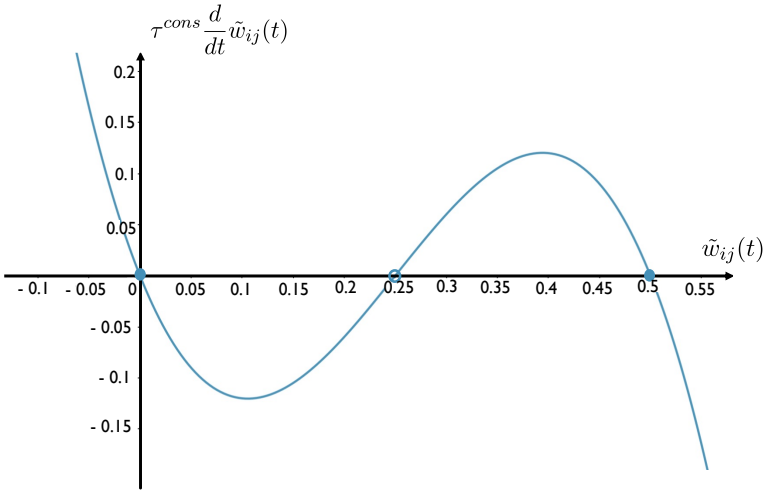

Figure 4.13 – **Evolution of the reference weight $\tilde{w}_{ij}(t)$ when the difference $(w_{ij} - \tilde{w}_{ij})$ is zero.** Plot drawn from equation 4.9. The filled points represent the stable equilibrium points and the unfilled point is the unstable equilibrium point.

The graph intercepts the x-axis at three points, which correspond to the equilibrium points, thus the points towards which $\tilde{w}_{ij}(t)$ will potentially converge. The slope of the curve at the equilibrium points $\tilde{w}_{ij}(t) = 0$ and $\tilde{w}_{ij}(t) = 0.5$ is negative, so these are stable equilibrium points. The slope of the curve at the point $\tilde{w}_{ij}(t) = 0.25$ is positive, so it is an unstable point.

In summary, when the difference between the current synaptic weight w_{ij} and the current reference weight $\tilde{w}_{ij}$ is zero (in this case, $w_{ij} = \tilde{w}_{ij}$), $\tilde{w}_{ij}(t)$ will converge to one of the two stable points, either to 0 or to 0.5. The bifurcation diagram of the dynamics of the reference weight $\tilde{w}_{ij}(t)$ is available in Appendix B.1. It shows that when w_{ij} is larger than $\tilde{w}_{ij}$, the equilibrium points of $\tilde{w}_{ij}$ increase. This can be interpreted as follows: if neurons learn information, the w_{ij} of the synapse will increase, and w_{ij} will then be greater than $\tilde{w}_{ij}$. Since, in this case, its equilibrium points are increased, $\tilde{w}_{ij}$ will converge to a larger value and the internal state of the synapse will increase. Learning therefore results in an increase in synapse size.

Note that in addition to the consolidation of plasticity that takes place through slow changes in the reference weight $\tilde{w}_{ij}$, [Zenke et al., 2015] introduces homeostatic plasticity that also takes place on a larger time scale. He does this by making the rate of LTD (the B parameter in equation 4.7) depend on time.

Model summary

To summarize, the model proposed by [Zenke et al., 2015] introduces several mechanisms of synaptic plasticity on several time scales. Indeed, they take into account traditional Hebbian plasticity combined with heterosyanatic plasticity as well as homeostatic plasticity (definition in Appendix B.2 and consolidation. The evolution of the synaptic weight $w_{ij}(t)$ therefore takes into account all these forms of plasticity and is a function of the reference synaptic weight $\tilde{w}_{ij}(t)$. The latter evolves as a function of the current $(w_{ij} - \tilde{w}_{ij})$ difference but much more slowly than the synaptic weight. In a simplified way, we can write:

$$\frac{d}{dt}w_{ij}(t) = f\left[(\text{pre})_j, (\text{post})_i, \tilde{w}_{ij}(t)\right] \tag{4.10}$$

and

$$\frac{d}{dt}\tilde{w}_{ij}(t) = g\left[(w_{ij} - \tilde{w}_{ij})\right] \tag{4.11}$$

where $(\text{pre})_j$ and $(\text{post})_i$ refer to presynaptic and postsynaptic activity, respectively.

This model has been shown to allow for the stable formation and retrieval of memories. The blocking of one or the other form of plasticity of the model prevents the proper functioning of the long-term memory. This highlights the importance of considering different forms of plasticity, and that traditional models of synaptic plasticity, alone, are not sufficient to explain long-term memory.

4.4.3 Others phenomenological models

There are many other models that can be classified in this category. A large group of these are that model the Synaptic Tagging and Capture (STC) hypothesis (which was defined in Part I of this thesis). One such example is the model proposed by [Lehr et al., 2022] [Jacquerie, 2023], in which the total synaptic weight consists of two contributions. Indeed, the first contribution is the early phase plasticity, which is based on calcium. The second contribution is late phase plasticity, which is based on STC and depends on neuromodulation. The model proposed by [Luboeinski and Tetzlaff, 2021] is also based on this same principle. The model proposed by [Li et al., 2016] is also based on a similar principle. In this model, late-phase plasticity depends on protein synthesis and synaptic tagging processes. Each of these two processes depends on a respective triggering threshold which in turn depends on early plasticity.

4.5 Conclusions

There is a wide variety of models of structural plasticity, and those we have mentioned are only a fraction of those present in the scientific literature. In fact, it is difficult to define a universal method used by these models, as they often differ significantly from each other. The only common element to all models is that structural plasticity is modeled on a slow time scale.

Nevertheless, it is possible to identify 3 main strategies adopted by these models, as suggested by [Jacquerie, 2023].

Mathematical models, like those of [Deger et al., 2012], [Helias, 2008] and [Zheng et al., 2013], rely on a lot of equations and statistics to describe structural plasticity. Moreover, they try to involve as few assumptions as possible concerning the underlying biophysical processes of structural plasticity.

Biological models, such as those in [Smolen et al., 2006], [Smolen et al., 2020] and [Amano et al., 2022], are based entirely on the biological processes involved in structural plasticity. Indeed, they describe structural plasticity through the dynamics of the biochemical reaction cascades that underlie it.

Phenomenological models, as proposed by [Fauth and van Rossum, 2019] and [Zenke et al., 2015], are in between the two previous types of model. They are based on the biological processes of structural plasticity, but in a simplified way to govern the model equations. Some, like [Lehr et al., 2022], [Luboeinski and Tetzlaff, 2021] and [Li et al., 2016], are based on the Synaptic Tagging and Capture hypothesis.

Each model has its own advantages and disadvantages. However, in general, we can say that the big advantage of mathematical models is that they do not require detailed knowledge of the bio-molecular mechanisms involved in structural plasticity. This is a big advantage since there is still a lack of knowledge on this subject. However, mathematical models are composed of many equations, sometimes very complex to understand. Concerning the biophysical models, in a global way, they have the advantage to provide a good understanding of the mechanisms underlying structural plasticity. However, since these models describe the dynamics of each molecule involved, they are often described by a large number of equations, which can make the implementation slow. Finally, concerning the phenomenological models, which are between the two previous models, it is difficult to give their general advantage or disadvantage since the models are very different from each other.

Chap 4 : a review of structural plasticity models

Mathematical models

[Deger et al., 2012] [Helias, 2008] [Zheng et al., 2013]

Use many equations and statistics to describe structural plasticity.

Ex.

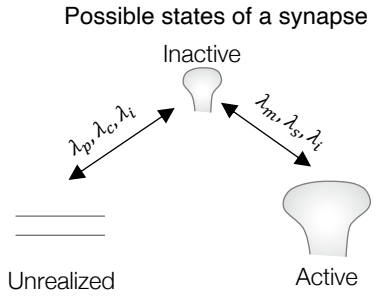

$$\begin{aligned}\frac{d}{dt}p_{(x,y)} = &-p_{(x,y)}\left[(x+2y)\lambda_i + (N-x-y)\lambda_c + x\lambda_s(x) + y\lambda_p(x) + y\lambda_m(x)\right] \\ &+ (x+1)p_{(x+1,y-1)}\left[\lambda_s(x+1) + \lambda_i\right] \\ &+ (y+1)p_{(x,y+1)}\left[\lambda_p(x) + \lambda_i\right] \\ &+ (y+1)p_{(x-1,y+1)}\left[\lambda_m(x-1) + \lambda_i\right] \\ &+ (N-x-y+1)p_{(x,y-1)}\lambda_c\end{aligned}$$

\+ Do not require detailed knowledge of biomolecular mechanisms

\− Sometimes difficult to understand

Biological models

[Smolen et al., 2012] [Smolen et al., 2012] [Amano et al., 2022]

Describe the dynamics of the biochemical reaction cascades.

Ex.

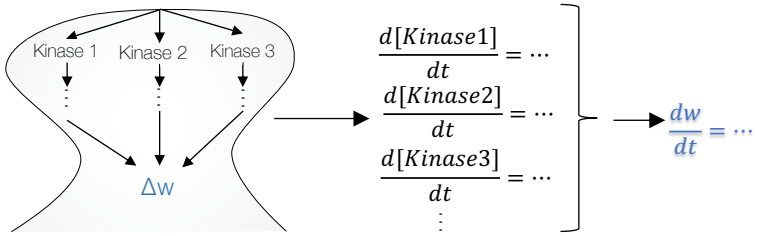

\+ Provide a good understanding of structural plasticity mechanisms

\− Difficult to implement

Phenomenological models

[Fauth and van Rossum, 2019] [Zenke et al.,2015]
[Lehr et al., 2015] [Luboeinski and Tetzlaff, 2021] [Li et al., 2016]

Based on the Synaptic Tagging and Capture hypothesis

Use simplified biological processes to govern the model equations.

Ex.

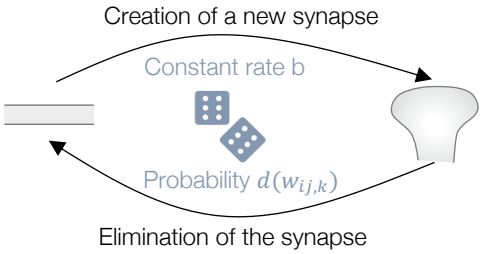

$$d(w_{ij,k}) = d_1 + \frac{d_0 - d_1}{1 + e^{(-\beta(w_{off} - w_{ij,k}))}}$$

Part III

Computational study

Chapter 5

Creation of a structural plasticity model

We saw in Chapter 2 that applying traditional synaptic plasticity rules during neuronal activity switches, in particular during the tonic-to-burst switch, led to homeostatic reset. All the learning acquired during tonic is thus forgotten when switching to burst. In this part of the thesis, we create a structural plasticity model for transferring learning, so that the combination of traditional synaptic plasticity rules and this structural plasticity is consistent with memory consolidation.

5.1 Preliminary model model proposed by [Jacquerie, 2023]

[Jacquerie, 2023] has proposed a preliminary model combining traditional synaptic plasticity rules with a structural plasticity rule to obtain a model consistent with memory consolidation. Specifically, it defines synaptic weight as the product of two terms: *early-weight* (w) and *late-weight* (l). The former term models E-LTP and refers to an increase in postsynaptic receptor efficiency and the rapid insertion of new receptors. The second term models L-LTP and refers to structural changes and protein synthesis. During burst activity, early-weights undergo the homeostatic reset, while late-weights consolidate the information learned during the preceding tonic. Specifically, strong learning during the tonic period leads to an increase in late-weight during the subsequent burst period. Conversely, weak learning leads to a decrease in late-weight during the burst.

5.1.1 Model

The early-weight, w, is defined by the traditional calcium-based rule of synaptic plasticity (more details on rule implementation in [Jacquerie et al., 2022a]). Concerning the late-weight, l, its evolution is described by the following equation:

$$\tau_l \dot{l} = \Delta l \tag{5.1}$$

where Δl is between -1 and 1 and the time constant τ_l modulates the speed of change.
During the burst activity, Δl follows the following law:

$$\tau_\Delta \dot{\Delta l} = \sigma(w) - \Delta l \tag{5.2}$$

where τ_Δ modulates the speed of the Δl and $\sigma(w)$ is a sigmoid function between -1 and 1, resembling the shape depicted in Figure 5.1.

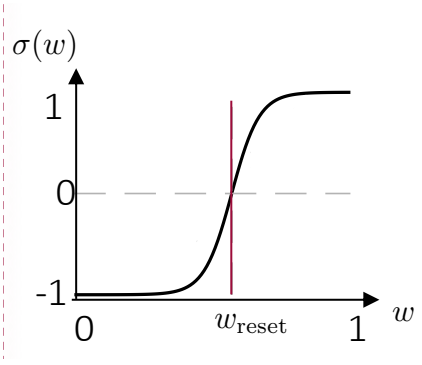

Figure 5.1 – **Curve of the $\sigma(w)$ function involved in the structural plasticity model proposed by [Jacquerie, 2023].** w_{reset} is the estimated homeostatic reset during burst activity. *Adapted from* [Jacquerie, 2023].

In this way, when w is greater than w_{reset} (representing strong learning), Δl is positive, resulting in an increase in

l as we intended. Conversely, when w is smaller than w_{reset} (representing weak learning), Δl is negative, resulting in a decrease in l.

5.1.2 Computational experiments

Scenarios

In this thesis, we study the synaptic plasticity that occurs between pairs of neurons (a presynaptic and a postsynaptic neuron) when their activity switches from one state to another. In particular, three scenarios, consisting of cycles of 2 states that can be repeated, will be tested. These scenarios are presented in Table 5.1. On the one hand, testing synaptic plasticity through these scenarios will highlight the role of different activities in learning. On the other hand, it will help determine in which activities structural plasticity should be implemented.

		State 1	**State 2**
Scenario 1	*Neuronal activity*	Tonic	Burst
	Structural plasticity	OFF	ON
Scenario 2	*Neuronal activity*	Tonic	Burst
	Structural plasticity	ON	ON
Scenario 3	*Neuronal activity*	Tonic	Inactive
	Structural plasticity	ON	ON

Table 5.1 – **Scenarios tested in computational experiments.**

Scenario 1 consists of switches from tonic to burst activity, in which structural plasticity is implemented only during the burst. During tonic activity, the late-weight (l) remains constant.

Scenario 2 also involves switching from tonic to burst activity, but here structural plasticity is implemented throughout the different states, even in tonic activity.

Scenario 3 consists of switches from tonic activity to inactivity, in which structural plasticity is implemented for both types of activity. In this scenario, it's as if burst activity has been blocked. This scenario serves to emphasize the importance of burst activity in the context of learning.

Neuronal network

In the experiments in this section, the neuronal network shown in Figure 5.2 is considered. It consists of 3 presynaptic neurons, all connected to 2 postsynaptic neurons, forming a total of 6 connections. The circuit has been implemented so as to have 3 correlated (black) and 3 uncorrelated (grey) connections. Correlated connections simulate learning, while uncorrelated connections simulate non-learning. To obtain correlated connections, both presynaptic and postsynaptic neurons must have high electrical activity, i.e. a high spike frequency. To obtain uncorrelated connections, one of the two neurons must have low activity and therefore a relatively low spike frequency. Furthermore, all neurons in the circuit are connected to an inhibitory neuron, to which a current I_{app}, selected based on the desired neuronal activity, is applied. I_{app} reproduces the effects of neuromodulators, which are responsible for triggering burst activity in neurons. Note that, initially, the neural network is considered to be homogeneous. In other words, the intrinsic properties of the neurons, such as their intrinsic conductance, are the same for all neurons in the network.

Generation of neuronal activity

To generate the tonic activity of the neurons, they are supplied with a high external current of $50nA/cm2$ for a duration of 3ms at a chosen frequency f_0. Spike times are generated with inter-spike intervals following independent normal distributions $\mathcal{N}\left(\frac{1}{f_0}, (\frac{0.1}{f_0})^2\right)$. For each experiment, the chosen frequency f_0 is indicated. During tonic activity, the current I_{app} applied to the inhibitory neuron is $3nA/cm^2$. To switch our neurons to burst activity, the inhibitory neuron is hyperpolarized with an $I_{app} = -1.2nA/cm^2$ current and external currents are blocked. Inactive activity is generated in a similar way to tonic activity, but at low f_0 frequencies ([0.1-1Hz]) [Jacquerie, 2023].

5.1.3 Results

The results obtained with the parameters just described and for the three scenarios are those shown in Figure 5.3.

Each graph represents 6 curves: the black curves correspond to correlated connections while the grey ones correspond to uncorrelated ones. The evolution of early-weight (w) is represented on the top graphs and the evolution of late-weight (l) on the middle graphs. The synaptic weight corresponding to the product of the two is visible on the lower graphs. For all 3 scenarios, during the tonic phase (blue panels), the early-weights (w) of correlated neurons increase, while those of uncorrelated neurons decrease.

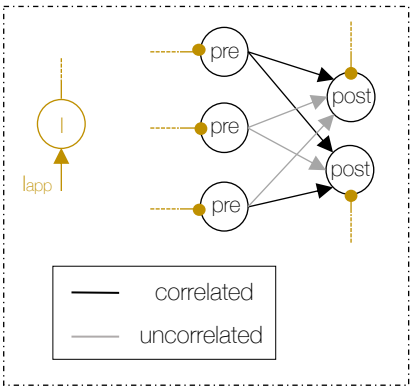

Figure 5.2 – **Neuronal network.** The circuit is composed of 3 presynaptic and 2 postsynaptic neurons, all interconnected in a feedforward manner. 3 connections are correlated (black) and 3 are uncorrelated (grey). An inhibitory neuron is connected to all neurons and an I_{app} current is applied to it. *Adapted from* [Jacquerie et al., 2022a].

Parameters:

- Frequency f_0 chosen to generate tonic activity:

Neuron	Pre	Post
1	70 Hz	30 Hz
2	5 Hz	40 Hz
3	20 Hz	/

- Initial values:

w_0	l_0	τ_l
0.5	0.1	$5e^5$

In scenario 1 (Figure 5.3, left), neurons switch from tonic (blue panel) to burst (pink panel) activity. As seen in section 2.4.3, the switch to burst activity leads to convergence of all early-weights, regardless of learning. To transfer the information learned during tonic activity, structural plasticity is implemented during burst activity, as in [Jacquerie, 2023]. In line with the model, the late-weight increases during burst for correlated connections, since the early-weight (w) is above the homeostatic reset. Conversely, the late-weight decreases for uncorrelated connections. Looking at the impact on total weight, we can see that there's a balance between homeostatic reset and structural plasticity. In other words, during burst activity, synaptic weight decreases a little for correlated connections and increases a little for uncorrelated connections (effect of homeostatic reset), but the forces don't all converge towards the same value (effect of structural plasticity). At the end of burst activity, it is now possible to distinguish between correlated and uncorrelated connections, whereas this was not the case without structural plasticity. In fact, the weight of correlated connections is now higher than the weight of uncorrelated connections.

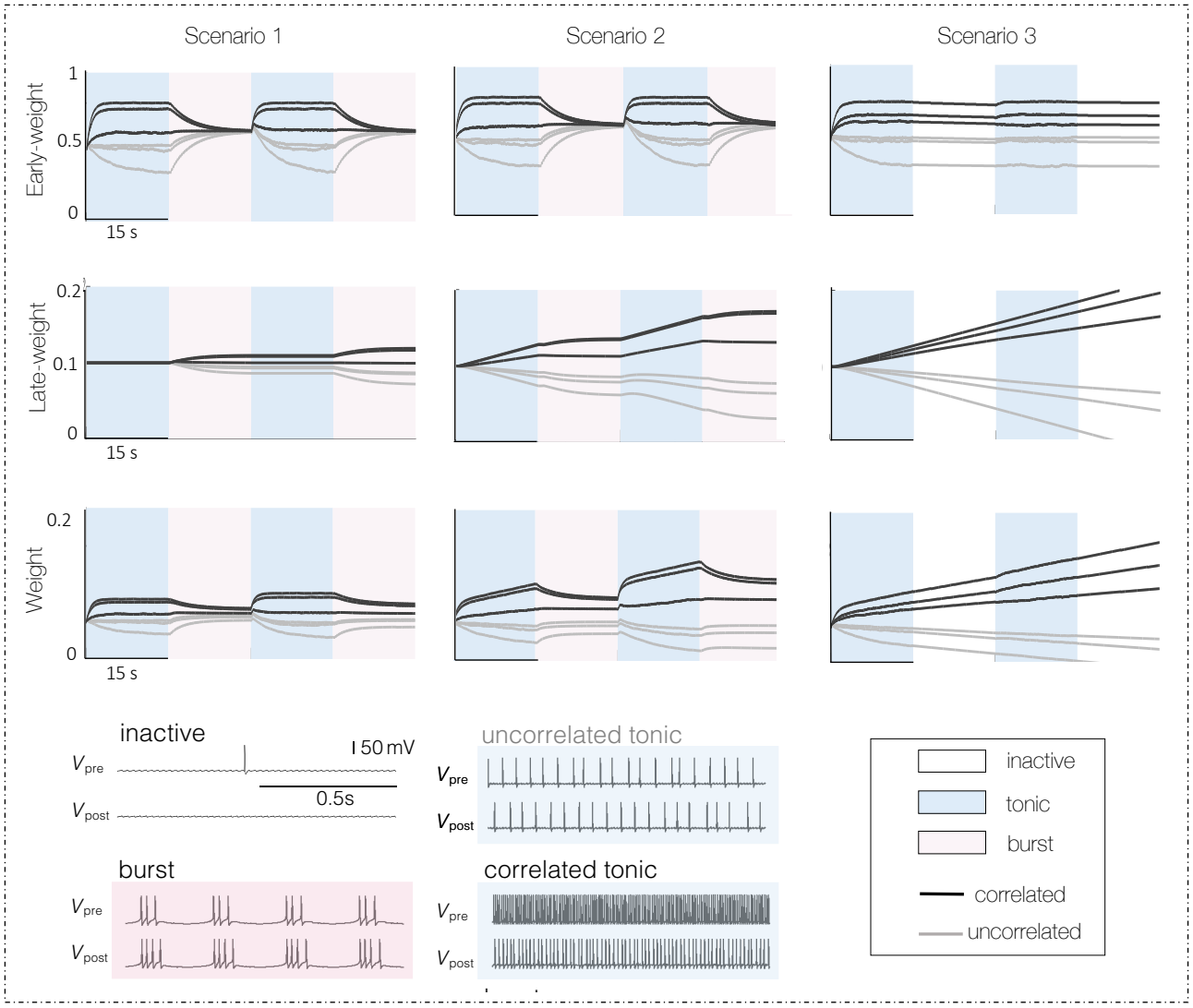

Figure 5.3 – **Results of the structural plasticity rule proposed by [Jacquerie, 2023] for different scenarios.** Scenario 1 (left) is a transition between tonic and burst activity. In this scenario, structural plasticity is implemented d-only during burst activity. Scenario 2 (middle) also transitions from tonic to burst activity, but this time structural plasticity is also implemented during the tonic phase. Scenario 3 (right) consists of a succession of tonic activities followed by a phase of inactivity, in which structural plasticity is implemented in both types of activity. For each of the 3 scenarios, curves showing the evolution of early-weight, late-weight and weight are plotted. Black curves correspond to correlated neurons and gray curves to uncorrelated neurons. The neuronal circuit used is that shown in Figure 5.2. Diagram of the different electrical activities taken from [Jacquerie, 2023].

In scenario 2 (Figure 5.3, middle), the activities are the same as in Scenario 1. The early-weight curves are therefore the same for both scenarios. The difference here is that structural plasticity is also implemented in tonic. However, the structural plasticity rule proposed by [Jacquerie, 2023] only allows late-weight to evolve during burst activity. Since there is no reset value in tonic, we can't use it to define when the late-weight is consolidated or depressed, as is done in the burst period. However, we have seen from simulations that the reset value in burst is around 0.55. This is why we decided to choose this value as the cutoff point between consolidation and depression. In this way, during tonic periods, when early-weight is above 0.55, late-weight increases. Conversely, when early-weight is below 0.55, late-weight decreases. This approach to varying late-weight during tonic periods is naive, but our aim here is just to get an idea of how the model works in scenario 2. For the evolution of late-weight, as

in the previous scenario, it increases for correlated connections and decreases for uncorrelated connections. The difference with scenario 1 is that the change is more rapid. Indeed, this is logical, since in this case, late-weight also evolves in this way during tonic phases. The impact on synaptic weight is therefore also the same as in scenario 1, but more pronounced. That is, at the end of the experiment, correlated connections have a higher weight than in scenario 1, and uncorrelated connections have a lower weight. This is due to the fact that the late-weight has higher values than in scenario 1 (since it evolves faster here) and therefore counterbalances the homeostatic reset in a more pronounced way.

Finally, in scenario 3 (Figure 5.3, right), after the tonic phase, comes an inactive phase (white panel) in which neurons have very little electrical activity. In this scenario, the burst is thus blocked. In the inactivity phase, early-weights remain stable or decrease slightly. In the next learning phase (2nd blue panel), we see that the early-weights of correlated connections increase only slightly. The early-weight curve therefore shows saturation. This saturation is in fact due to the use of soft bounds, which makes high early-weights difficult to potentiate. Concerning late-weight, it is implemented during tonic and inactivity in the same way as during tonic in scenario 2. That is, with the cut-off value of 0.55 between consolidation and depression. It can be seen that in this scenario, the late-weight explodes in its values, which also translates into an explosion of synaptic weight values. What's more, even when neurons are not learning (during the inactive phase), the late-weight continues to increase, as the trace of the early-weight is above the threshold value of 0.55.

Conclusion

The results in Figure 5.3 showed that transferring learning through structural plasticity could be a good solution to overcome the problem of learning loss due to homeostatic reset. Indeed, scenarios 1 and 2 showed that, at the end of burst activity, the learned information was not completely forgotten, since the weights of correlated connections are increased compared with the reset. What's more, the neurons are capable of learning through multiple occurrences, since the weights of the correlated connections continue to increase over the course of the states. At this stage, it's hard to say which of scenarios 1 and 2 is better at providing a model consistent with memory consolidation. However, as the weight and late weight curves evolve more rapidly for scenario 2, there is a risk that too large values will be reached too quickly, which could be problematic since a neural network does not have infinite capacity. In scenario 3, the early-weight curves showed saturation, making it impossible to learn new things. Furthermore, the late-weight curves are not consistent with memory consolidation, since the values explode even when there is no learning.

From a biological point of view, the model can be interpreted as follows: the evolution of early-weight, which, as a reminder, models E-LTP, characterizes changes in postsynaptic receptor efficacy. Whereas the evolution of late-weight, which models L-LTP, characterizes structural changes and the formation of new receptors. In the transition to burst activity, on the one hand, receptor efficiency is restored as early-weights undergo homeostatic reset. This enables the neurons to learn new information at a later stage. At the same time, changes in receptor efficiency during tonic activity are transferred to morphological changes through the evolution of late-weight. Learned information is thus retained by the neurons.

However, there remain certain bothersome aspects associated with this rule governing structural plasticity. The evolution of late-weight is calculated from the value of the homeostatic reset, referred to here as the w_{reset}. In fact, the way in which the value of l is updated is governed by the value of w in relation to this value of w_{reset}. It is therefore necessary to predict this w_{reset} value in advance, which requires certain assumptions to be made. The idea of creating a new structural plasticity rule that does not require this prediction of w_{reset} then emerges.

5.2 New structural plasticity model

5.2.1 Model

The idea in developing a new rule was to start directly from the dynamics of early-weight, i.e. $\dot{w}$, to uncover structural plasticity. With the calcium rule, the evolution of synaptic weight is defined as follows:

$$\dot{w} = \frac{1}{\tau_w([Ca])}(\Omega([Ca]) - w) \tag{5.3}$$

where the time constant $\tau_w([Ca])$ and the steady-sate value $\Omega([Ca])$ are both depedndent of the concentration of calcium. $\Omega([Ca])$ is determined by two sigmoid functions, which are used to create a U-shape. From this equation we have defined the dynamics of the late-weight l as follows:

$$\tau_l \dot{l} = \zeta \frac{1}{\tau_w([Ca])}(\Omega([Ca]) - w) \tag{5.4}$$

where τ_l is the time constant. The choice of sign depends on the activity in which the neurons find themselves. Like neuronal activity (inactivity, tonic or burst), ζ is controlled by neuromodulators. We therefore define $\zeta = 1$ in tonic or inactivity activities to ensure consistency with learning. In this way, if the early-weight (w) increases, the late-weight (l) also increases. During burst activity, we define $\zeta = 1$ because, during burst activity, the early-weights of correlated connections decrease, while they increase for uncorrelated connections. In this way, the late-weight will increase for strong connections and decrease for weak ones, which is more consistent with memory consolidation.

With this new structural plasticity rule, unlike the rule proposed in section 5.1, it is no longer necessary to predict the value of w_{reset} in advance. Simplified, equation 5.4 can be rewritten in this form:

$$\tau_l \dot{l} = \zeta \dot{w} \tag{5.5}$$

5.2.2 Results

The same experiments as those described in section 5.1.2 were carried out with this new structural plasticity rule. The parameters used are also the same, apart from τ_l which here is 10 and has been chosen so that changes in l are of the same order of magnitude as with the rule proposed by [Jacquerie, 2023]. The results are shown in Figure 5.4.

The early-weight curves for the three scenarios are the same as in Figure 5.3 and will not be discussed again here. Concerning the evolution of the late-weight, for scenario 1 (Figure 5.4, left), in which structural plasticity is implemented only during burst activity, it increases for correlated connections and it decreases for uncorrelated connections. Moreover, the curves do not saturate and continue to evolve during the different states. As far as total weight is concerned, there is once again a counterbalance between homeostatic reset and structural plasticity. This results in a slight increase in weight for correlated connections and a slight decrease for uncorrelated connections at the end of burst activity. For scenario 2 (Figure 5.4, middle), the observations are similar to those for the previous scenario. The difference is that the late-weight is also implemented during tonic activity and therefore evolves more rapidly than for scenario 1. This is reflected in the synaptic weight curve, which also evolves more rapidly. At the end of burst activity, correlated connections are more pronounced than in scenario 1. The same applies to uncorrelated connections, which are reduced more sharply. However, no saturation of the curves can yet be observed. Finally, in scenario 3 (Figure 5.4, right), where tonic phases are followed by inactive phases, the late-weight curve saturates with the early-weight curve. In the first phase of tonic activity, late-weight increases for correlated connections, but then remains virtually stable for all subsequent phases. Here, unlike in Figure 5.3, late-weights remain constant during inactive phases, i.e. when there is no learning, which is more consistent.

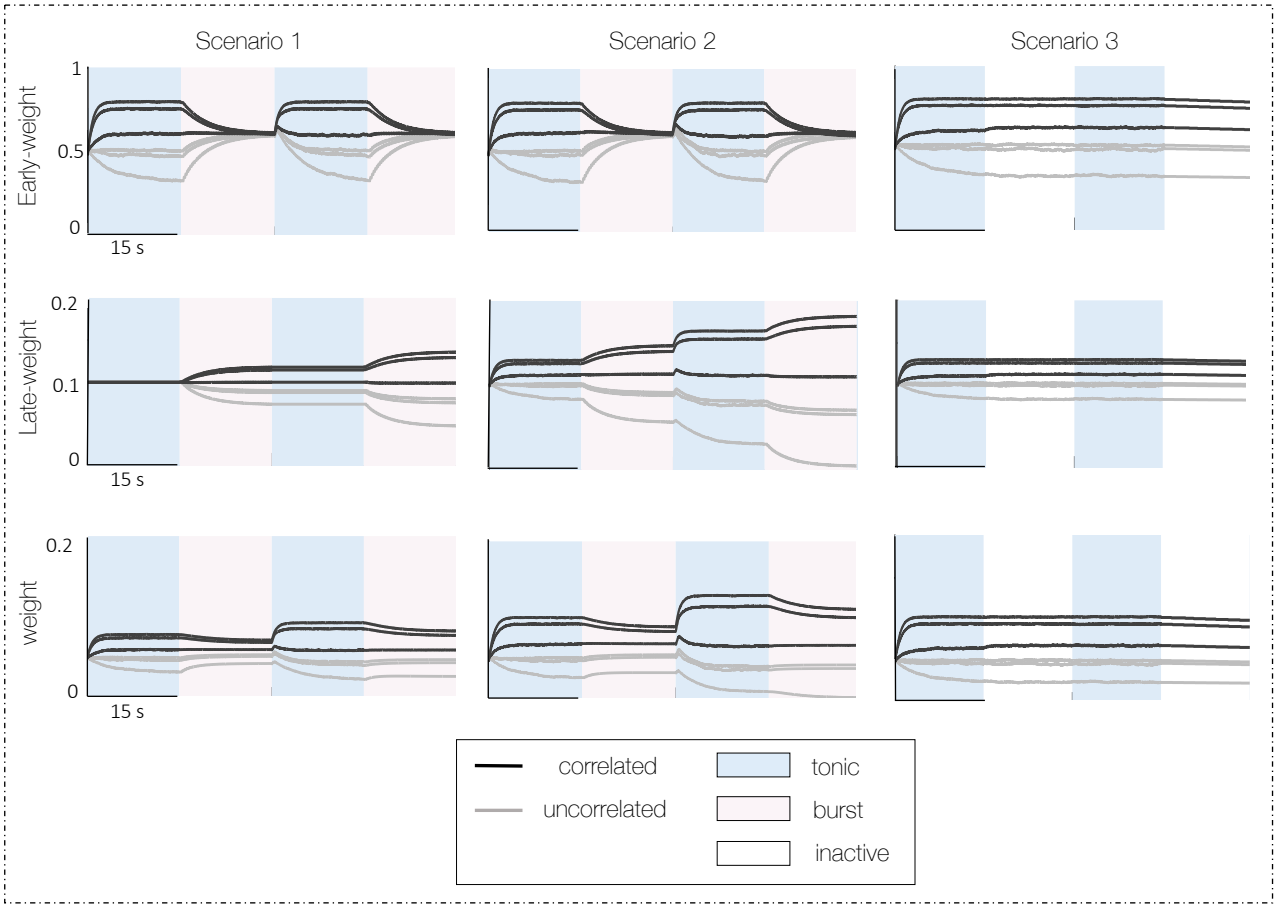

Figure 5.4 – **Implementation of the new structural plasticity rule (equation 5.4) for different scenarios.** The scenarios are the same as those shown in Figure 5.3 (see Caption). The early-weight, late-weight and weight curves are plotted for each scenario (black curve for correlated neurons and gray curve for uncorrelated neurons).

.

5.2.3 Conclusions

The results showed that the new structural plasticity rule seems to be a good solution to overcome the homeostatic reset problem. Indeed, information learned during tonic is no longer forgotten, since synaptic weight is increased for correlated connections and decreased for uncorrelated ones. Moreover, neurons are able to learn through multiple occurrences, as weights continue to evolve across different states without saturation. Scenarios 1 and 2 both led to this result: implementing the structural plasticity rule only in burst activity or also in burst activity seems to be a good solution for memory consolidation. Changes in receptor efficiency (E-LTP) could be transformed into structural changes in synapses (L-LTP). Scenario 3 also produced very interesting results. The saturation they show leads to the conclusion that burst periods are essential for memory consolidation. Indeed, neurons are no longer able to learn through multiple occurrences when burst activity is blocked.

5.3 Model analysis

In this section, the model, and in particular the behavior of the late-weight (l), is analyzed in greater depth. This will provide a clear understanding of how it evolves. In addition, the influence of the various model parameters is studied, so that their values can be chosen appropriately.

5.3.1 Analytical calculation of late-weight convergence

The aim here is to predict the value towards which the late-weight (l) converges at the end of a state. More precisely, we calculate the convergence value at the end of burst activity, once the early-weights (w) have converged to the homeostatic reset. Since we are in burst mode, we consider $\zeta = -1$.

The curve for the evolution of late-weight can be expressed using an integral such as:

$$\begin{aligned} l(t) &= \int_{-\infty}^{t} \dot{l}(t^*)dt^* \\ &= l_0 + \int_{0}^{t} \dot{l}(t^*)dt^* \end{aligned}$$

where l_0 is the initial value of the late-weight at the start of the burst activity under consideration. By the definition given to the late-weight (equation 5.4 and equation 5.3), it can be expressed as a function of the evolution of early-weight as follows:

$$l(t) = l_0 - \frac{1}{\tau_l} \int_{0}^{t} \dot{w}(t^*)dt^* \tag{5.6}$$

However, during burst activity, early-weight (w) can be approximated by the following expression:

$$\hat{w}(t) = w_{reset} + (w_0 - w_{reset})e^{-\frac{t}{\tau_w}}$$

where w_0 is the initial value of the early-weight at the start of burst activity. The w_{reset} is the value towards which the early-weights converge at the end of the burst and τ_w is the time constant of the evolution of w. Deriving this equation gives :

$$\hat{\dot{w}}(t) = \left(\frac{w_{reset} - w_0}{\tau_w}\right) e^{-\frac{t}{\tau_w}} \tag{5.7}$$

Equation 5.7 can then be injected into equation 5.6, giving an approximation of the late-weight:

$$\begin{aligned} \hat{l}(t) &= l_0 - \frac{1}{\tau_l} \int_{0}^{t} \left(\frac{w_{reset} - w_0}{\tau_w}\right) e^{-\frac{t^*}{\tau_w}} dt^* \\ &= l_0 - \frac{w_{reset} - w_0}{\tau_l \tau_w} \left[-\tau_w e^{-\frac{t^*}{\tau_w}}\right]_0^t \\ &= l_0 + \frac{w_{reset} - w_0}{\tau_l} \left(e^{-\frac{t}{\tau_l}} - 1\right) \end{aligned}$$

To find the convergence value, we then tend this last equation towards infinity, which gives:

$$\hat{l}(\infty) = l_0 - \left(\frac{w_{reset-w_0}}{\tau_l}\right) \tag{5.8}$$

Equation 5.8 therefore gives us the value towards which the late-weight converges at the end of the burst. It is a function of the initial early-weight (i.e. the early-weight at the start of burst activity), w_0, the initial late-weight at the start of the burst, l_0, the time constant τ_l and the value of w_{reset}. The latter is known and has been demonstrated by [Ponnet, 2022].

5.3.2 Experimental verification of the early-weight convergence value

Methods

To verify the convergence value of the late-weight, a simple circuit consisting of 3 presynaptic neurons and 1 post-synaptic neuron is used. The spike frequencies of the neurons were chosen so as to have one correlated and two uncorrelated connections. The neuronal circuit is illustrated in Figure 5.5 and is simulated during 2 tonic/burst cycles in which structural plasticity varies only during the burst (it remains constant during tonic phases). The parameters used are those described below:

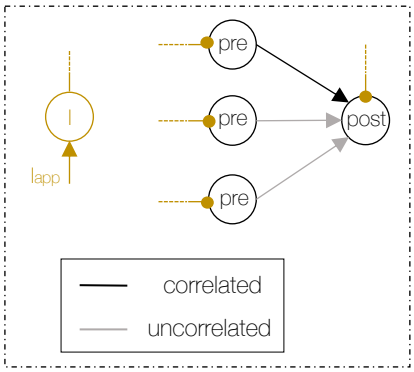

Figure 5.5 – **Neuronal network.** It consists of 3 presynaptic neuron connected to one post-synaptique neuron, in a feedforward manner. 2 connections are correlated (black) and 1 is uncorrelated (grey). An inhibitory neuron is connected to all neurons and an I_{app} current is applied to it.

Parameters:

- Frequency f_0 chosen to generate tonic activity:

Neuron	Tonic 1	Tonic 2
Pre 1	70 Hz	70 Hz
Pre 2	5 Hz	10 Hz
Pre 3	10 Hz	0.2 Hz
Post	40 Hz	30 Hz

- Initial values:

w_0	l_0	τ_l
0.5	0.1	10

Results

The evolution of late-weight during the two tonic/burst cycles is shown in Figure 5.6. Analytical predictions of its convergence at the end of burst activity for each connection are represented by the purple crosses. They match the different curves, thus verifying equation 5.8.

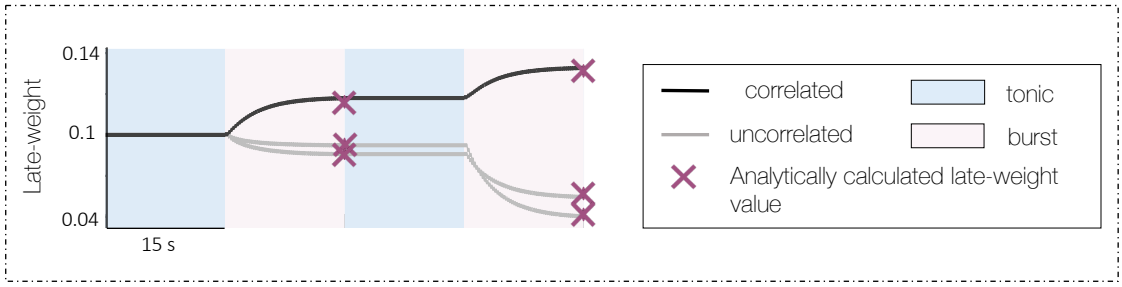

Figure 5.6 – **Experimental verification of equation 5.8.** The evolution of late weight is plotted for the three neural network connections (black curve for the correlated connection and grey curves for the two uncorrelated connections). The prediction of the convergence value at the end of the burst is represented by the purple crosses.

.

Now that the convergence equation has been verified by the simulations, the various parameters influencing it can be studied. In particular, the effect of the time constant τ_l and the effect of the w_{reset} value are studied.

5.3.3 Analysis of parameters influencing late-weight

We look at how the late weight change (Δl) is impacted by the various parameters. It is defined, on the basis of equation 5.8, as follows:

$$\Delta l = -\left(\frac{w_{reset} - w_0}{\tau_l}\right)$$

Effect of τ_l

The τ_l effect on Δl is illustrated in Figure 5.7 **i**. For this purpose, w_{reset} was set to 0.55 and w_0 to 1 to represent strong connections (black curve) or to 0 to represent weak connections. Note that Δl is represented on the y-axis in percent and corresponds to the value $\left(\frac{l-l_0}{l_0}\right)$. For strong connections, Δl is positive, so the late-weight increases well, and for weak connections, it is the other way around, the late-weight decreases. Moreover, the evolution of Δl as a function of τ_l follows an exponential which decreases for strong connections and increases for weak ones. The smaller the τ_l, the greater the change in late-weight. When τ_l is close to 1, the late-weight undergoes a variation of around 500%, whereas when it is close to 100, it undergoes a variation close to 0%. So it is important to choose an adequate τ_l, so that the late-weight changes neither too much nor too little. A τ_l of around 10 seems a good choice. With this value, the late-weight will vary by around 45%. However, depending on the goal we're aiming for, the value can be modulated. If we're aiming for rapid consolidation, it's best to choose a τ_l value below 10, whereas if we're aiming for slow consolidation, a τ_l value above 10 would be preferable.

Effect of w_{reset}

It is interesting to see what impact the w_{reset} has on the late-weight, because as we'll see in Chapter 6, the w_{reset} can change over time. Indeed, it is driven by the burst activity of neurons, which can change over time.

Figure 5.7 **ii.** shows the change in late-weight (y-axis) as a function of the initial connection early-weight (x-axis) for different values of w_{reset} (blue shading). The darker the blue, the higher the w_{reset}. We can see that for a high w_{reset} (dark blue line), depression will be stronger than potentiation. Indeed, for $w_{reset} = 0.8$, a strong connection (due to strong learning) will see its late-weight increase by 20%, while a weak connection will see its late-weight decrease by 80%. Conversely, for a low w_{reset} (light blue line), potentiation will be stronger than depression. Indeed, for $w_{reset} = 0.3$, a strong connection will see its late-weight increase by 70%, while a weak connection will see it decrease by 30%.

This phenomenon is illustrated in a different way in Figure 5.7 **iii.** to aid understanding. For weak connections (left graphs), early-weights at the end of tonic activity are low. If the w_{reset} is high, the early-weight will have to travel a long distance to reach it, which has repercussions on the late-weight, which will undergo a big change. On the contrary, if the w_{reset} is low, the early-weight will have to travel a shorter distance to reach its value, so the late-weight will change less. The opposite phenomenon occurs for strong connections (graphs on the right). Indeed, at the end of the tonic, early-weights are high. They will therefore have to travel a shorter distance to reach a high w_{reset} than to reach a low one. The late-weight will therefore change less for a high w_{reset} than for a low one.

What's great about these observations is that the value of the w_{reset}, which is determined by the neuronal rhythm, fine-tunes the balance of how much we consolidate or depress.

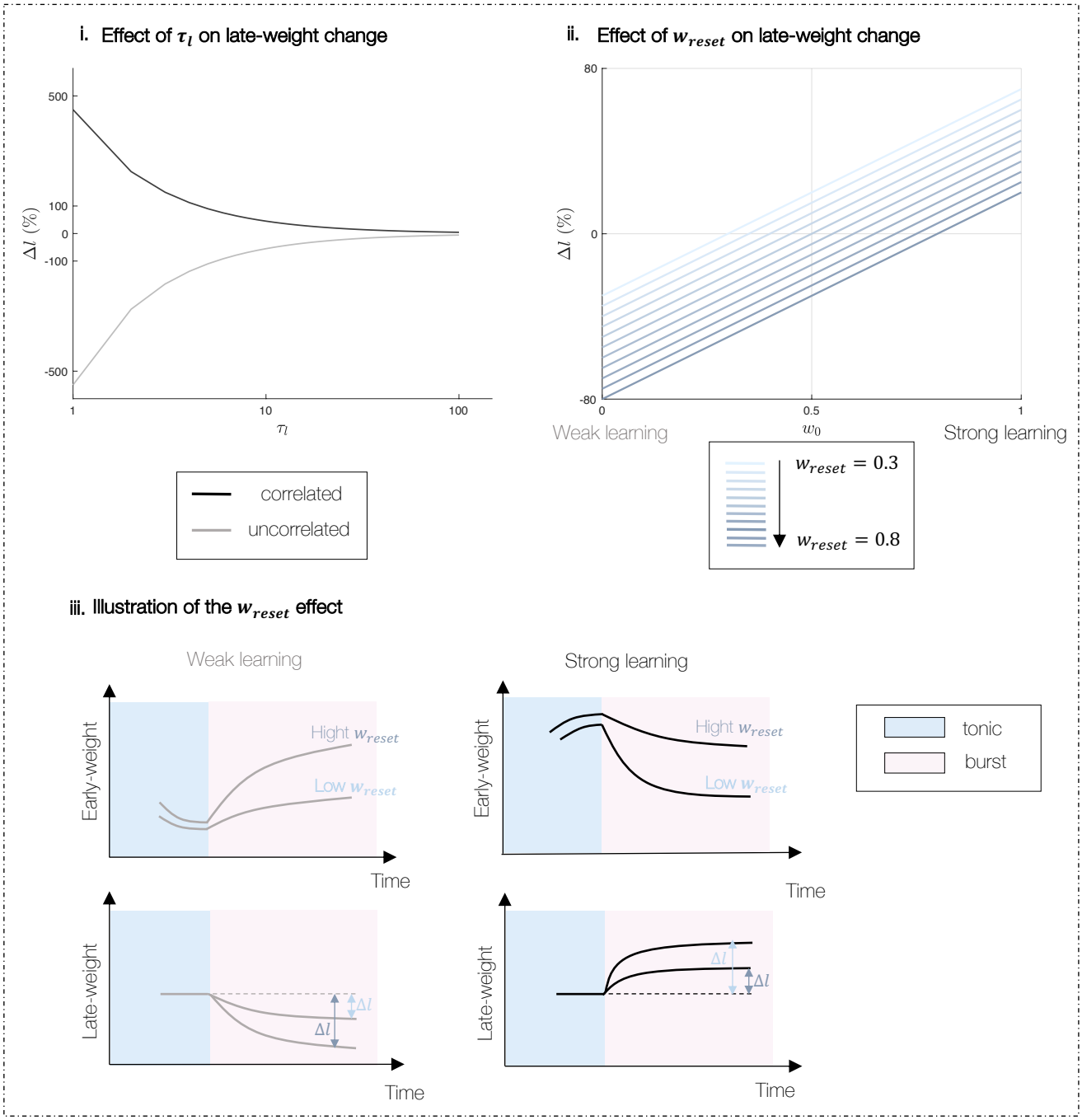

Figure 5.7 – **Effect of parameters on late weight change. i.** Change in late-weight (Δl in percentage) as a function of τ_l (x-axis graduation in logarithmic scale) for a strong connection (black) and for a weak connection (grey). The lower the τ_l, the greater the change in late-weight. **ii.** Change in late-weight (Δl in percentage) as a function of initial early-weight (w_0) for different values of w_{reset} (blue gradient: from light to dark for increasing w_{reset}). For a low w_{reset}, late-weight potentiation dominates its depression. The opposite is true for a high w_{reset}. **iii.** Illustration of the effect of w_{reset} for weak connections (left) and strong connections (right). Evolution of early-weight on top graphs for high and low w_{reset}. Impact on late-weight represented on lower graphs.

5.4 Adding heterogeneity to the neuronal network

In real life, neuronal networks are not as simple as the ones we've just illustrated. In fact, they are often much larger, and the network is not homogeneous. For the moment, we've only considered networks made up of neurons with the same properties. This is why, in this section, we add heterogeneity to the network, so that the intrinsic properties of its constituent neurons differ from one neuron to the next. More specifically, we vary the intrinsic conductances. We will also increase the size of the network.

5.4.1 Experiments

The experiments in this section are performed in the case of scenario 1. That is, when tonic activity is followed by burst activity and structural plasticity is implemented only during burst activity. This scenario was chosen because it seemed to be suitable for memory consolidation. Although this is also the case for scenario 2, the aim of this section is to show how the model behaves in the face of heterogeneity in the neuronal network, so it was not necessary to implement several scenarios.

Experiment 1: Adding heterogeneity to a small neuronal network

For this experiment, the same neuronal network as in section 5.2.2 (visible in Figure 5.2) is used with $\tau_l = 10$. It is thus composed of 3 presynaptic neurons connected to 2 postsynaptic neurons, forming 6 synaptic connections. The difference here is that we've added a 15% variability in the intrinsic conductances of the neurons in the network, which is now heterogeneous.

Experiment 2: Increasing the size of the neuronal network

In this experiment, a larger neuronal network consisting of 10 presynaptic and 10 postsynaptic neurons is considered. Again, all presynaptic neurons are connected to all postsynaptic neurons in a feedforward manner, forming a total of 100 synaptic connections. The spike frequencies of the neurons were chosen so as to have some correlated and some uncorrelated connections. The network is illustrated in Figure 5.8.

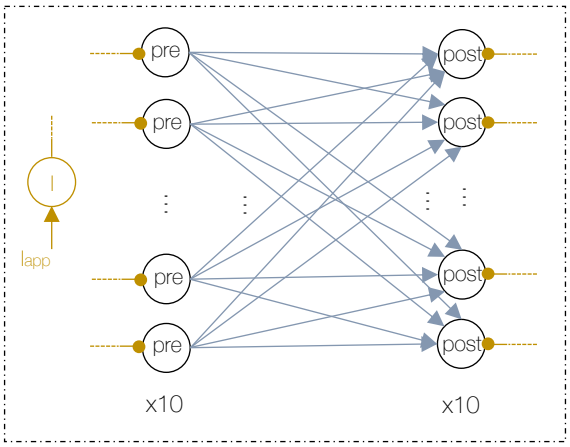

Figure 5.8 – **Neuronal network.** It is composed of 10 presynaptic neuron all connected to 10 postsynaptic neuron in a feedforward manner. An inhibitory neuron is connected to all neurons and an I_{app} current is applied to it.

Parameters:

- Frequency f_0 chosen to generate tonic activity:

Neuron	Tonic 1	Tonic 2
Pre 1 → 3	60 Hz	60 Hz
Pre 4 → 5	30 Hz	30 Hz
Pre 6 → 10	[0.1 - 2] Hz	[0.1 - 2] Hz
Post 1 → 4	40 Hz	40 Hz
Post 5 → 10	50 Hz	50 Hz

- Initial values:

w_0	l_0	τ_l
0.5	0.1	10

Experiment 3: Adding heterogeneity to the large neuronal network

The same compound neuronal network as in Experiment 2 is used (shown in Figure 5.8). It comprises 100 synaptic connections (formed by 10 presynaptic and 10 postsynaptic neurons). Here, as in Experiment 1, a 15% variability in neuron conductance is added.

5.4.2 Results

The results of the 3 experiments are shown in Figure 5.9. The graphs of early-weight evolution show that adding heterogeneity to the model results in heterogeneity in w_{reset} values. Indeed, in Experiments 1 and 3, where there is variability in the intrinsic conductances of neurons, not all early-weights converge to the same weight at the end of burst activity. This is due to the fact that neurons now have different properties, so they show different patterns of activity during burst. We know that the value of the w_{reset} is directed by the burst activity of the neurons, so if the burst pattern is different, the w_{reset} will also be different. In Experiment 2, the convergence value of the early-weights is the same for all connections, because in this case all neurons have the same intrinsic conductances and therefore present the same pattern of activity during the burst.

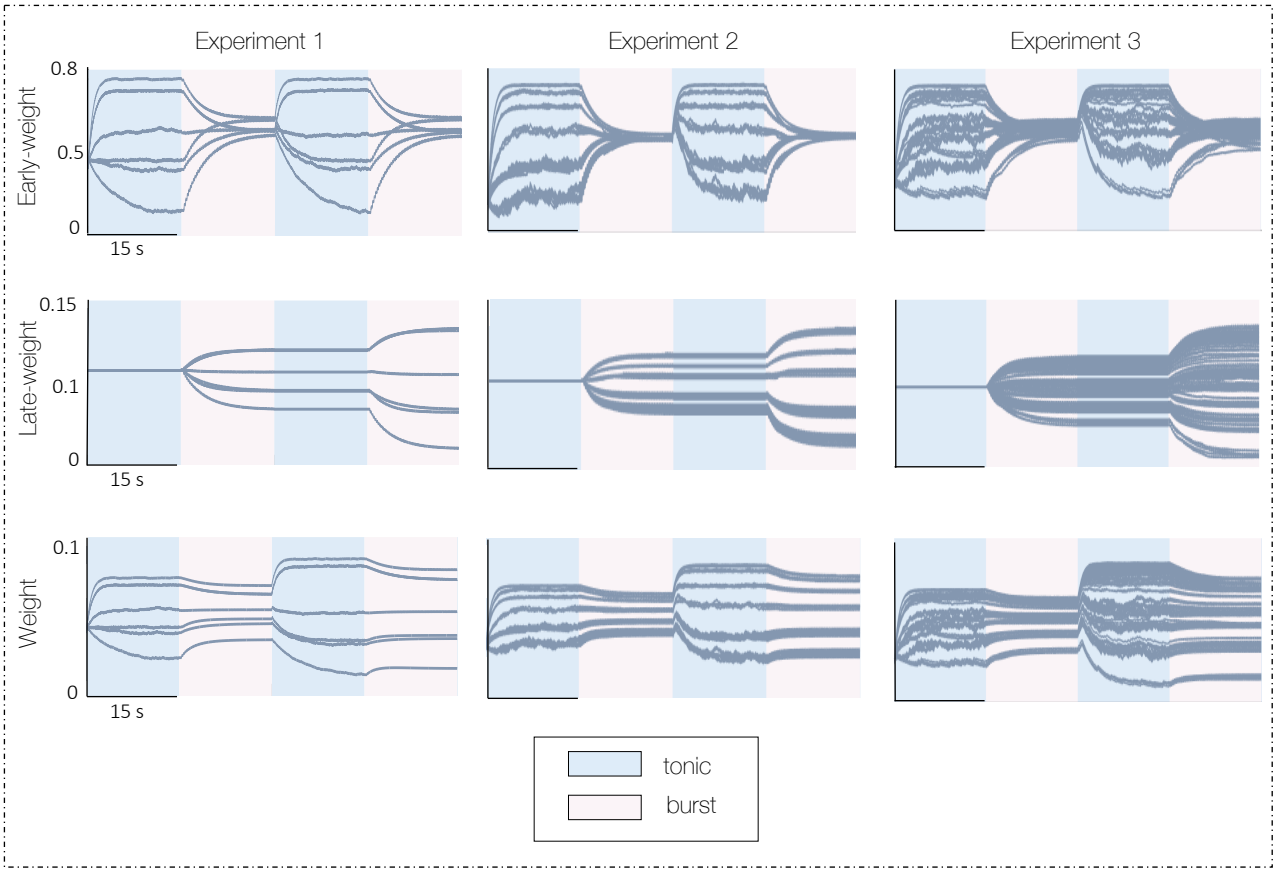

Figure 5.9 – **Results of the new structural plasticity rule with variability in the neuronal network.** Scenario 1 is implemented. That is, the simulation is carried out over two tonic/burst cycles and structural plasticity is only implemented during burst activity. For each experiment, early-weight, late-weight and weight curves are plotted. Experiment 1 uses the neuronal network illustrated in Figure 5.2, adding 15% variability in the intrinsic conductances of the neurons. In this network, there are therefore 6 connections in all. Experiment 2 uses the neuronal network shown in Figure 5.8, with a total of 100 synaptic connections. Experiment 3 uses the same network as Experiment 2, but adds 15% variability in neuron conductance.

As regards changes in late-weight and total weight, the size of the network or the addition of heterogeneity

seems to have no significant impact on their behavior. The only small impact it has is that the curves are more differentiated from each other in cases where there is variability in the properties of the neurons. Indeed, if we compare the curves of Experiments 2 and 3, the curves of Experiment 3 are more dispersed in values than those of Experiment 2. This result is to be expected, since the evolution of late-weight (which therefore also impacts the synaptic weight) is affected by the evolution of early-weight during burst activity, which, as we have just seen, was impacted by the addition of heterogeneity. Indeed, the early-weights converged to different w_{reset} at the end of the burst. Overall, however, the model's behavior is the same as in the experiments carried out in section 5.2.2. That is, strong connections see their synaptic weight increase and weak connections see their weight decrease relative to the initial weight value. The neuronal networks are thus able to retain information learned during tonic, but are also capable of learning new things. We can therefore conclude that the structural plasticity model proposed in this thesis appears to be robust to variability and neural network size.

5.5 New structural plasticity model with the phenomenological rule

Until now, early-weight was implemented using the traditional calcium-based plasticity rule. However, as we saw in Chapter 2, there is also a phenomenological model to describe the evolution of early-weight. This section is therefore dedicated to testing the new structural plasticity rule with this phenomenological model.

5.5.1 Model

It is necessary to adapt the structural plasticity model since the evolution of late weight is directed by a calcium-dependent equation (equation 5.4). We start from the same idea of using early-weight evolution to direct late-weight evolution. In the phenomenological model (more details on rule implementation in [Jacquerie et al., 2022a]), the evolution of the early-weight is based on the spike times of pre- and post-synaptic neurons, denoted t_{pre} and t_{post} respectively. The model (triplet model) is described as follows:

$$w(t) \longrightarrow \begin{cases} w(t) + x_1(t)(1-w)\left(A_2^+ + A_3^+ y_2(t)\right) & if \quad t = t_{post} \\ w(t) - y_1(t)w\left(A_2^- + A_3^- x_2(t)\right) & if \quad t = t_{pre} \end{cases} \tag{5.9}$$

where $x_1(t)$ and $x_2(t)$ are the traces of the presynaptic neurons and $y_1(t)$ and $y_1(t)$ are the traces of the postsynaptic neurons. A_2^- and A_3^- are the depression constants and A_2^+ and A_3^+ are the potentiation constants. Based on this equation, we defined the evolution of late-weight as follows:

$$\begin{cases} \tau_l \dot{l} = x_1(t)(1-w)\left(A_2^+ + A_3^+ y_2(t)\right) & if \quad t = t_{post} \\ \tau_l \dot{l} = -y_1(t)w\left(A_2^- + A_3^- x_2(t)\right) & if \quad t = t_{pre} \end{cases} \tag{5.10}$$

The closer the presynaptic neuron spikes and just before the postsynaptic neuron spikes, the more potentiation is promoted. Conversely, if the presynaptic spike is just after the postsynaptic spike, this favors depression.

5.5.2 Experiments

The neuronal network used is illustrated in Figure 5.10. In fact, we consider 6 small circuits consisting of one presynaptic and one postsynaptic neuron. In each circuit, an inhibitory neuron is connected to the presynaptic and postsynaptic neurons to modulate their electrical activity. Of the 6 synaptic connections, 3 are correlated and 3 uncorrelated. Since potentiation and depression of the weights depend on the spike times of the neurons, the protocol for obtaining correlated and uncorrelated connections is different from that used with the calcium rule. In this case, to obtain potentiation, we need to ensure that we have pre-post spike pairs, and to obtain depression, we need to have post-pre spike pairs. Spike frequencies used are the same for correlated and uncorrelated connections, but with different spike times, so that for correlated connections the presynaptic neuron spikes before the postsynaptic neuron, and for uncorrelated connections it's the other way around. Note that in this section, τl is set to 0.1, which

is smaller than in the calcium rule. This is because the change in early-weight with the phenomenological model is faster than with the calcium model. τl has been chosen so that the late-weight evolves with similar amplitudes as previously, when the calcium rule was used.

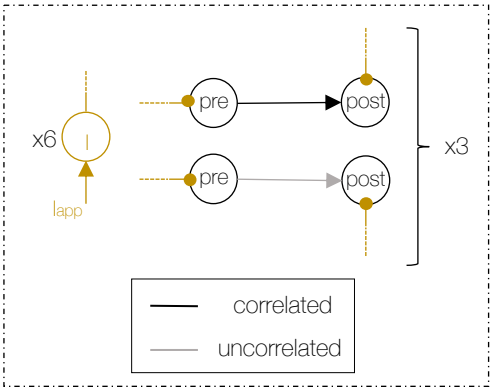

Figure 5.10 – **Neuronal network used with the phenomenological model.** It consists of 6 small circuits, each composed of a presynaptic neuron connected to a postsynaptic neuron. 3 of the circuits form a correlated connection and the other 3 an uncorrelated connection. Each circuit contains an intbiting neuron connected to presynaptic and postsynaptic neurons.

Parameters:

- Frequency f_0 chosen to generate tonic activity:

Neuron	Pre	Post
1	5 Hz	5 Hz
2	10 Hz	10 Hz
3	20 Hz	20 Hz

- Initial values:

w_0	l_0	τ_l
0.5	0.1	0.1

5.5.3 Results

The results are shown in Figure 5.11. Scenarios 1 and 2 were used, as both appeared to be consistent with memory consolidation. The neural network is therefore simulated over two successive periods of tonic activity and burst activity. In scenario 1 (graphs on the left), structural plasticity is implemented only during the burst period, whereas in scenario 2 (graphs on the right), it is implemented throughout the simulation.

For both scenarios, all curves (early-weight, late-weight and weight) have the same shape as those with the calcium rule (see Figure 5.4). Correlated connections have their overall weight increased over time (although it is slightly decreased during burst activity). On the contrary, uncorrelated connections show an overall decrease in weight. What differentiates scenario 1 from scenario 2 is that, at the end of the simulation (at the end of the 4 states), for correlated connections, the final value of late-weight and weight are higher in scenario 2. The opposite is observed for uncorrelated connections. This is due to the fact that, for scenario 2, the late-weight evolves during all the states of the simulation, whereas for scenario 1, it only evolves during every other state. However, over two tonic/burst cycles, the evolution remains reasonable and weights do not saturate.

We can conclude that, whatever the traditional synaptic plasticity rule used, the structural plasticity model we are proposing enables memory consolidation. Indeed, it takes advantage of the homeostatic reset observed with traditional rules to consolidate memory. By combining the two plasticity rules (traditional rule and structural plasticity rule), neurons are able to retain information even when their electrical activity changes, and are also capable of learning new things.

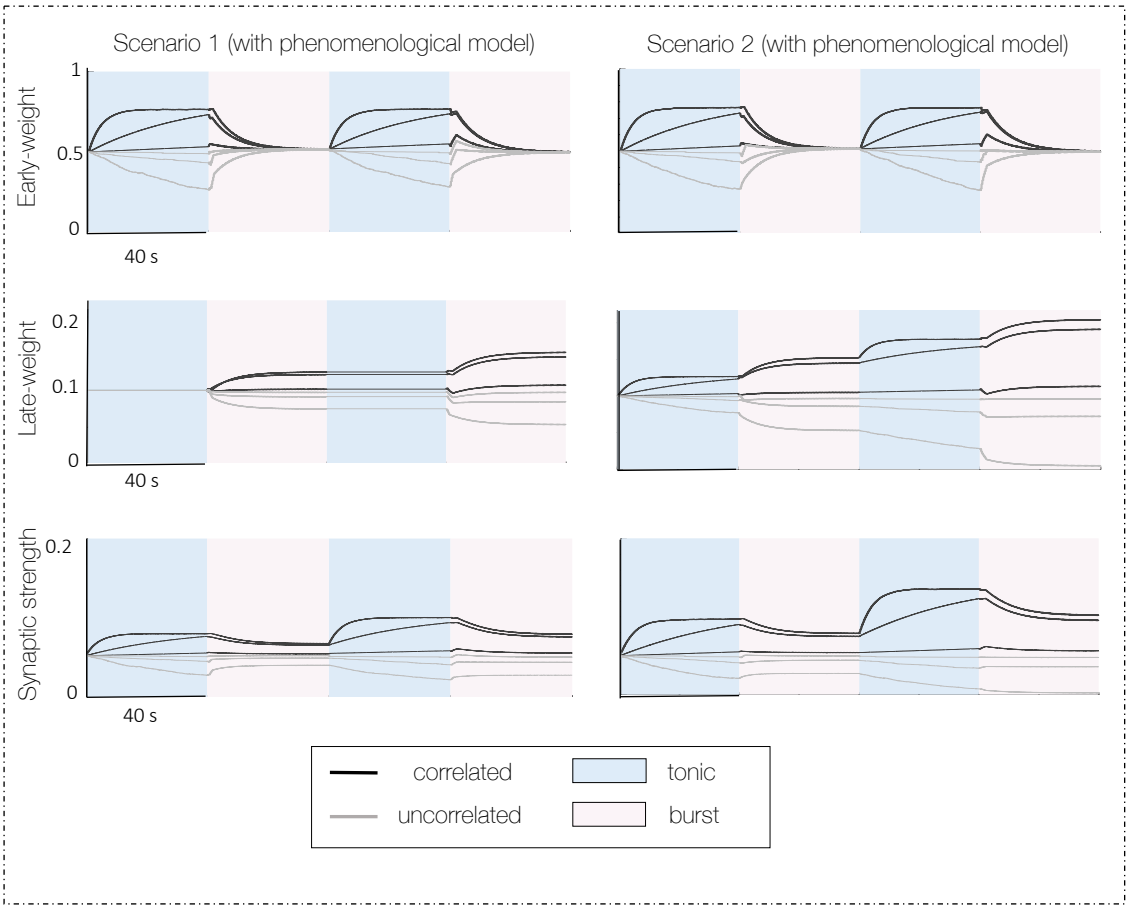

Figure 5.11 – **Results of the new structural plasticity rule with the phenomenological model.** Scenario 1 consists of a succession of tonic and burst periods, with structural plasticity implemented only during burst activity. Scenario 2 is the same as scenario 1, with the difference that structural plasticity is implemented throughout the simulation (in both tonic and burst periods). Early-weight, late-weight and weight curves are shown (in black for correlated connections and in grey for uncorrelated ones). The neuron circuit used is that shown in Figure 5.10.

Chap 5 : creation of a structural plasticity model

Model

Simplified form:

$$\tau_l \, \dot{l} = -\dot{w}$$

(during the burst activity)

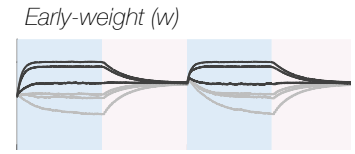

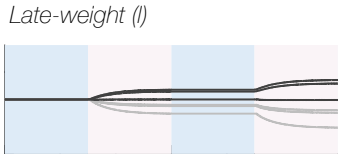

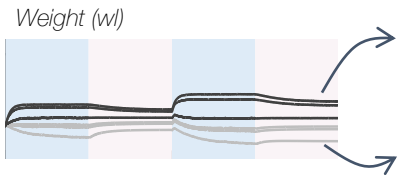

Model able to take advantage of homeostatic reset to transfer learning

Robustness test

Increased network size ✓

Adding heterogeneity to neuron conductances ✓

With phenomenological model ✓

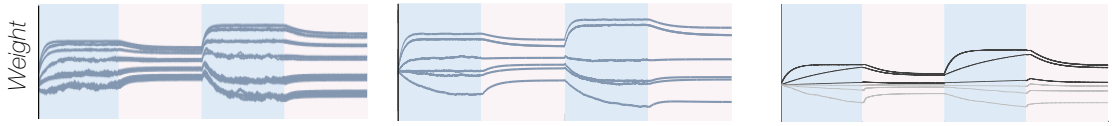

Influence of parameters

Effect of w_{reset}

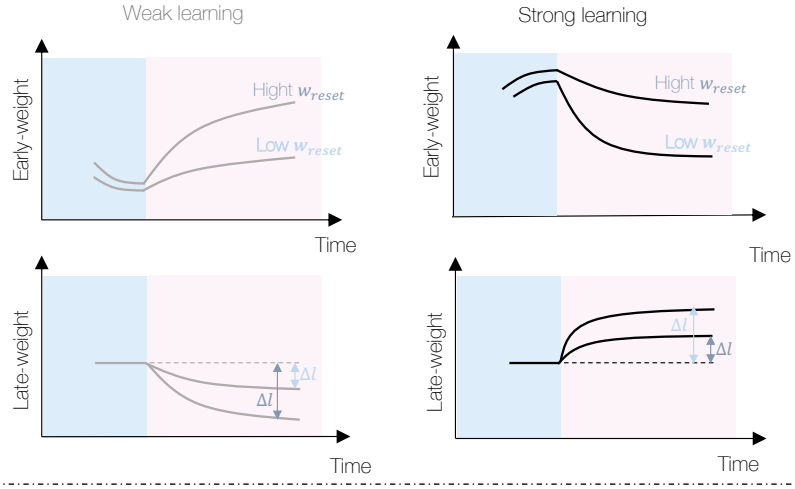

The value of w_{reset} (driven by neuronal rhythm during the burst activity) dictates the extend to which consolidation and depression occur

Chapter 6

Application of the new structural plasticity model

6.1 Model efficiency

6.1.1 Experiments

To test the effectiveness of our proposed plasticity model, a memory task similar to that proposed by [González-Rueda et al., 2018] is performed. This will enable us to study memory consolidation when neurons switch activity. Initially, we use a smaller network than that proposed by [González-Rueda et al., 2018]. Indeed, as illustrated in Figure 6.1, here we first use a network composed of 10 presynaptic neurons connected to 1 postsynaptic neuron in a feedforward manner. One of the 10 presynaptic neurons is paired with the postsynaptic neuron, while the other 9 are not. The way in which neuron activity is generated is the same as that used in Chapter 5, described in section 5.1.2. As a reminder, spike times are generated with inter-spike intervals following independent normal distributions $\mathcal{N}\left(\frac{1}{f_0}, (\frac{0.1}{f_0})^2\right)$ where f_0 is chosen according to the desired activity. To obtain the correlated connections, f_0 is chosen high and for the 9 uncorrelated connections, it is chosen low, between 0.1 and 2 Hz.

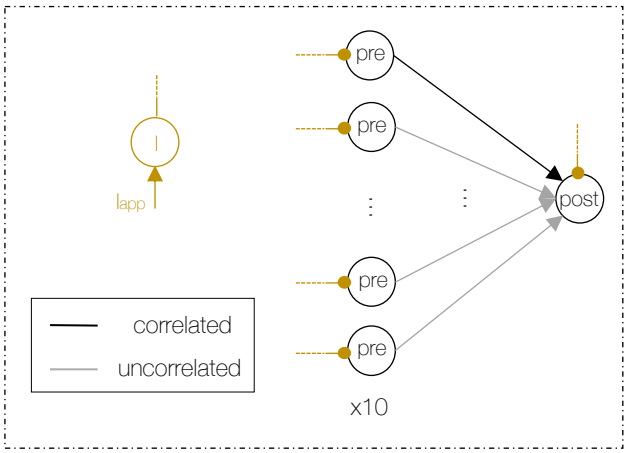

Figure 6.1 – **Neural network used to test model efficiency.** It consists of 10 presynaptic neurons connected to 1 postsynaptic neuron. One connection is correlated, while the other 9 are uncorrelated. An inhibitory neuron is connected to the neurons to modulate their electrical activity.

Parameters:

- Frequency f_0 chosen to generate tonic activity:

Neuron	frequency
Pre 1	60 Hz
Pre 2-10	[0.1-2] Hz
Post	40 Hz

- Initial values:

w_0	l_0	τ_l
0.5	0.1	10

The three scenarios described and tested in Chapter 5 are used again here and compared with each other. Moreover, a scenario 0 is also implemented to show the full benefit of structural plasticity in memory consolidation. This scenario is presented in Table 6.1 and is similar to scenario 1 (tonic-to-burst activity switches), but where structural plasticity is not implemented. As a reminder, scenario 1 consists of a succession of activity switches from tonic to burst, in which structural plasticity is implemented in burst only. Scenario 2 is the same as scenario 1, with the difference that structural plasticity is also implemented in tonic activity. For scenario 3, burst activity is blocked and consists of a succession of tonic and inactive periods (scenarios shown in Table 5.1). In this section, It should also be noted that the simulations are carried out over a duration of 150 s (i.e. 10 states of 15 seconds each).

		State 1	**State 2**
Scenario 0	*Neuronal activity*	Tonic	Burst
	Structural plasticity	OFF	OFF

Table 6.1 – **Scenario 0 settings.**

To analyze the results and interpret the neuronal network's ability to store information, the signal-to-noise ratio (SNR) is calculated. To calculate it, we use the formula proposed by [González-Rueda et al., 2018]:

$$\text{SNR} = \frac{max(wl)}{mean(wl)} \tag{6.1}$$

6.1.2 Results

The results of the simulations described above are shown in Figure 6.2. For each scenario, the weight curves (product of early-weight (w) and late-weight (l)) are shown on the top graphs. In addition, the SNR calculated at each end of state is shown on the lower graphs.

In scenario 0 (Figure 6.2, top left), where no structural plasticity is implemented, the weight curves undergo homeostatic reset. This is reflected in the SNR, which follows the same trend as the weight curve. In fact, during tonic periods, SNR is increased, but with each switch to burst activity, it is decreased. Switching to burst activity therefore leads to a downscaling of the neural network, preventing SNR from improving over the course of the simulation. Indeed, it never exceeds the value of 2 during the 10 states, showing that the neuronal network is unable to consolidate memory in this case.

In scenario 1 (Figure 6.2, top right), where structural plasticity is implemented in burst activities, the weight curves no longer show the homeostatic reset and increase for correlated connections and decrease for uncorrelated connections over time. This is reflected in the SNR, which has an increasing trend over time, since the SNR after the first state is less than 2 and reaches a value close to 6 after the 10th state. This means that the neural network is consolidating information over time. However, it is interesting to note that the evolution of the SNR is not monotonic throughout the simulation. Indeed, the first switches to burst activity (e.g. from state 1 to state 2) will show a downscaling of the network as observed in scenario 0, as the SNR decreases. However, it is important to note that this downscaling is less pronounced than in scenario 0, meaning that "less" information is lost when switching to burst activity. After a certain state, this downscaling phenomenon disappears and the switch to burst activity leads to an increase in SNR (as can be seen from the switch from state 9 to state 10). This is a brilliant phenomenon, because during the burst, the neuronal network receives no information to learn, yet manages to consolidate the information.

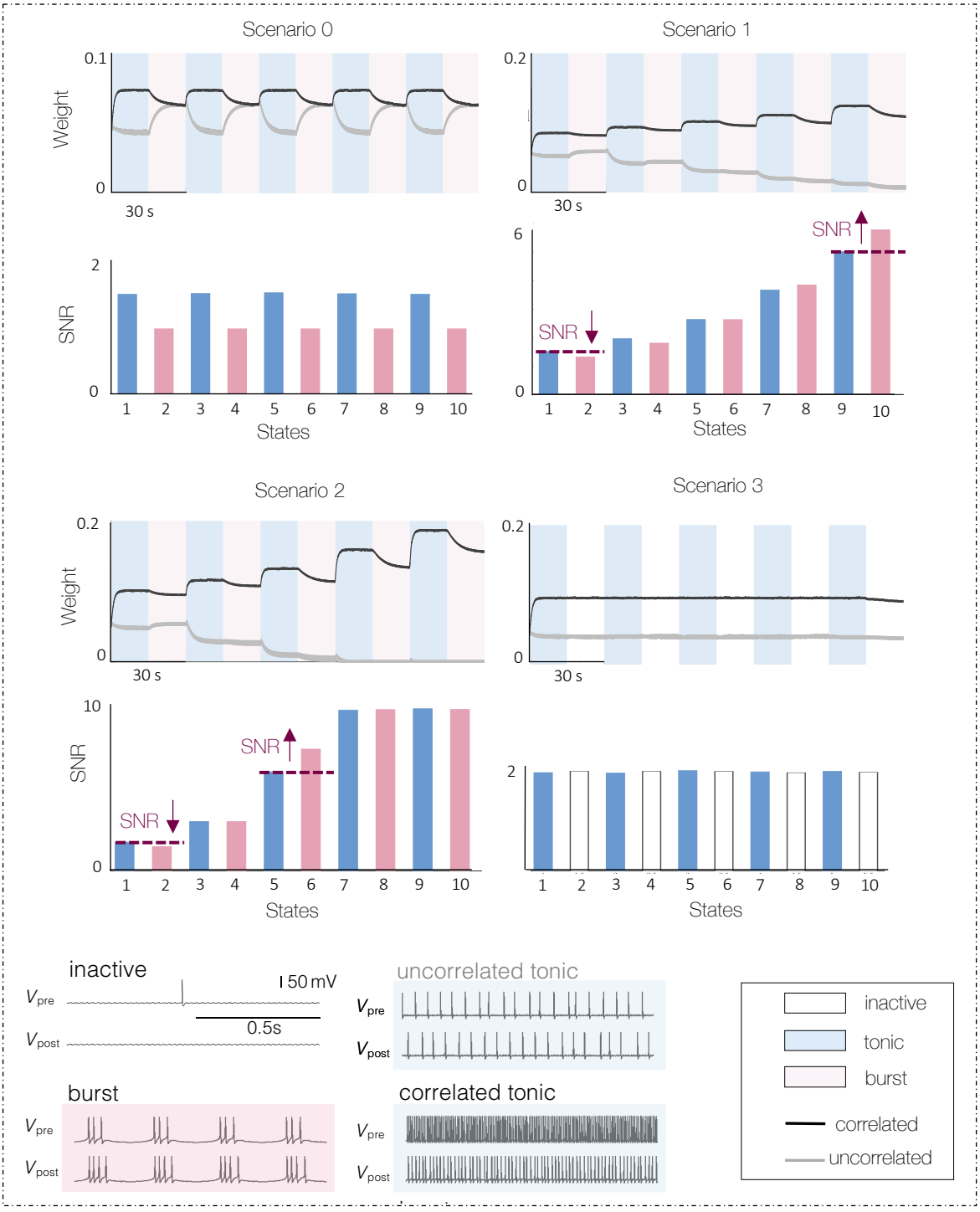

Figure 6.2 – **Results of the simple memory task for different scenarios.** 4 scenarios were tested: scenario 0 consists of a succession of tonic and burst periods in which no structural plasticity is present; scenario 1 is similar but with structural plasticity present during burst; scenario 2 is also the same but in which structural plasticity is implemented during tonic and burst; scenario 3 consists of a succession of tonic and inactive periods, in which structural plasticity is implemented throughout the simulation. For each scenario, the evolution of weight (product of early weight (w) and late weight (l)) is shown, along with the SNR (calculated for each state from equation 6.1). Implementing structural plasticity improves SNR over time. During the initial cycles, the SNR decreases with the transition to burst activity, while after a certain time, it increases (shown in burgundy). The neural network used is the one depicted in Figure 6.1. Diagram of the different electrical activities taken from [Jacquerie, 2023]

In scenario 2 (Figure 6.2, bottom left), the weight and SNR curves behave in the same way as in scenario 1. The difference is that their evolution is more rapid, since structural plasticity is also implemented during tonic periods. In the first cycles, a downsclaing of the network is observed during the transition to burst activity (decrease in SNR), whereas after a while, the transition to burst activity leads to memory consolidation (increase in SNR). However, an additional phenomenon can be observed in this scenario: from state 7 onwards, an SNR saturation occurs. Indeed, during the last 4 states, the SNR remains at the same value. This is due to the fact that the weights of uncorrelated connections have reached their lower limit (i.e. 0). This can be interpreted by the fact that there are no longer any connections between neurons. If we draw a parallel with the models proposed by [Deger et al., 2012] and [Fauth and van Rossum, 2019] described in Chapter 4, these "no longer existing" connections between uncorrelated neurons can be seen as the transformation of the synapse from functional to non-functional. At this stage, information is neither forgotten nor consolidated. We will see later (in section 6.3) what happens when the simulation runs longer.

Finally, for scenario 3 (Figure 6.2, bottom right), where burst activity is blocked, the saturation observed on the weight curves (from state 2 to state 10, the curves hardly change at all) is reflected on the SNR, which also saturates and remains at the same value throughout the simulation. Although the neuronal network seems to retain information (as the SNR remains at 2), it is unable to consolidate it or learn anything new. It should be noted that a slight decrease in weight, and therefore SNR, can be observed in the inactive period (as in state 10, for example). This is due to the fact that the neurons spike very little and therefore the weight depresses slightly.

6.1.3 Conclusion

The results show that combining our structural plasticity rule with a traditional plasticity rule enables an improvement in SNR over time in the presence of tonic-to-burst switches. This model thus enables information storage and memory consolidation, which was not the case without structural plasticity. Indeed, without structural plasticity, when switching to burst activity, there is a downscaling of the neuronal network that forgets the learned information due to the homeostatic reset of the weight. Furthermore, the results showed that without burst activity, the neural network was unable to consolidate memory, given the saturation of the SNR. Finally, an interesting phenomenon was highlighted when structural plasticity is implemented. After a certain point, bursting plays a different role in memory consolidation. Initially, SNR decreases with the transition to burst activity and network downscaling occurs. Then, it increases with the transition to burst activity and memory consolidation takes place. From this point onwards, neurons continue to learn during burst periods, when they no longer receive external stimulation. This is a powerful phenomenon, and it is interesting to know when it occurs and what causes it. This will be discussed in the next section.

6.2 Why does bursting play a different role in memory consolidation from a certain point onwards?

6.2.1 Cause

To answer this question, it is necessary to take a closer look at the early-weight curve, late-weight curve, and total weight curve. These are shown in Figure 6.3 for scenario 1. In the graph of the early-weight curve (top-left graph), it can be observed that the value of w_{reset} decreases during the simulation. In Chapter 5, we learned that this has an influence on the evolution of the late-weight. Specifically, the value of w_{reset} determines the extent to which late weights are consolidated, and the extent to which they are exceeded. A high value of w_{reset} (as in the early cycles of the simulation) favors depression over consolidation, while a low value of w_{reset} (as towards the end of the simulation) favors consolidation over depression. This effect can be directly seen in the late-weight curve (middle-left graph), which shows a decreasing depression over the course of the simulation.

But what causes the change in the value of w_{reset} over time?

We know that w_{reset} is influenced by the burst activity of neurons, and we can see that it is modified during the simulation. As shown in the two insets of Figure 6.3, during the first burst activity, the postsynaptic neuron exhibits bursts of 5 spikes, while during the last burst activity, it only exhibits 4 spikes. This is because the connectivity between neurons changes over time, and therefore the activity of the postsynaptic neuron is influenced by the activity of the presynaptic neurons. In fact, everything is interconnected: the electrical rhythm of neurons affects structural plasticity and, in turn, the SNR. However, structural plasticity, which defines the connectivity between neurons, also affects their rhythm, as the influence neurons have on each other changes (due to the change in connectivity).

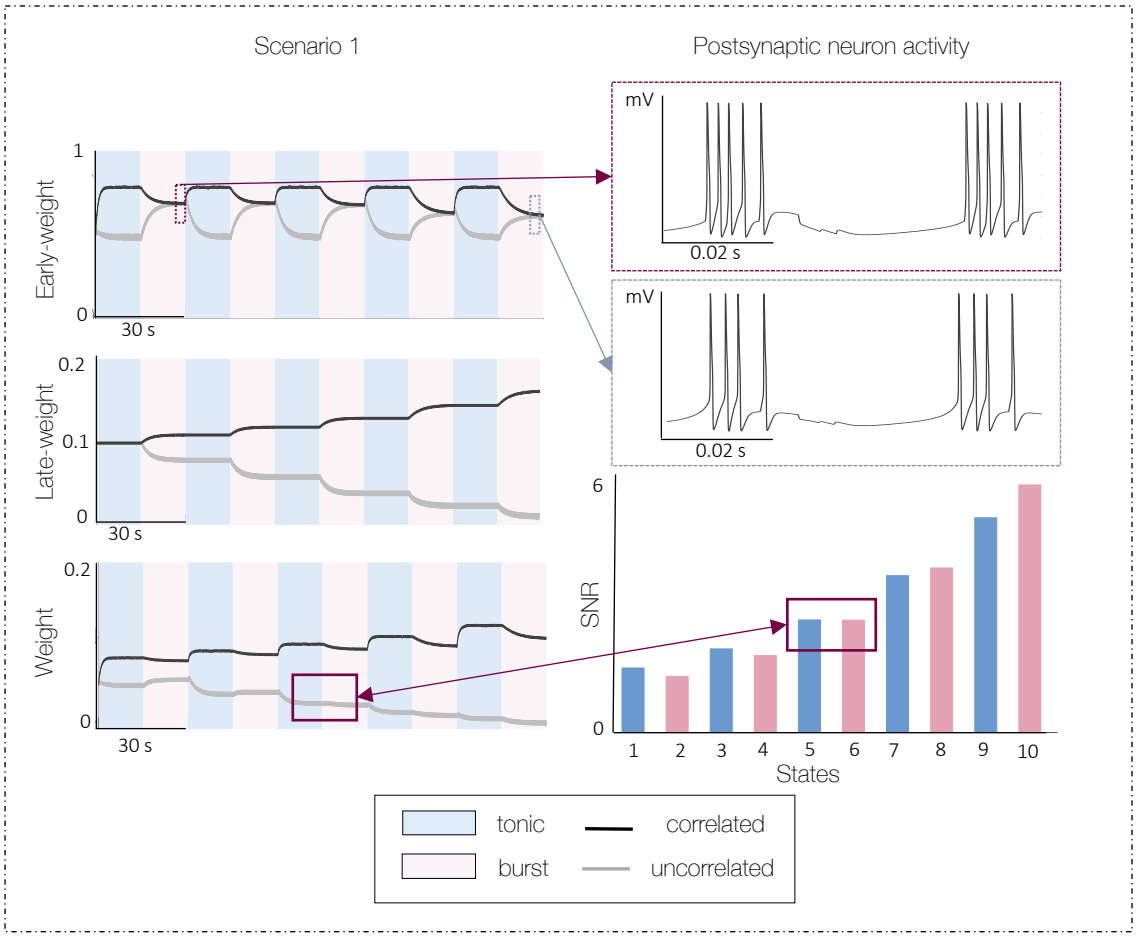

Figure 6.3 – **Causes of the change in SNR behavior.** To highlight this phenomenon, early-weight, late-weight and weight curves are shown (for scenario 1). The w_{reset} decreases over the course of the simulation, due in particular to the change in postsynaptic neuron activity during the burst period. This is shown by the two dotted boxes illustrating the neuron's electrical activity during the first burst (in burgundy) and during the last burst (in blue). The SNR begins to increase in burst from the moment the slope of the weight at the start of burst activity is negative for the uncorrelated connections (shown by the burgundy rectangles in solid lines).

6.2.2 Calculating the moment at which memory consolidation emerges during burst activities

Naive approach

If we take a closer look at the weight curve (bottom graph) and SNR in Figure 6.3, we can see that the change in SNR behavior occurs when there is a change of sign in the weight curves of uncorrelated connections (gray curves). Indeed, in the second burst (state 4), the low weights increase, resulting in a decrease in SNR. At the fourth burst (state 8), however, low weights decrease, resulting in an increase in SNR. I have illustrated this phenomenon in Figure 6.4 for a clearer understanding.

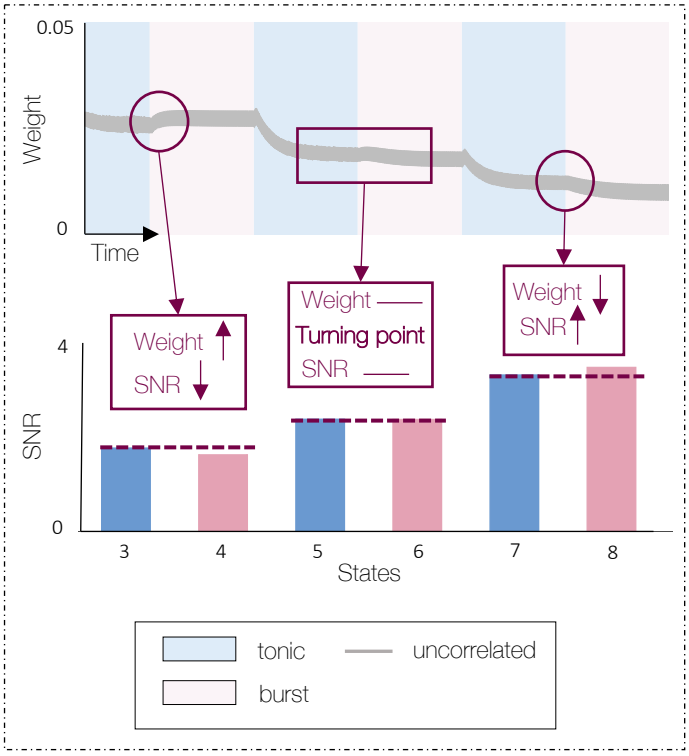

Figure 6.4 – **Configuration at which memory consolidation emerges during burst activities.** The evolution of synaptic weights (product of early weight (w) and late weight (l)) for uncorrelated connections is shown in the top graph (graph zoomed in at bottom left of Figure 6.3). The SNR is shown on the lower graph for states present on the weight evolution graph (also zoomed in from the SNR graph in Figure 6.3). When the weight of uncorrelated connections increases during burst activity (as in state 4), this results in a decrease in SNR. When the weight decreases during burst (as in state 8), this results in an increase in SNR. SNR remains stable when the weight remains constant at the transition to burst activity. This is the turning value between downscaling and consolidation.

The naive approach is to say that the moment of transition between the downscaling of the neuronal network and its consolidation at the switch to burst activity is when the synaptic weight remains constant (as shown in Figure 6.4). However, it is important to note that this approach is only valid when the weights have not yet reached their lower limit, i.e. 0. Indeed, once they reach 0, the SNR remains constant. Mathematically, the transition from downscaling to consolidation occurs when, for uncorrelated connections:

$$w_{tonic} l_{tonic} = w_{burst} l_{burst} \tag{6.2}$$

where w_{tonic} and l_{tonic} are respectively the early and late weights at the end of the tonic period, and w_{burst} and l_{burst} are respectively the early and late weights at the end of the burst period. It is worth noting that here we

are only focusing on uncorrelated connections, because according to observations, it's their behavior that drives SNR behavior. The fact that they have more influence than the correlated connections could simply be due to the fact that there are 9 uncorrelated connections, whereas there is only one correlated connection. In chapter 5, we showed that during the burst period, the late-weight converges to $l_0 - \left(\frac{w_{reset}-w_0}{\tau_l}\right)$ (Equation 5.8). In our case, l_0 and w_0 correspond respectively to the late-weight and early-weight at the end of tonic, i.e. l_{tonic} and w_{tonic}, and w_{reset} corresponds to the early-weight at the end of burst, i.e. w_{burst}. We can therefore rewrite: $l_{burst} = l_{tonic} - \left(\frac{w_{burst}-w_{tonic}}{\tau_l}\right)$. In this way, we have

$$\begin{aligned} w_{tonic}l_{tonic} &= w_{burst}\left(l_{tonic} - \left(\frac{w_{burst} - w_{tonic}}{\tau_l}\right)\right) \\ w_{tonic}l_{tonic} - w_{burst}l_{tonic} &= -\left(\frac{w_{burst}^2 - w_{burst}w_{tonic}}{\tau_l}\right) \\ l_{tonic}\left(w_{tonic} - w_{burst}\right) &= -\frac{w_{burst}}{\tau_l}\left(w_{burst} - w_{tonic}\right) \end{aligned}$$

This results in

$$l_{tonic} = \frac{w_{burst}}{\tau_l} \tag{6.3}$$

In order to be even more precise, it is better to average out the uncorrelated connections and therefore consider l_{tonic_mean} in equation 6.3 instead of l_{tonic}. The term l_{tonic_mean} corresponds to the average of the values of the late-weights of the uncorrelated connections at the end of the tonic period. This equation means that as soon as the late-weight of uncorrelated connections at the end of the tonic (l_{tonic}) becomes smaller than the early-weight at the end of the burst (w_{burst} which corresponds to the w_{reset}) divided by τ_l (the time constant of the late-weight), the weight curve decreases during the burst. This means that from then on, burst periods reinforce the forgetting of uncorrelated connections. This was not the case before, as the weight curves increased during the burst, resulting in the memory of uncorrelated connections being reinforced. The SNR is therefore improved as "useless information" (which can be considered as noise) is "eliminated". The fact that neurons forget useless information means, in a way, that learned information is consolidated. Although somewhat simplified, the term *memory consolidation* is used in this section to refer to an increase in SNR. It is also interesting to note that the value of w_{reset} can be predicted in advance. Indeed, [Ponnet, 2022] demonstrated the value to which it converges. We can therefore predict at the end of tonic activity whether the neuronal network will be able to consolidate the information during the burst that follows. Although this result seems to be verified by simulations, it remains an approximation and a naive approach. A more realistic approach is preferable.

Realistic approach

There are various approaches to finding the point at which SNR improves during bursts. We have just seen that this moment corresponds to the instant when the slopes of the weight curves of uncorrelated connections change sign during burst activity. As a reminder, SNR decreased during bursts when the weight curves increased (positive slope), and increased when the curve decreased (negative slope) (see Figure 6.4). One approach is therefore to develop the expression for the slope of the weight curves as follows:

$$\begin{aligned} \frac{d}{dt}(wl) &= \dot{w}l + w\dot{l} \\ &= -\tau_l\dot{l}l + w\dot{l} \end{aligned}$$

because $\tau_l\dot{l} = -\dot{w}$ during the burst activity (see definition of late-weight in Chapter 5). So we have:

$$\frac{d}{dt}(wl) = (w - \tau_l l)\,\dot{l} \tag{6.4}$$

Equation 6.4 means that, depending on the sign of $(w - \tau_l l)$, the slope of the weight (wl) will be of the same sign or not as the slope of the late-weight (l). In our case, for the network to consolidate memory during the burst, we want the slope of the weight to be negative for uncorrelated connections (as shown in Figure 6.4). We know that for an uncorrelated connection, the slope of the late-weight is negative, as shown in Figure 6.5. To consolidate memory, wg must therefore have a slope of the same sign as the slope of l. To achieve this, $(w - \tau_l l)$ must be positive, i.e. when $l < \frac{w}{\tau_l}$, which verifies equation 6.3.

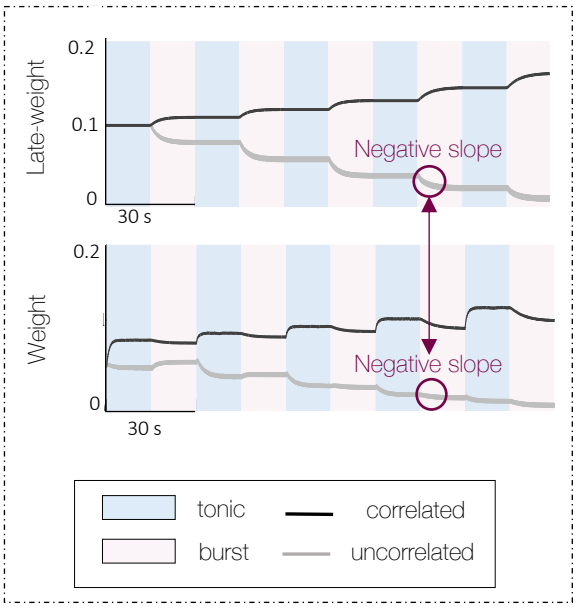

Figure 6.5 – **Late-weight and weight slopes highlighted.** The graphs of late-weight (top graph) and weight (bottom graph) are taken from Figure 6.3. When the slope of the weight for uncorrelated connections is negative, the slope of the late-weight is also negative. At this point, weight and late-weight have the same sign of slope.

To conclude this paragraph, in the simple memory task proposed here, the neuronal network begins to consolidate memory in burst period when at time t, $l(t) < \frac{w(t)}{\tau_l}$ for uncorrelated connections, $l(t)$ representing the late-weight at time t and $w(t)$ the early-weight at the same time. When the late-weight has not yet reached this value, the neuronal network forgets information when switching to burst activity.

6.3 Influence of parameters on SNR

6.3.1 Effect of τ_l

First, the effect of the late-weight time constant (τ_l) on SNR behavior is analyzed. The results are shown in Figure 6.6. The greater the τ_l, the slower the increase in SNR over time. Indeed, we can see that for $\tau_l = 5$ (left graph), as early as state 2, the neuronal network consolidates memory during the burst. In addition, the SNR reaches a value of 10 as early as state 8 and saturates thereafter. In contrast, when $\tau_l = 15$, 10 states is not enough for memory consolidation during the burst, and by state 10, the SNR has not even reached a value of 4. By tuning the value of τ_l, we can determine the speed at which the neuronal network learns.

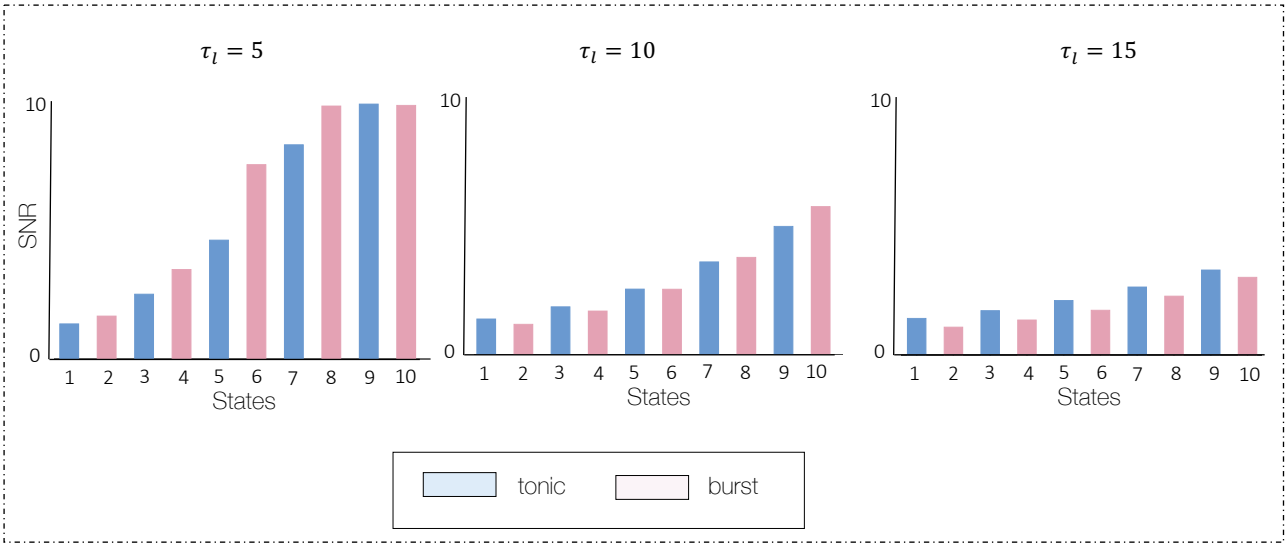

Figure 6.6 – **Effect of τ_l on SNR.** SNR is plotted for $\tau_l = 5$ (left graph), for $\tau_l = 10$ (middle graph) and for $\tau_l = 15$ (right graph). As τ_l increases, SNR rises more slowly. The neuronal network simulated is that shown in Figure 6.1.

6.3.2 Influence of a longer simulation period

To see the effect of a longer simulation period, a smaller tau_l is used, i.e. $\tau_l = 5$. In this way, as we have just seen, the SNR will evolve more rapidly. The results are shown in Figure 6.7.

First of all, around state 9, there is a period of SNR saturation. This has already been discussed in section 6.1.2, as it has already been observed. As a reminder, this saturation occurs because the late-weight reaches its minimum value and saturates at 0. After this saturation period, the SNR starts to decrease. This is due to the fact that the late-weight curve starts to rise again, as can be seen in the middle graph in Figure 6.7. This is explained by the fact that there is an over-connection occurring in the neuronal network (i.e. the connections between neurons become too strong). On the early-weight curve (top graph in Figure 6.7), from a certain point onwards, uncorrelated connections are no longer able to depress during tonic periods. These connections are therefore potentiated. Biologically, this happens because the correlated connection becomes so strong that it brings a large quantity of calcium into play. This calcium will then influence the uncorrelated connections, which will potentiate. If we want to avoid this phenomenon of over-connections, we need to define an appropriate maximum value for the late-weight. This has been extensively discussed in the Master thesis of Emmy Kellens.

6.3.3 Effect of l_0

Up to now, l_0 has always been set to 0.1, which means that we initialize the late-weight of all connections to this value. However, as Emmy Kellens shows in her Master thesis, this initialization value is high. Indeed, by choosing a value of l_0 that is too high, l will quickly reach large values, and there is a risk of encountering the over-connection situation described earlier, at a faster pace. That is why in this section, several lower values of l_0 are tested to see the impact this has on the SNR. The neuronal network used for the simulation is always the one shown in Figure 6.1, with its corresponding parameters. Weight curves and SNR are shown for three different values of l_0 in Figure 6.8 (left for $l_0 = 0.04$, middle for $l_0 = 0.07$ and right for $l_0 = 0.1$).

Concerning the weight curves, we can see that the smaller l_0 is chosen, the faster the uncorrelated connections (gray curves) saturate at 0. This result is logical, since by choosing a smaller value of l_0, fewer values remain for the late weight to reach the value of 0. As a result, saturation of the SNR occurs earlier in the simulation. Indeed,

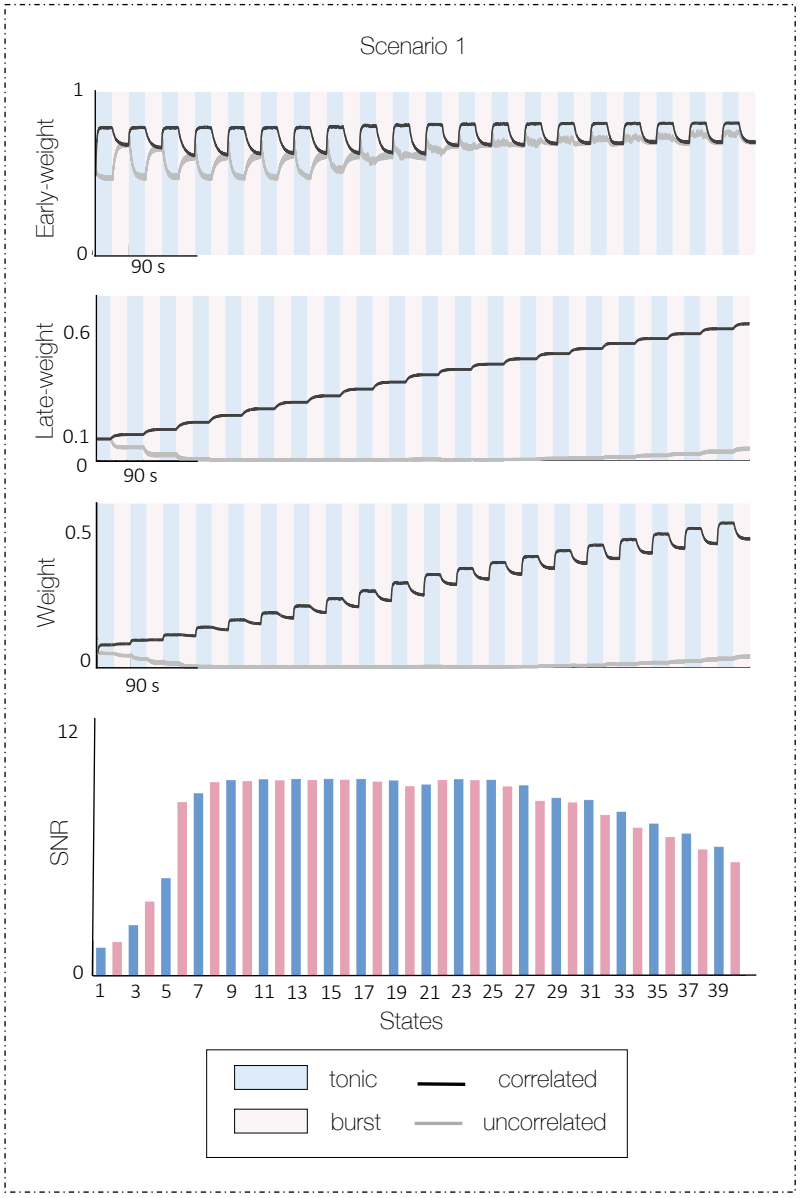

Figure 6.7 – **Effect of a long simulation period on SNR.** The neuronal network shown in Figure 6.1 with $\tau_l = 5$ was simulated over a period of 600 seconds (i.e. 40 states). The evolution of early-weight (top left graph), late-weight (middle graph) and weight (bottom graph) are shown, along with the SNR calculated at the end of each state (right graph). The SNR exhibits saturation due to the late-weight saturating at 0. Subsequently, the SNR decreases as a result of neuronal network over-connection, which leads to the potentiation of early-weights in uncorrelated connections.

for $l_0 = 0.04$, a saturation of the SNR is observable whereas for $l_0 = 0.07$ and $l_0 = 0.1$ there is no saturation yet after a simulation of a succession of 10 states. Furthermore, when $l_0 = 0.04$, it can be observed that from the initial states onwards, the SNR increases during burst periods, indicating that the neural network consolidates the learned information right from the beginning. This is not the case for larger l_0 values, whose SNR shows a decrease in the first states when switching to burst activity, signifying lost information. It takes a little longer for the neuronal network to start consolidating learned information during the burst, compared to the case where $l_0 = 0.04$.

What we can learn from these results is that whatever the initial value of the late-weight (within reasonable

values), the SNR tends to increase over time. What's more, the neuronal network ends up consolidating the information (learned during tonic periods) during burst periods. Indeed, even when the neuronal network is no longer subject to external stimulation, SNR increases. The choice of the value of l_0 just modulates the evolution of the SNR.

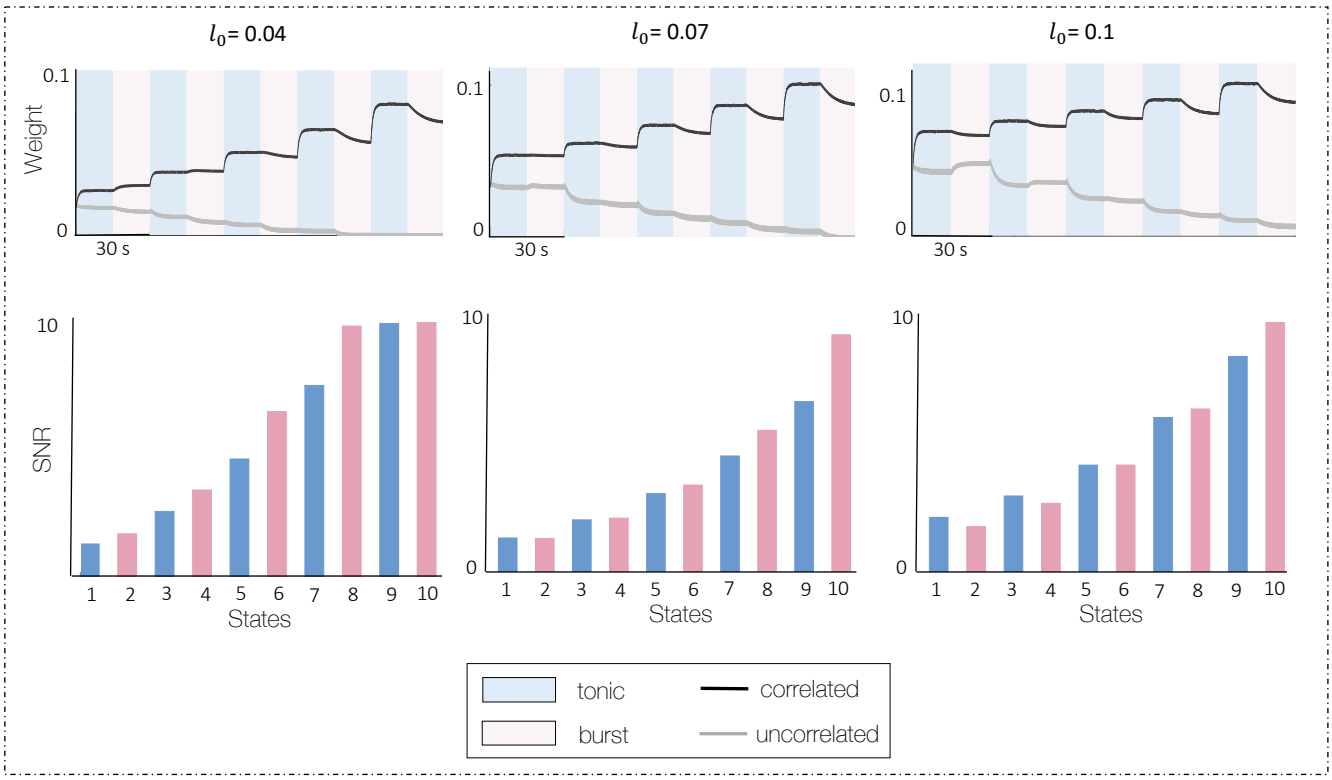

Figure 6.8 – **Effect of choice of initial late weight on SNR.** The weight curves (top graph) and corresponding SNR are shown for different values of l_0 (for $l_0 = 0.04$ (left), for $l_0 = 0.07$ (middle) and for $l_0 = 0.1$ (right)). In all three cases, the SNR tends to increase over time.

6.3.4 Effect of network size

Experiments

The memory task proposed by [González-Rueda et al., 2018] applies to a larger network than the one we have just used. In [González-Rueda et al., 2018], a network of 100 presynaptic neurons and 1 postsynaptic neuron is used. For this reason, in this section, a network of the same size is used to see how the SNR behaves in this case. The simulated neuronal network is shown in Figure 6.9 and the parameters used are specified. The way in which neuron activity is generated is the same as that used in the previous sections (described in section 5.1.2). In this network, 5 connections are correlated as their neurons spike at a high frequency. The remaining 95 connections are uncorrelated since their presynaptic neurons spike at a low frequency. For these neurons we have defined f_0 between 0.1 and 2 Hz. The initial parameters (l_0 and τ_l) were chosen so as not to have any over-connection or saturation in the neuronal circuit during the simulation time, i.e. 10 states. To achieve this, l_0 was set to 0.07 and τ_l to 12.

Results

The results for the large neural network are shown in Figure 6.10.

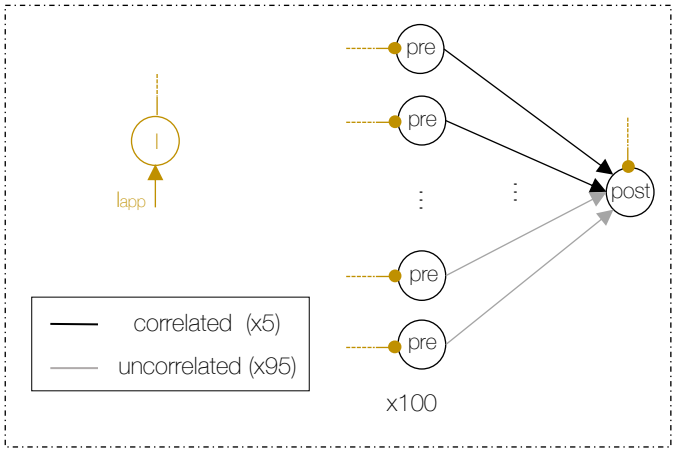

Figure 6.9 – **Neural circuit used to see the effect of increasing network size on SNR.** It consists of 100 presynaptic neurons connected to 1 postsynaptic neuron. Five connection are correlated, while the other 95 are uncorrelated. An inhibitory neuron is connected to the neurons to modulate their electrical activity.

Parameters:

- Frequency f_0 chosen to generate tonic activity:

Neuron	frequency
Pre 1-5	60 Hz
Pre 6-100	[0.1-2] Hz
Post	40 Hz

- Initial values:

w_0	l_0	τ_l
0.5	0.07	12

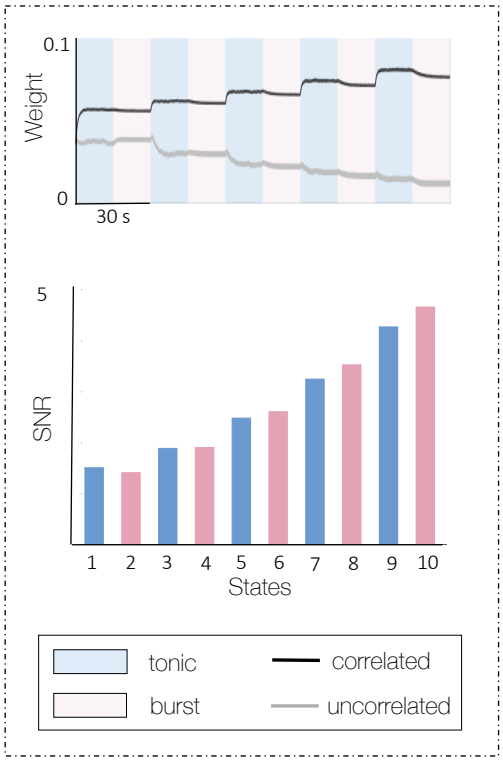

Figure 6.10 – **SNR evolution for a larger neuronal network.** The evolution of weight (product of early-weight and late-weight) is shown on the top graph (5 correlated connections in black and 95 uncorrelated connections in grey). The SNR calculated at the end of each state is shown on the bottom graph. The SNR tends to increase over time. The simulated circuit is that shown in Figure 6.9.

The behavior of the SNR is the same as that observed for the smallest neuronal network. Indeed, we can see that during the first few states, SNR decreases at the switch to burst activity. This represents a downscaling of

the neuronal network and indicates that information is being forgotten during burst periods. Subsequently, the opposite behavior is observed. Indeed, SNR continues to increase even during burst activity, indicating that the neural network is consolidating the learned information.

Even by increasing the size of the neural network, the structural plasticity model we propose seems consistent with memory consolidation.

6.3.5 Conclusions

In conclusion, the effects of the various parameters on SNR do not affect its overall behavior. In other words, whatever the parameters chosen, SNR tends to increase over time. Moreover, the neuronal network ends up consolidating memory even during burst periods. Parameters influence the rate of SNR evolution. Indeed, a small τ_l will cause the SNR to increase faster than a large τ_l. Memory consolidation during burst periods will therefore begin at an earlier state than with a larger τ_l. As for the initial value of the late-weight (l_0), the smaller it is chosen, the faster the SNR will reach saturation. The choice of parameters remains at the discretion of the user, depending on the desired objective.

6.4 Applying the structural plasticity model to a learning task

In this section, a simple learning task is performed to illustrate memory consolidation during neuronal activity switches. This allows us to test the model proposed in this thesis, which combines a traditional synaptic plasticity rule with a structural plasticity rule. This task was inspired by one proposed by [Jacquerie, 2023].

6.4.1 Experiment

The task consists in teaching the neural network to identify a pattern composed of 4 pixels on a 3x3 grid. This pattern and the neuronal network used are illustrated in Figure 3. The neuronal network consists of 9 presynaptic neurons and one postsynaptic neuron. Each presynaptic neuron is associated with a grid pixel. To learn the pattern, the neurons associated with the pattern (presynaptic neurons 1 to 4) are stimulated to spike at a frequency of around 55Hz. Neurons not associated with the pattern (presynaptic neurons 5 to 9) spike at a frequency of around 1Hz. In addition, the postsynaptic neurons are simultaneously activated at a frequency of 40Hz.

In this section, we experiment with Scenario 0 and Scenario 1 and the simulation runs for 150 seconds, i.e. for 10 states. As a reminder, scenario 0 corresponds to a succession of tonic and burst periods in which no structural plasticity is implemented. Scenario 1 is the same as scenario 0, but in which structural plasticity is implemented during burst periods. By experimenting with these two scenarios, we can demonstrate the effectiveness and usefulness of implementing structural plasticity in our model.

To illustrate results and interpret learning, we display the receptive field of each output neuron, as proposed by [Jacquerie, 2023]. The receptive field represents the matrix of weights assigned to each output neuron, i.e. the weights of the 9 presynaptic neurons remodeled in a 3x3 grid. Here, the weight in question is the product of the early-weight and the late-weight (wl). The color of each pixel in the grid is proportional to the normalized weight obtained at the end of each state.

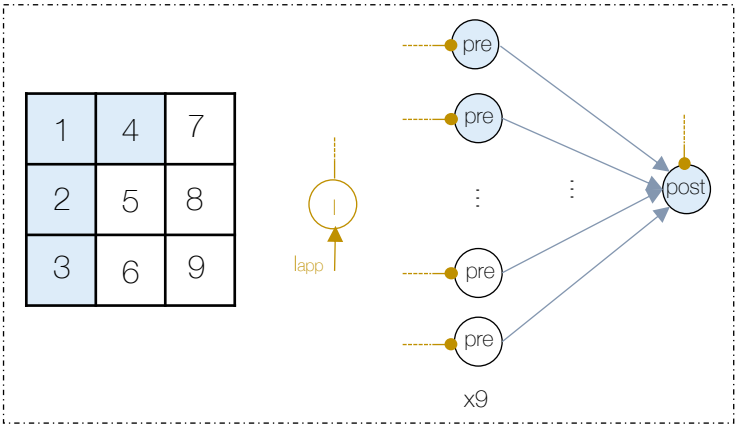

Figure 6.11 – **Pattern and Neuronal network.** The pattern is composed of 4 pixels on a 3x3 pixel grid. The neuronal network consists of 9 presynaptic neurons, each associated with a pixel in the pattern. These neurons are connected to a postsynaptic neuron, in a ffedforward manner. An inhibitory neuron is connected to the neurons to modulate their electrical activity.

Parameters:

- Frequencies used to generate neuron spikes:

Neuron	**frequency**
Pre 1-4	55 Hz
Pre 5-9	1 Hz
Post	40 Hz

- Initial values:

w_0	l_0	τ_l
0.5	0.03	10

6.4.2 Results

The receptive fields for each state and scenario are shown in Figure 6.12. Those at the top are those obtained with the implementation of structural plasticity and those at the bottom without the implementation of structural plasticity. The lighter the color, the higher the synaptic weight. It is important to note that the synaptic weight considered to give the pixel color is normalized for each scenario considered. This means that, for the same pixel color between scenario 0 and scenario 1, this does not necessarily correspond to the same synaptic weight.

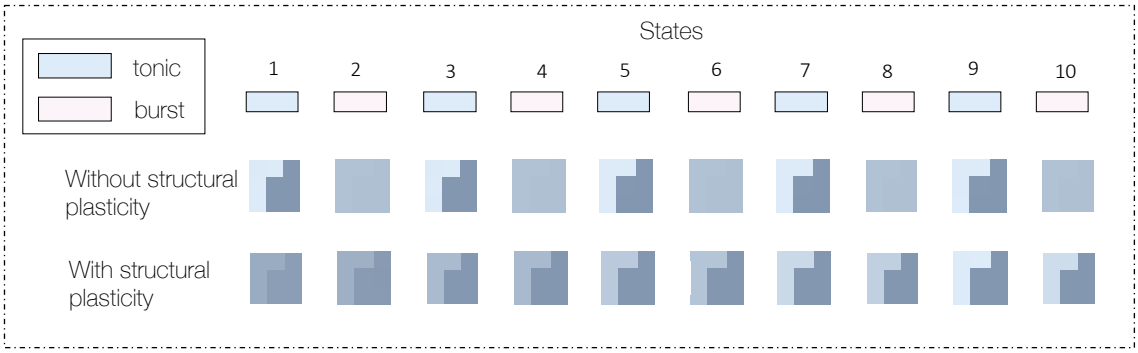

Figure 6.12 – **Results of the learning task.** At the top are the receptive fields when no structural plasticity is implemented. The color intensity of each pixel is proportional to the normalized synaptic weight. The lighter the color, the higher the weight. Below are the receptive field when structural plasticity is implemented during the burst. Experiments are performed for a succession of tonic and burst periods over a total of 10 states, using the neural network shown in Figure 6.11.

The results show that, in the presence of structural plasticity, the pattern becomes better and better learned over the course of the states. Indeed, we see that the pattern is lighter in color in state 10 than in state 1. However, at

each burst period, we see that the neural network forgets some of the information, since the pattern is represented in slightly darker color. But the pattern is still visible, which means that not all the information is forgotten. Concerning the results when there is no structural plasticity, we see that at each burst period, the neuronal network forgets the information, since the pattern is invisible during these periods. In addition, over the entire period of simulations, the network is unable to consolidate the learned information. Indeed, the color of the pattern in state 9 is the same as in state 1, which means that the network does not know the information any better at the end of the simulation.

In conclusion, in the presence of structural plasticity, the neural network is able to consolidate learned information, even if a small amount of information is forgotten with each switch to burst activity. Without structural plasticity, the network is unable to consolidate learned information, since every time it switches to burst activity, it forgets all the information it has learned. Implementing structural plasticity is therefore a prerequisite for memory consolidation.

Chap 6 : effectiveness of the model

Our structural plasticity model improves the SNR across several tonic/burst cycles

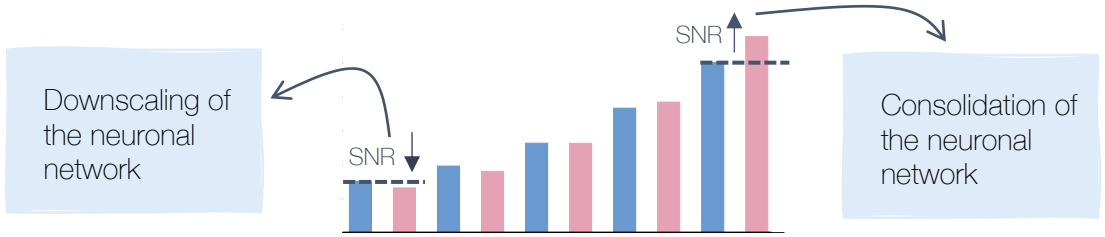

Influence of parameters on SNR

Effect of τ_l

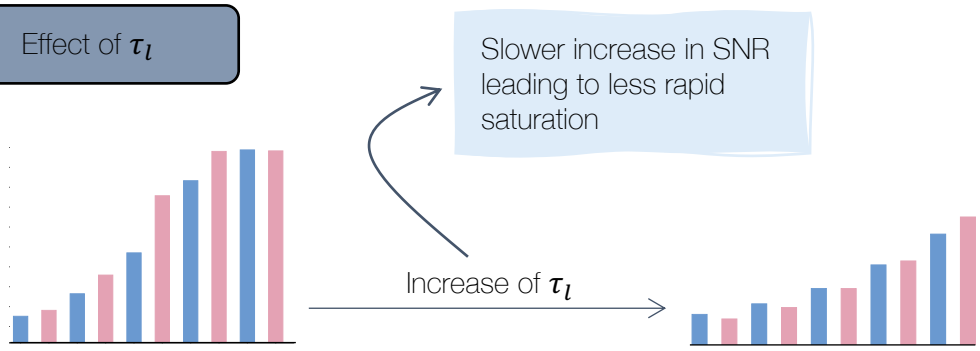

Effect of l_0

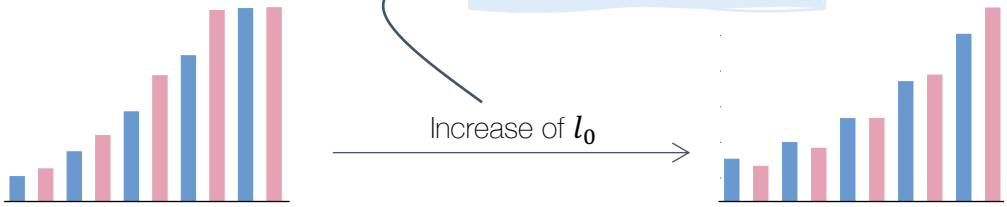

But it is important to choose a l_0 that is not too large to avoid the problem of over-connection of neurons

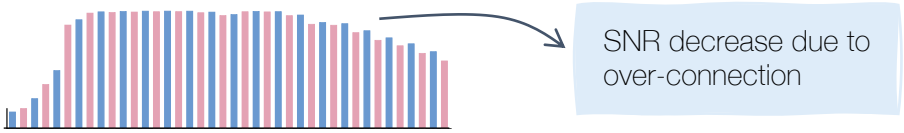

Neuron learning improves during simulation with our structural plasticity rule.

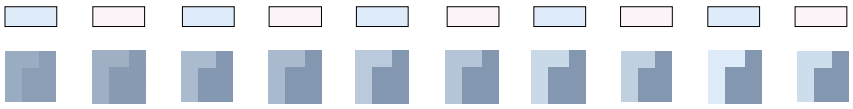

Part IV

Conclusion and perspectives

Chapter 7

Conclusion and perspectives

7.1 Thesis summary

This thesis aimed to develop a model of structural plasticity capable of taking advantage of the homeostatic remnant observed with traditional rules of synaptic plasticity during changes in neuronal firing patterns. The goal was to obtain a model consistent with memory consolidation during quiet waking states. To achieve this objective, the following key questions were addressed:

- *What is synaptic plasticity, how is it modeled, and what are the limitations of these models for changes in neuronal firing pattern?* (Chapter 2)
  Synaptic plasticity refers to the ability of neurons to modify their neuronal connections. In the literature, it exists in two forms: E-LTP and L-LTP. The first type, E-LTP, is characterized by a modification of receptor efficiency and the rapid insertion of new receptors, and it has been extensively investigated from a computational standpoint. Two major categories of models are encountered: biophysical models and phenomenological models. However, as [Jacquerie et al., 2022a] has shown, when these synaptic plasticity rules are used as they are in changes in firing patterns (particularly from tonic to burst), the homeostatic reset is observed. Indeed, when switching to burst activity, all synaptic weights converge to the same baseline value, whatever their initial value. This phenomenon is inconsistent with memory consolidation, since all the information learned during tonic is forgotten.

- *What is structural plasticity from a biological point of view* (Chapter 3) *and how is it modeled in the literature?* (Chapter 4)
  Structural plasticity, often referred to as L-LTP in the literature, is characterized by structural changes in dendritic spines. It also involves protein synthesis, unlike E-LTP. We first investigated it from a biological point of view, so as to have all the tools needed to understand the models proposed in the literature. In brief, the calcium influx resulting from LTP induction triggers a whole cascade of biochemical reactions leading to the rearrangement of the actin cytoskeleton. Small GTPases play a key role in this cascade. In addition, CREB activation triggers the synthesis of new receptors.
  From a computational model point of view, L-LTP models have been much less investigated than E-LTP models. As proposed by [Jacquerie, 2023], they can be classified into three categories: mathematical models (using a lot of equations and statistics to describe structural plasticity) like the one proposed by [Deger et al., 2012], biological models (describing the dynamics of biochemical reactions) like that of [Smolen et al., 2006] , and phenomenological models (using simplified biological processes to govern the model equations) like that of [Fauth and van Rossum, 2019].

- *Can we create a structural plasticity rule that takes advantage of homeostatic reset to transfer learning and be consistent with memory consolidation?* (Chapter 5)

We have developed a structural plasticity rule that models L-LTP through the evolution of late-weight. The rule is based directly on the dynamics of early-weight, which in turn models E-LTP. Synaptic weight is then defined as the product of early-weight and late-weight. The model was tested during the change in neuronal activity (in particular from tonic to burst) and showed that it was able to take advantage of the homeostatic reset to transfer learning. Indeed, over time, correlated connections (representing learning) were potentiated and uncorrelated connections depressed. The model thus demonstrated its ability to retain learned information and learn through multiple occurrences. An analysis of the parameters was carried out in order to determine their effect and to define them appropriately for the desired objective. In particular, it was shown that the value of the homeostatic reset (driven by neuronal rhythm during the burst activity) had an important effect on the model, as it dictates the extent to which consolidation and depression occur. A small value, for example, favors consolidation over depression. In addition, the model proposed in this thesis proved robust to the heterogeneity of the neuronal network and to the choice of the traditional synaptic plasticity rule used.

- *Is the proposed model effective for memory consolidation?* (Chapter 6)
  To test the effectiveness of the model, a simple task inspired by [González-Rueda et al., 2018] was carried out. Efficiency is assessed by calculating the signal-to-noise ratio (SNR). The results showed that our model improved the SNR across several tonic/burst cycles, which was not the case without structural plasticity. The SNR showed very interesting behavior. Indeed, during the first states, it decreased when switching to burst activity (reflecting a loss of information), then from a certain state onwards, the SNR continued to increase even when switching to burst activity (reflecting a consolidation of information). The behavior of the SNR was analyzed in depth, and the effects of different parameters on it were also highlighted. A time constant that was too small or a simulation period that was too long, for example, led to SNR saturation. Finally, the effectiveness of our model is illustrated in a simple pattern recognition learning task and the results showed that neurons learned better in the presence of structural plasticity.

7.2 Limitations and perspectives

Given that the structural plasticity model proposed in this thesis has only just been developed, many future prospects are open. Some of them are proposed below.

7.2.1 Variability in simulation times

In this thesis, we have always assumed that the different states had an equivalent duration. Specifically, we have almost always considered that a state lasted for 15 seconds, whether it was the tonic state or the burst state. However, in real life, this is not always the case. That is why it would be interesting to introduce variability in the durations of the states to better reflect reality. Additionally, investigating the impact of this variability on learning would be worthwhile. *Would shorter burst periods enhance learning? Conversely, would longer burst periods not result in better learning?* These are the types of questions that could be explored.

We have already begun exploring this task, and the results can be found in Figure 7.1. We repeated the same simple task inspired by [González-Rueda et al., 2018] discussed throughout Chapter 6 in which the signal-to-noise ratio (SNR) is calculated. Here, however, we cut the states in time and, more specifically, defined the following durations:

Duration	**Tonic**	**Burst**
Experiment 1	15 s	15 s
Experiment 2	15s	7.5 s
Experiment 3	7.5s	15s

Experiment 1 is just there for comparison.

At first glance, the impact of time variability is not obvious. Indeed, for all 3 experiments, the SNR improves over time, reaching a value of around 5 at the end of the 10th state. This is due to the fact that we did not shorten the states enough, so the early-weights had time to converge towards their convergence value. However, in Experiment 2, this is not quite the case, as we can see that the homeostatic reset is not quite reached at the end of the burst. But the values are still very close to the reset, so this has very little impact on the SNR, which reaches a slightly lower value than in the other experiments. Therefore, considering even shorter states remains an avenue to explore, which is expected to have an impact on learning.

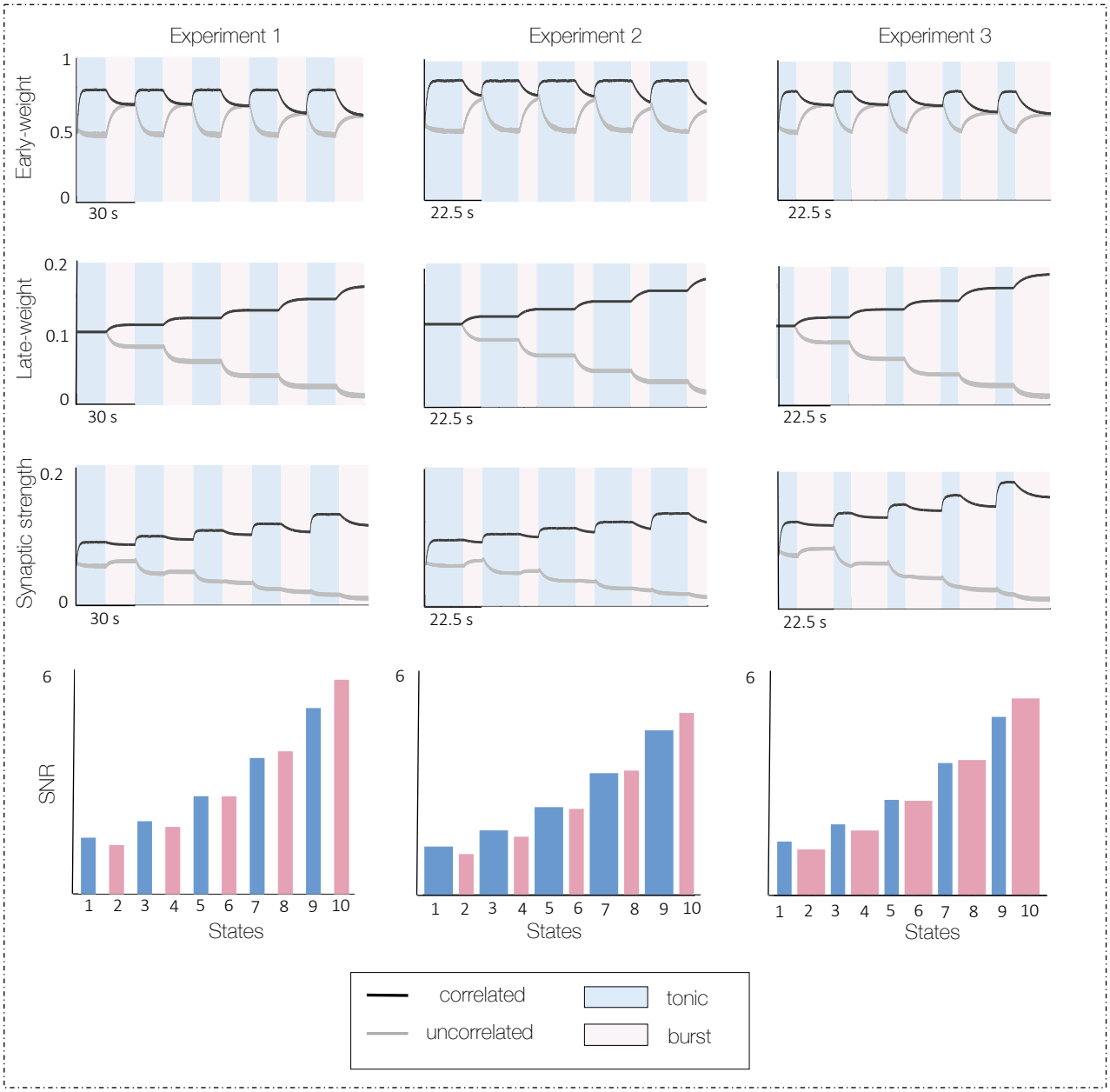

Figure 7.1 – **Effect of state duration variability on SNR.** In Experiment 1 (left), the tonic duration is the same as the burst duration, and is 15 seconds. In Experiment 2 (middle), the burst duration has been halved to 7.5 seconds. In experiment 3 (right), the tonic duration was halved.

7.2.2 Others perspectives

- In this thesis, we have illustrated the effectiveness of the proposed structural plasticity model through a simple pattern recognition task. However, these patterns were very simplistic, consisting of just 4 pixels. To really test the effectiveness of our model in learning tasks, more complex patterns would have to be used. A well-known and much-used pattern in the machine learning sector is the MNIST, shown in Figure 3. This pattern consists of a set of digitized handwritten digits ranging from 0 to 9. The patterns are 28x28 pixels in size, for a total of 784 pixels. It would be very interesting to see whether our model is capable of performing these complex memory tasks.

Figure 7.2 – **MNIST dataset.** *From* [ActiveLoop, 2023]

- In the experiments of this thesis, we mainly used the calcium-based plasticity rule to describe the evolution of early weight. Although we tested our structural plasticity model with the phenomenological models, no learning tasks were performed using them. It could therefore be interesting to further explore the structural plasticity rule with phenomenological models.

Bibliography

[ActiveLoop, 2023] ActiveLoop (2023). MNIST Dataset. https://datasets.activeloop.ai/docs/ml/datasets/mnist/. Accessed on June 8, 2023.

[Adem et al., 2016] Adem, S., Chang, C., and Fleming, M. (2016). Impact of Demyelination Disease on Neuronal Networks.

[Amano et al., 2022] Amano, R., Nakao, M., Matsumiya, K., and Miwakeichi, F. (2022). A computational model to explore how temporal stimulation patterns affect synapse plasticity. *PLOS ONE*, 17(9):e0275059.

[Bear et al., 2007] Bear, M. F., Conners, B. W., and Paradiso, M. A. (2007). *Neuroscience: Exploring the Brain*. Lippincott Williams and Wilkins, 3rd edition.

[Benghalem, 2022] Benghalem, N. (2022). Master thesis : Neuromodulation of phenomenological plasticity rules.

[Butz et al., 2009] Butz, M., Wörgötter, F., and van Ooyen, A. (2009). Activity-dependent structural plasticity. *Brain Research Reviews*, 60(2):287–305.

[Carlezonjr et al., 2005] Carlezonjr, W., Duman, R., and Nestler, E. (2005). The many faces of CREB. *Trends in Neurosciences*, 28(8):436–445.

[Citri and Malenka, 2008] Citri, A. and Malenka, R. C. (2008). Synaptic Plasticity: Multiple Forms, Functions, and Mechanisms. *Neuropsychopharmacology*, 33(1):18–41.

[Costa et al., 2020] Costa, J. F., Dines, M., and Lamprecht, R. (2020). The Role of Rac GTPase in Dendritic Spine Morphogenesis and Memory. *Frontiers in Synaptic Neuroscience*, 12:12.

[Deger et al., 2012] Deger, M., Helias, M., Rotter, S., and Diesmann, M. (2012). Spike-Timing Dependence of Structural Plasticity Explains Cooperative Synapse Formation in the Neocortex. *PLoS Computational Biology*, 8(9):e1002689.

[Domart, 2019] Domart, F. (2019). *Nano-imagerie corrélative de fluorescence X synchrotron et de super résolution des métaux et des protéines dans les synapses de neurones d'hippocampe*. PhD thesis.

[Fauth and van Rossum, 2019] Fauth, M. J. and van Rossum, M. C. (2019). Self-organized reactivation maintains and reinforces memories despite synaptic turnover. *eLife*, 8:e43717.

[Fu and Ip, 2017] Fu, A. K. and Ip, N. Y. (2017). Regulation of postsynaptic signaling in structural synaptic plasticity. *Current Opinion in Neurobiology*, 45:148–155.

[Furness, 2000] Furness, J. (2000). Types of neurons in the enteric nervous system. *Journal of the Autonomic Nervous System*, 81(1-3):87–96.

[González-Rueda et al., 2018] González-Rueda, A., Pedrosa, V., Feord, R. C., Clopath, C., and Paulsen, O. (2018). Activity-Dependent Downscaling of Subthreshold Synaptic Inputs during Slow-Wave-Sleep-like Activity In Vivo. *Neuron*, 97(6):1244–1252.e5.

[Hedrick and Yasuda, 2017] Hedrick, N. G. and Yasuda, R. (2017). Regulation of Rho GTPase proteins during spine structural plasticity for the control of local dendritic plasticity. *Current Opinion in Neurobiology*, 45:193–201.

[Helias, 2008] Helias, M. (2008). Structural plasticity controlled by calcium based correlation detection. *Frontiers in Computational Neuroscience*, 2.

[Hering and Sheng, 2001] Hering, H. and Sheng, M. (2001). Dentritic spines : structure, dynamics and regulation. *Nature Reviews Neuroscience*, 2(12):880–888.

[Holtmaat and Caroni, 2016] Holtmaat, A. and Caroni, P. (2016). Functional and structural underpinnings of neuronal assembly formation in learning. *Nature Neuroscience*, 19(12):1553–1562.

[Jacquerie, 2023] Jacquerie, K. (July 2023). *Modeling brain-state dependent memory consolidation*. PhD thesis, ULiège - Université de Liège [Applied Sciences], Liege, Belgium.

[Jacquerie et al., 2022a] Jacquerie, K., Minne, C., Ponnet, J., Benghalem, N., Sacré, P., and Drion, G. (2022a). Switches to slow rhythmic neuronal activity lead to a plasticity-induced reset in synaptic weights. preprint, Neuroscience.

[Jacquerie et al., 2022b] Jacquerie, K., Minne, C., Ponnet, J., and Drion, G. (November 2022b). Is the homeostatic reset an artefact or a feature of synaptic plasticity rules for sleep-dependent memory consolidation? F.R.S.-FNRS - Fonds de la Recherche Scientifique [BE].

[Lai and Ip, 2013] Lai, K.-O. and Ip, N. Y. (2013). Structural plasticity of dendritic spines: The underlying mechanisms and its dysregulation in brain disorders. *Biochimica et Biophysica Acta (BBA) - Molecular Basis of Disease*, 1832(12):2257–2263.

[Lamprecht and LeDoux, 2004] Lamprecht, R. and LeDoux, J. (2004). Structural plasticity and memory. *Nature Reviews Neuroscience*, 5(1):45–54.

[Larousse, 2023a] Larousse (2023a). Endocytose. https://www.larousse.fr/dictionnaires/francais/endocytose/188111. Accessed on May 21, 2023.

[Larousse, 2023b] Larousse (2023b). Exocytose. https://www.larousse.fr/dictionnaires/francais/exocytose/188114. Accessed on May 21, 2023.

[Lee and Dan, 2012] Lee, S.-H. and Dan, Y. (2012). Neuromodulation of Brain States. *Neuron*, 76(1):209–222.

[Lehr et al., 2022] Lehr, A. B., Luboeinski, J., and Tetzlaff, C. (2022). Neuromodulator-dependent synaptic tagging and capture retroactively controls neural coding in spiking neural networks. *Scientific Reports*, 12(1):17772.

[Li et al., 2016] Li, Y., Kulvicius, T., and Tetzlaff, C. (2016). Induction and Consolidation of Calcium-Based Homo- and Heterosynaptic Potentiation and Depression. *PLOS ONE*, 11(8):e0161679.

[Luboeinski and Tetzlaff, 2021] Luboeinski, J. and Tetzlaff, C. (2021). Memory consolidation and improvement by synaptic tagging and capture in recurrent neural networks. *Communications Biology*, 4(1):275.

[Mark Lefers, 2004] Mark Lefers, H. L. (2004). Gene product. https://groups.molbiosci.northwestern.edu/holmgren/Glossary/Definitions/Def-G/gene_product.html.

[Mateos-Aparicio and Rodríguez-Moreno, 2020] Mateos-Aparicio, P. and Rodríguez-Moreno, A. (2020). Calcium Dynamics and Synaptic Plasticity. In Islam, M. S., editor, *Calcium Signaling*, volume 1131, pages 965–984. Springer International Publishing, Cham. Series Title: Advances in Experimental Medicine and Biology.

[Minne, 2021] Minne, C. (2021). Interactions between synaptic plasticity and switches in brain states for memory consolidation: a modeling study.

[Muller et al., 2002] Muller, D., Nikonenko, I., Jourdain, P., and Alberi, S. (2002). LTP, Memory and Structural Plasticity. *Current Molecular Medicine*, 2(7):605–611.

[Nakahata and Yasuda, 2018] Nakahata, Y. and Yasuda, R. (2018). Plasticity of Spine Structure: Local Signaling, Translation and Cytoskeletal Reorganization. *Frontiers in Synaptic Neuroscience*, 10:29.

[Nishiyama and Yasuda, 2015] Nishiyama, J. and Yasuda, R. (2015). Biochemical Computation for Spine Structural Plasticity. *Neuron*, 87(1):63–75.

[Patterson and Yasuda, 2011] Patterson, M. and Yasuda, R. (2011). Signalling pathways underlying structural plasticity of dendritic spines: Structural plasticity of dendritic spines. *British Journal of Pharmacology*, 163(8):1626–1638.

[Pchitskaya and Bezprozvanny, 2020] Pchitskaya, E. and Bezprozvanny, I. (2020). Dendritic Spines Shape Analysis—Classification or Clusterization? Perspective. *Frontiers in Synaptic Neuroscience*, 12:31.

[Pereira-Leal and Seabra, 2000] Pereira-Leal, J. B. and Seabra, M. C. (2000). The mammalian Rab family of small GTPases: definition of family and subfamily sequence motifs suggests a mechanism for functional specificity in the Ras superfamily 1 1Edited by M. Yaniv. *Journal of Molecular Biology*, 301(4):1077–1087.

[Poirazi and Mel, 2001] Poirazi, P. and Mel, B. W. (2001). Impact of Active Dendrites and Structural Plasticity on the Memory Capacity of Neural Tissue. *Neuron*, 29(3):779–796.

[Ponnet, 2022] Ponnet, J. (2022). Master thesis : Neuromodulation of calcium-based plasticity rules.

[Runge et al., 2020] Runge, K., Cardoso, C., and de Chevigny, A. (2020). Dendritic Spine Plasticity: Function and Mechanisms. *Frontiers in Synaptic Neuroscience*, 12:36.

[Saura and Valero, 2011] Saura, C. A. and Valero, J. (2011). The role of CREB signaling in Alzheimer's disease and other cognitive disorders. *revneuro*, 22(2):153–169.

[Sheng and Lee, 2001] Sheng, M. and Lee, S. H. (2001). AMPA Receptor Trafficking and the Control of Synaptic Transmission. *Cell*, 105(7):825–828.

[Shibata et al., 2021] Shibata, A. C. E., Ueda, H. H., Eto, K., Onda, M., Sato, A., Ohba, T., Nabekura, J., and Murakoshi, H. (2021). Photoactivatable CaMKII induces synaptic plasticity in single synapses. *Nature Communications*, 12(1):751.

[Shivarama Shetty and Sajikumar, 2017] Shivarama Shetty, M. and Sajikumar, S. (2017). 'Tagging' along memories in aging: Synaptic tagging and capture mechanisms in the aged hippocampus. *Ageing Research Reviews*, 35:22–35.

[Smolen et al., 2006] Smolen, P., Baxter, D. A., and Byrne, J. H. (2006). A Model of the Roles of Essential Kinases in the Induction and Expression of Late Long-Term Potentiation. *Biophysical Journal*, 90(8):2760–2775.

[Smolen et al., 2020] Smolen, P., Baxter, D. A., and Byrne, J. H. (2020). Comparing Theories for the Maintenance of Late LTP and Long-Term Memory: Computational Analysis of the Roles of Kinase Feedback Pathways and Synaptic Reactivation. *Frontiers in Computational Neuroscience*, 14:569349.

[Song et al., 2019] Song, S., Cong, W., Zhou, S., Shi, Y., Dai, W., Zhang, H., Wang, X., He, B., and Zhang, Q. (2019). Small GTPases: Structure, biological function and its interaction with nanoparticles. *Asian Journal of Pharmaceutical Sciences*, 14(1):30–39.

[Wikipédia, 2023] Wikipédia (2023). Endosome. https://fr.wikipedia.org/wiki/Endosome. Accessed on May 21, 2023.

[Zagha and McCormick, 2014] Zagha, E. and McCormick, D. A. (2014). Neural control of brain state. *Current Opinion in Neurobiology*, 29:178–186.

[Zenke et al., 2015] Zenke, F., Agnes, E. J., and Gerstner, W. (2015). Diverse synaptic plasticity mechanisms orchestrated to form and retrieve memories in spiking neural networks. *Nature Communications*, 6(1):6922.

[Zheng et al., 2013] Zheng, P., Dimitrakakis, C., and Triesch, J. (2013). Network Self-Organization Explains the Statistics and Dynamics of Synaptic Connection Strengths in Cortex. *PLoS Computational Biology*, 9(1):e1002848.

Part V

Appendix

Appendix A

Elements of neurophysiology

A.1 Short-term plasticity

This type of plasticity, which temporarily alters synaptic transmission following repeated stimuli, can last from a few milliseconds to several minutes. It is often due to changes in the probability of neurotransmitter release. There are two main types of short-term plasticity: *facilitation* and *depression*. Indee, when two stimuli are applied in succession, the response to the second stimulus may be either enhanced or reduced compared to the first response [Citri and Malenka, 2008].

Depression This plasicity occurs when the stimuli are very close in time (less than 20ms) and the response to the second stimulus is weaker than the response to the first stimulus. It therefore involves a decrease in the release of neurotransmitters in response to a second stimulus [Citri and Malenka, 2008]. This plasticity can be explained by the fact that the first stimulus triggers the release of a large number of vesicles containing neurotransmitters present in the presynaptic neuron. If the second stimulus arrives too quickly, the released vesicles do not have enough time to be replaced, resulting in fewer vesicles available to respond to the second stimulus. This results in a decrease in the number of neurotransmitters released in response to the second stimulus [Mateos-Aparicio and Rodríguez-Moreno, 2020].

Facilitation It occurs when the interval between stimuli is slightly longer (20-500ms) and the response to the second stimulus is stronger than the response to the first stimulus. It therefore involves an increase in the release of neurotransmitters in response to a second stimulus [Citri and Malenka, 2008]. This plasticity would be explained by the fact that following the first stimulus, there is residual calcium in the presynaptic neuron. When the second stimulus occurs, the increase in calcium in the neuron that it causes is added to the residual calcium of the first stimulus. The presynaptic neuron therefore contains more calcium than during the first stimulus, which causes an increase in the number of neurotransmitters released [Mateos-Aparicio and Rodríguez-Moreno, 2020].

It should be noted that these forms of plasticity depend on the history of synapse activation. Indeed, synapses that started with a very high probability of neurotransmitter release tend to reduce their response to the second stimulus, whereas those that started with a low probability of release tend to increase their response to the second stimulus. In addition, the probability of neurotransmitter release is partly controlled by receptor occupancy on presynaptic terminals [Citri and Malenka, 2008].

Appendix B

Structural plasticity from a modeling point of view

B.1 Model proposed by [Zenke et al., 2015]

The bifurcation diagram of the dynamics of the reference weight $\tilde{w}_{ij}(t)$, which thus includes the different equilibrium values, is plotted in Figure B.1. The solid line represents stable points and the dotted line represents unstable points. In addition, the control parameter is the difference $(w_{ij} - \tilde{w}_{ij})$. When this difference is zero, we have the two stable equilibrium points at 0 and 0.5 and the unstable equilibrium point at 0.25, which is therefore in agreement with Figure 4.13. When w_{ij} is slightly larger than $\tilde{w}_{ij}$, two stable equilibrium points are also possible but the value of these two stable points is slightly increased. And finally, when w_{ij} is significantly larger than $\tilde{w}_{ij}$, only one high stable point is possible.

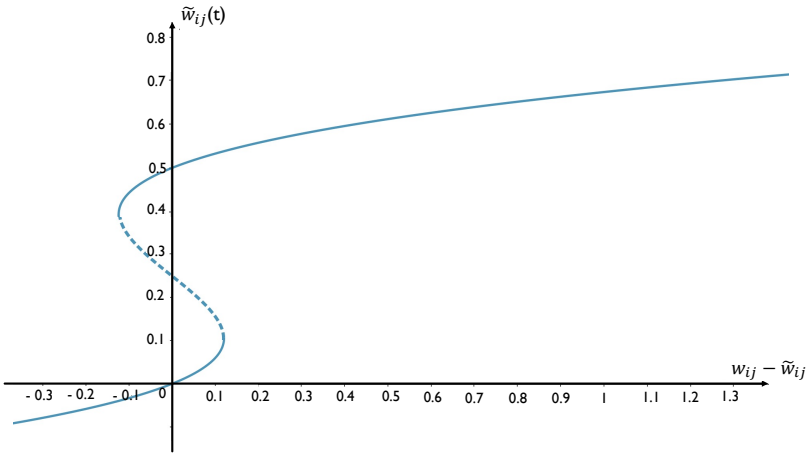

Figure B.1 – **Bifurcation diagram of the dynamics of the reference synaptic weight.** Evolution of the reference weight $\tilde{w}_{ij}(t)$ as a function of the difference between the current synaptic weight $w_{ij}(t)$ and the current reference weight $\tilde{w}_{ij}(t)$. Plot drawn from equation 4.9 when $\tilde{w}_{ij}(t)$ has reached its convergence and thus when $\frac{d}{dt}\tilde{w}_{ij} = 0$. The solid line represents stable equilibrium points while the dashed train corresponds to unstable points.

B.2 Homeostatic plasticity

The main form of homeostatic plasticity is *synaptic scaling*. This maintains balanced neuronal activity and avoids excessive excitation or total inhibition of neuronal circuits. Unlike long-term forms of plasticity such as LTP and LTD, which act specifically on individual synapses, synaptic scaling affects the overall transmission across all synapses of a neuron. This form of plasticity occurs when network activity is dramatically decreased or increased for prolonged periods exceeding 12 hours. When activity decreases, the strength of all excitatory synapses on excitatory neurons increases, whereas when it increases, the strength of all excitatory synapses decreases. The molecular mechanisms underlying this form of plasticity include changes in the number of AMPARs and NMDARs at individual synapses, as well as presynaptic changes [Citri and Malenka, 2008].